Mémoire

Auteur : Peffer, Tom
Promoteur(s) : Kittel, Christoph; Fettweis, Xavier
Faculté : Faculté des Sciences
Diplôme : Master en sciences géographiques, orientation global change, à finalité approfondie
Année académique : 2021-2022
URI/URL : http://hdl.handle.net/2268.2/15761

FACULTÉ DES SCIENCES

Département de Géographie

Long-term historical climate and surface mass balance over the Antarctic Ice Sheet

Mémoire présenté par

Tom PEFFER

en vue de l'obtention du titre de

Master en sciences géographiques
orientation global change
à finalité approfondie

Année acadmémique

2021-2022

Membres du jury

Christoph KITTEL (Promoteur

Xavier FETTWEIS (Co-Promoteur)

Aurélia HUBERT

Acknowledgments

Abstract *(English)*

Although the climate of the Antarctic Ice Sheet has been subject to simulations for many years, they are generally limited to the past few decades, rendering a good assessment of the past climate including the processes linked to the variability of the latter difficult. In this study, a recently released back extension of the ERA5 reanalysis produced by the European Centre for Medium-Range Weather Forecasts (ECMWF) was used for forcing the polar-oriented regional climate model $MAR_{v3.12}$ over the Antarctic Ice Sheet from 1950 to 2020 using a 35 km resolution. Regarding near-surface pressure and temperature (SAT), $MAR_{v3.12}$ displays good performance for the back-extension period (1950–1978) and properly reproduces the SAT variability across the AIS. The model slightly underestimates near-surface temperature along the coastline and tends to overestimate values on the Antarctic Plateau. Likewise, $MAR_{v3.12}$ forced by ERA5 appears to accurately portray surface mass balance (SMB) for both 1950–1978 (r = 0.85) and 1979–2020 (r = 0.85). Mean biases (-8.5 kg m-2 yr-1and -37.8 kg m^{-2} yr^{-1}) are to a certain extent the result of drifting snow processes as well as atmospheric sublimation not being included in model calculations. An assessment of the evolution of the climate reveals an overall increase in SAT, SMB, and surface melt (SM) over time. Especially high temperature increases (> 2°C between the 1951–1980 and 1981–2010 mean) are found in East Antarctica. In summer, across the area Ross ice shelf, both SAT and SMB exhibit a decrease. Interestingly, $MAR_{v3.12}$ forced by ERA5 produces a pronounced surge in SAT and SMB in the late 1970s, notably during austral winter (JJA). Since the same pattern is displayed by the reanalysis itself, this jump may be artificial and a result of the assimilation of stratospheric ozone measurements into the ERA5 dataset around 1979. This hypothesis is supported by the fact that the abnormal rise in temperature does not appear to be present in observation-based climate records. Moreover, in recent studies, a switch in the relationship between the SAT and the Southern Annular Mode (SAM) was identified in the late 1970s, a feature also replicated in this study using $MAR_{v3.12}$ forced by ERA5. It remains unclear if there is a connection between these two events occurring around 1980, however, in future studies MAR could be forced by different reanalyzes also spanning over a longer period or the results presented in this study could be directly compared to ice core measurements. Either way, this study demonstrates the usability of the ERA5 reanalysis for early climate simulations and identifies areas where further research is necessary for assessing the evolution of the Antarctic climate.

Abstract *(French)*

Même si le climat de la calotte glaciaire antarctique a fait l'objet de simulations depuis de nombreuses années, celles-ci sont généralement limitées aux dernières décennies, ce qui rend une bonne évaluation du climat passé difficile. Le « European Centre for Medium-Range Weather Forecasts » (ECMWF) a récemment publiée une nouvelle version de la réanalyse ERA5 contenant des valeurs à partir de 1950. Dans cette étude, ERA5 a été utilisée pour forcer le modèle climatique régional MAR$_{v3.12}$ sur l'Antarctique entre 1950 et 2020 en utilisant une résolution de 35 km. En ce qui concerne la pression et la température à proximité de la surface (SAT), MAR$_{v3.12}$ affiche de bonnes performances pour la période 1950-1978 et reproduit correctement la variabilité du climat à travers l'AIS. Le modèle sous-estime légèrement la température proche de la surface le long du littoral et a tendance à surestimer les valeurs sur le plateau antarctique. De même, MAR$_{v3.12}$ forcé par ERA5 semble représenter avec précision le bilan de mass en surface (SMB) pour les périodes 1950-1978 (r = 0,85) et 1979-2020 (r = 0,85). Les biais moyens (-8,5 kg m-2 an-1 et -37,8 kg m-2 an-1) sont, dans une certaine mesure, le résultat de processus de « blowing snow » ainsi que de la sublimation atmosphérique qui ne sont pas inclus dans les calculs du modèle. Une évaluation de l'évolution du climat révèle une augmentation globale de la température, du SMB et de la fonte de surface (SM) au fil du temps. Des augmentations de température particulièrement élevées (> 2°C entre 1951-1980 et 1981-2010) sont constatées dans l'Antarctique de l'Est. En été, dans toute la zone de la plate-forme glaciaire de Ross, le SAT et le SMB présentent une diminution. Il est intéressant de noter que MAR$_{v3.12}$ forcé par l'ERA5 produit une augmentation prononcée du SAT et du SMB à la fin des années 1970, notamment pendant l'hiver austral (JJA). Comme la même tendance est affichée par la réanalyse elle-même, ce saut peut être artificiel et résulter de l'assimilation des mesures de l'ozone stratosphérique dans l'ensemble de données ERA5 vers 1979. Cette hypothèse est soutenue par le fait que l'augmentation anormale de la température ne semble pas être présente dans les enregistrements climatiques basés sur des observations. De plus, dans des études récentes, un changement dans la relation entre le SAT et le mode annulaire sud (MAS) a été identifié à la fin des années 1970, une caractéristique également reproduite dans cette étude utilisant MAR$_{v3.12}$ forcé par ERA5. On ne sait toujours pas s'il existe un lien entre ces deux événements survenus autour de 1980. Toutefois, dans les études futures, MAR pourrait être forcé par différentes réanalyses couvrant également une période plus longue ou les résultats présentés dans cette étude pourraient être directement comparés aux mesures des

carottes de glace. Quoi qu'il en soit, cette étude démontre l'utilité de la réanalyse ERA5 pour les simulations climatiques précoces et identifie les domaines où des recherches supplémentaires sont nécessaires pour évaluer l'évolution du climat de l'Antarctique.

Abbreviations

AIS	Antarctic Ice Sheet
ASL	Amundsen Sea Low
AWS	Automatic Weather Station
D	Discharge
DJF	December-January-February (austral summer)
ENSO	El Niño Southern Oscillation
ESM	Earth-System Model
GCM	General Circulation Model
JJA	June-July-August (austral winter)
MAM	March-April-May (austral autumn)
masl	meter above sea level
MAR	Modèle Atmosphérique Régional
M_{basal}	Basal Melt
MSLP	Mean Sea Level Pressure
r	Correlation coefficient
RF	Rainfall
RCM	Regional Climate Model
RMSE	Root mean squared error
RU	Meltwater Runoff
SAM	Southern Annular Mode
SAT	Surface Air Temperature
SD	Standard Deviation
SF	Snowfall
SIC	Sea-ice concentration
SISVAT	Soil Ice Snow Vegetation Atmosphere Transfer
SM	Surface Melt
SMB	Surface Mass Balance
SO	Southern Ocean
SON	September-October-November (austral spring)
SST	Sea-surface temperature
SU	Sublimation

Figures

Figures
_____

Tables

Contents

FIG. 1. Map of Antarctica showing elevation contours with 200-m intervals (topography from Liu et al. 2001).

Figure 1.1: Map of the Antarctic Ice Sheet displaying ice shelves and elevation contours (from Bromwich and Nicolas, 2011)

1. Introduction

1.1. Generalities

The Antarctic continent hardly requires an introduction. For the past decades, even centuries, the Antarctic continent, home of the most southern point on Earth, the South Pole, has been an area of interest for the scientific community (e.g., Murray, 1898). The continent has been a battle ground for explorers, as illustrated by the famous race to the South Pole by Scott and Amundsen in the early 20th century. It has also been studied by scientists for its unique ecosystem (e.g., Wace, 1960; McKnight *et al.*, 2007; Pertierra *et al.*, 2019). Finally, the importance of the Antarctic Ice Sheet (AIS) is revealed from a climatological point of view. Apart from providing valuable data regarding past climates using ice cores for example, looking at more recent evolutions of the Antarctic Ice Sheet can give us an idea about the climate of the future and its implications. For instance, the continent is almost entirely covered by ice and snow (98%), making it the largest store of frozen water on Earth (70%) (King & Turner, 1997). Melting of the entire AIS would result in a rise of the global sea level of approximately 58 m. Greenland, on the other hand, the second-largest store of ice and snow, would only contribute around 7 m to sea-level rise, were its ice to melt completely (Fretwell *et al.,* 2013; Bamber *et al.*, 2013). The global surface reflectivity, the albedo, would also lower considerably in the case of complete melting, thereby further contributing to global warming. This clearly points to the relevance of studying the past, present, and future climate of the AIS.
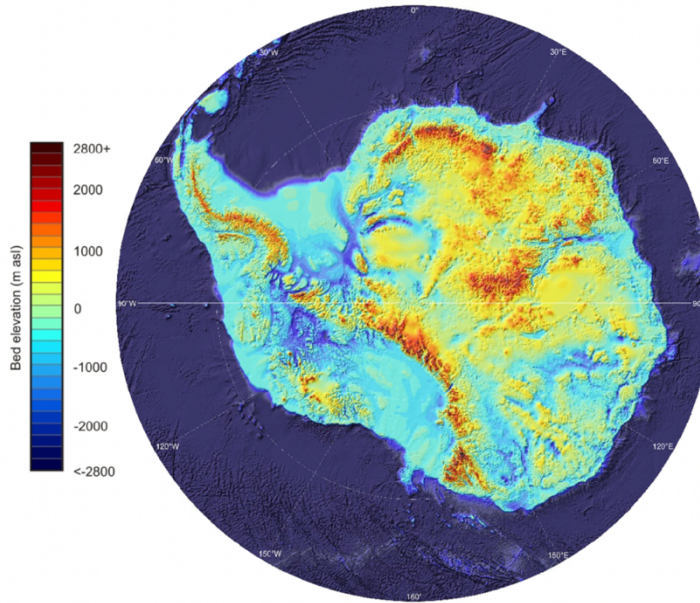
Figure 2.2: Antarctica topography below the ice sheet (from Fretwell *et al.*, 2013)

1.2. Antarctic climate

1.2.1. Near-surface temperatures and winds

Near-surface temperatures across the Antarctic Ice Sheet depend on several key factors (e.g., location, season). There are for instance differences between coastal and inland regions (Fig. 1.3). The presence of sea ice near coastal regions influences the heat fluxes coming from the ocean (King, 1994). At the same time, topography plays a significant role through interactions with the atmosphere (e.g., Foehn effect). Moreover, regions at higher altitudes generally display lower near-surface temperatures. In addition to the spatial variability, AIS near-surface temperatures also exhibit interannual and seasonal variability. During the winter months, sunshine hours are reduced to zero. This phenomenon is referred to as the polar night, when no solar energy is received by the continent, due to the Earth's rotational axis being inclined towards the sun. During its counterpart, the midnight sun, the sun shines 24 hours per day. Thus, the energy budget is significantly altered throughout the year, resulting in different near-surface temperatures. Lastly, changes in ice and snow cover (e.g., thickness and composition) result in regional differences in albedo, thereby creating further regional biases of the energy budget. Given the reasons mentioned above, it comes as no surprise that throughout several years, across the continent, an extreme range of temperatures can be observed. For instance, the mean observed summer temperature between 1969 and 2000 at a station on the Antarctic

Peninsula is +1.2 °C, while on the Antarctic Plateau, mean annual temperatures of around - 50 °C have been measured (Turner, 2004).
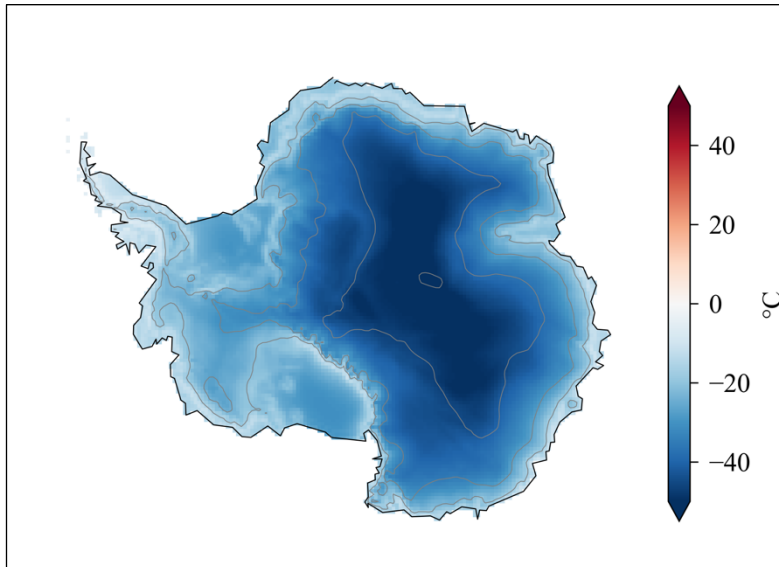
Figure 3.3: Mean annual near-surface temperature (°C) simulated by MAR over 1979–2020

Near-surface wind speed depends largely on the topography. The lowest wind speeds are generally found on the flat Antarctic Plateau, while coastal regions with their steep margins generally exhibit higher wind speeds (Fig. 1.4). The topography of the AIS also creates ideal conditions for the formation of katabatic winds. Katabatic wind corresponds to the downslope movement of colder and denser near-surface air, accelerated by gravity. Low surface temperatures lower the near-surface air temperature, thus creating a temperature inversion. The cold and dense masses of air will then flow from the centre of the AIS towards the coastal regions, thereby favouring the formation of katabatic winds. Moreover, the formation of Foehn winds is promoted by the combination of the westerly flow and the steep topography of the Antarctic Peninsula. They are the result of moist maritime air being forced upslope, resulting in a reduction of the relative humidity. This creates warm dry winds moving downslope on the lee side. Their strength and frequency depend on both location and season, being the strongest at the base of the Peninsula and the most persistent in spring (Turton *et al.*, 2017). Foehn winds have important implications for near-surface temperatures and melt rates on the eastern side of the Peninsula. Studies suggest that the increased Foehn winds that are promoted by a stronger westerly flow during a positive SAM phase (e.g., Marshall *et al.*, 2006) are responsible for the collapse of the Larsen A and B ice shelves and might be associated with the recent calving events of the Larsen C ice shelf (Orr *et al.*, 2008; Turton *et al.*, 2017).
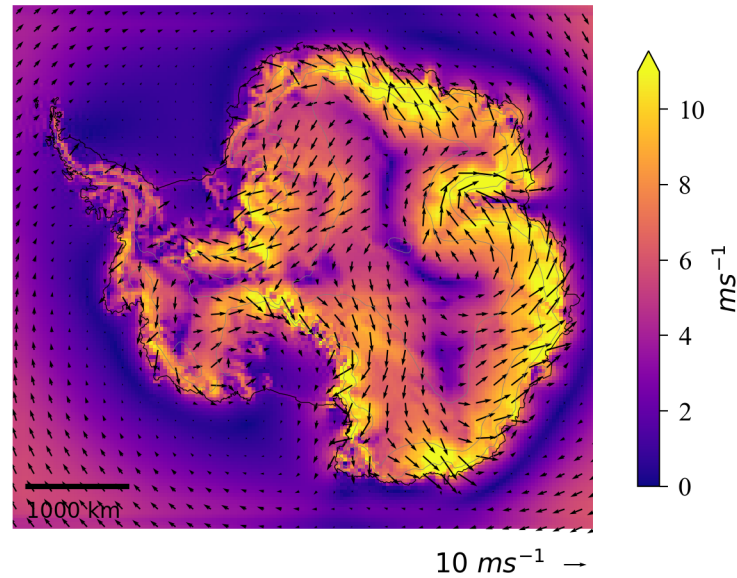
Figure 4.4: Mean annual near-surface wind speed (ms^{-1}) and direction simulated by MAR over 1981–2010

1.2.2. Atmospheric circulation

The atmospheric circulation in the Antarctic region is partially governed by the Southern Annular Mode (SAM), the EL Nino Southern Oscillation (ENSO) and to a certain extent, the Amundsen Sea Low (ASL).

1.2.2.1. Southern annular mode

The Southern Annular Mode is known as the most important mode of variability in the Southern Hemisphere atmospheric circulation. A positive (negative) SAM is linked to periods of weaker (stronger) westerly winds in the mid to high latitudes in the Southern Hemisphere. The SAM index represents the difference in zonal mean sea-level pressure between the latitudes of 40°S and 65°S. The SAM is mostly known for being a primary climate driver regarding the weather over Australia, bringing in cold fronts from the west. However, changes of the SAM also translate into changes of the Antarctic weather, mostly in terms of temperature and ocean circulation. Thus, the SAM is also referred to as "Antarctic Oscillation" (Thompson & Solomon, 2002; Marshall, 2003).

From an Antarctic Point of view, the SAM can be regarded as an expansion and contraction of the polar vortex, which results in a southerly or northernly movement of the mid-latitude jet. Recent observations indicate a dominantly positive SAM (Fig. 1.5), resulting in lower surface

pressures across Antarctica, accompanied by more westerly winds in the coastal region. Marshall *et al.* (2017) found that a positive SAM causes an increase in precipitation, primarily over the western part of the continent. The Antarctic Peninsula is also affected by this, however, only over its western parts because stronger westerly winds encountering the elevated terrain enhance the Foehn effect, losing moisture through precipitation as air passes over the mountainous terrain. While the reasons for this change in behaviour are still uncertain, it may be linked to the increasing greenhouse gas concentration in the atmosphere or the stratospheric ozone depletion (e.g., Turner, 2004).
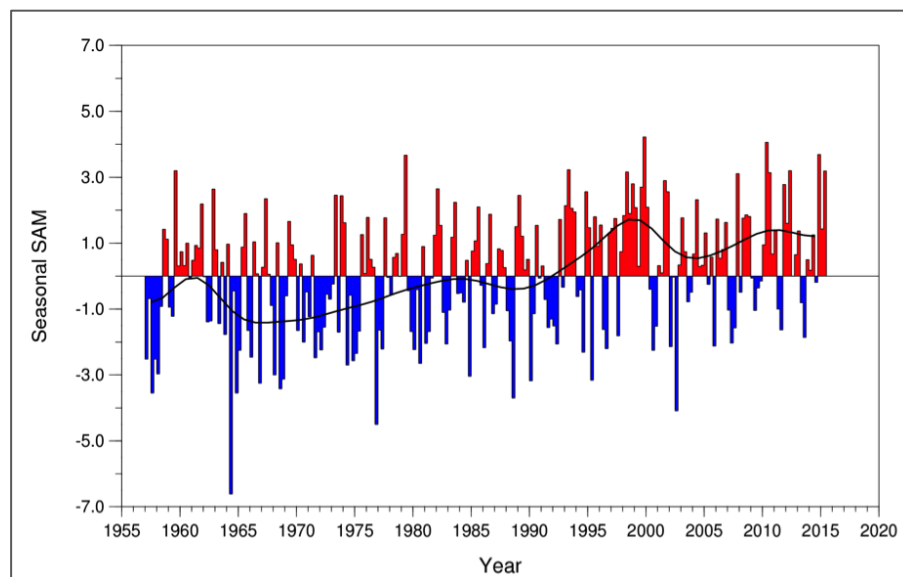
Figure 6.5: Seasonal values of the observation-based Southern Annular Mode index. Decadal variations are shown by the black curve (from Trenberth *et al.*, 2007)

1.2.2.2.　El Niño Southern Oscillation

The El Niño Southern Oscillation is made up of two parts, (1) El Nino and (2) its counterpart La Nina, which are two periodic events associated with episodes of warmer or cooler sea surface temperatures respectively, in the equatorial Pacific Ocean. ENSO has a significant impact on the weather, by changing pressure patterns, wind and precipitation. The fact that both the El Nino and La Nina events affect the weather not only locally but that their influence can be observed in remote locations such as Antarctica is referred to as teleconnections. Thus, taking these teleconnections into consideration, studying the ENSO patterns can provide us with valuable information regarding the climate variability across Antarctica (Turner, 2004; Scott *et al.*, 2018; Paolo *et al.*, 2018). Being a phenomenon that occurs in the Pacific Ocean, its influence can mostly be found in the Pacific Sector of the Southern Ocean, more specifically,

across the Antarctic Peninsula and the Bellingshausen Sea. Many studies have been conducted in the past; however, the main issue remains the lack of a long climate record over the AIS, which renders a thorough analysis of the relationship between ENSO and the Antarctic climate difficult (Turner, 2004).

1.2.2.3.   Amundsen sea low

The Amundsen Sea low is a low-pressure area located in the Pacific Sector of the Southern Ocean, in particular the Bellingshausen Sea, the Amundsen Sea, and the Ross Sea (Fig. 1.6). The climatological low is generally situated between 60°-70 °S. It is one of the main components of the nonzonal climatological circulation and is the result of the interaction between the high topography of the Victoria Land, which is situated west of the Ross Sea, and the mean westerly flow. Regarding its exact location, the ASL features a cyclic behaviour. During summer the low can be observed west of the Antarctic Peninsula, while during winter it can be seen in the Ross Sea. Moreover, the ASL moves to higher and lower latitudes in winter and summer respectively. The absolute depth of the ASL varies throughout the year but is also significantly influenced by both the El Nino-Southern Oscillation (ENSO) and the Southern Annular Mode (SAM) (Raphael *et al.*, 2016).

The ASL affects the climate over West Antarctica and to a certain degree across the Antarctic Peninsula, which, according to Hosking *et al.* (2013), primarily depends on the location and strength of the low. While predicting the future changes of the ASL is a difficult task, the ASL is expected to become stronger (except during summer) with the rise of greenhouse gas concentrations, thereby causing an increase in temperature, wind, and precipitation, notably around Ellsworth Land (Raphael *et al.*, 2016).
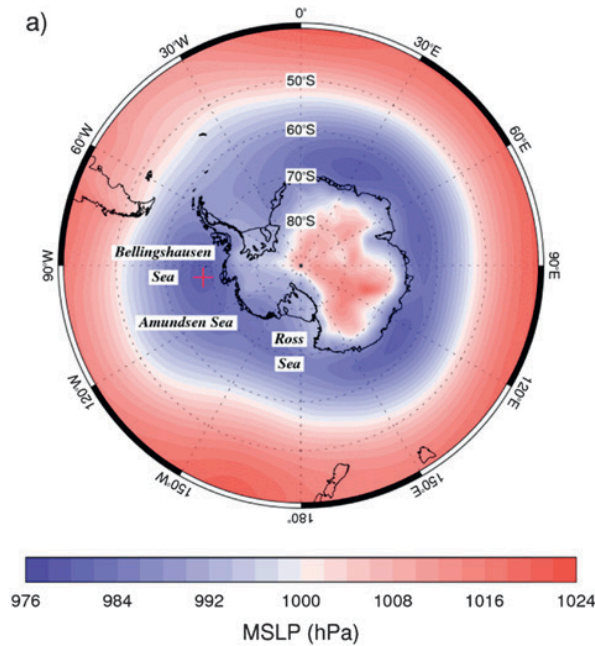
Figure 8.6: Mean MSLP around Antarctica for austral fall months in 1995 from ERA-Interim. The location Amundsen Sea Low during that season is marked by a red cross (from Raphael *et al.*, 2016)

The relative contribution of the SAM, ENSO and ASL to changes in the climate over Antarctica also exhibits seasonal differences. For instance, Clem *et al.* (2016) found that during MAM over the Antarctic Peninsula, temperature changes are mostly associated with the SAM, while the impact of ENSO remains weaker. Moreover, during summer (DJF), additional differences regarding the response to positive SAM conditions exist between the western and northeastern part of the Peninsula. Overall, many uncertainties still exist regarding the relationship between the SH atmospheric circulation and the climate over Antarctica. However, recent studies (e.g., Clem *et al.*, 2016; Raphael *et al.*, 2016; Marshall & Thompson, 2016; Marshall *et al.*, 2022) provide important insight to improve our understanding of the patterns and processes involved.

1.2.3. Mass Balance

The mass balance (MB) represents the balance between the gain and loss of ice/snow. It is determined, by taking into consideration the processes of accumulation and ablation across the entire AIS, using the formula given below. Since the mass balance represents the balance between the gain and loss of ice/snow, its evolution indicates the contributing factor of the AIS to sea level rise. Ablation for the Antarctic glacier includes, on the one hand, ice discharge (D) and on the other hand, basal melting (M_{basal}). The third factor, surface mass balance includes

both ablation (except for basal melting and ice discharge) and accumulation processes and is described below.

$$MB = SMB - D - M_{basal},$$

Between 1992 and 2017, ice sheet mass balance has reduced by approximately 2720 ± 1390 billion tons of ice, which equals almost 8 mm of global sea-level rise (Fig. 1.7) (Shepherd *et al.*, 2018)
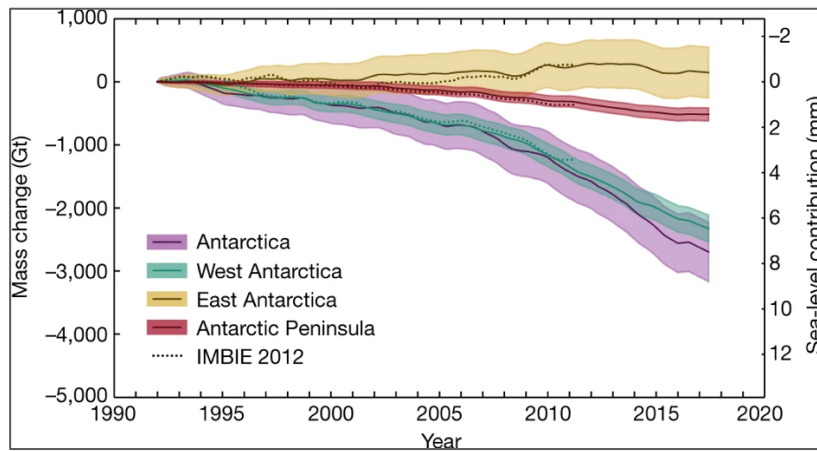
Figure 10.7: The cumulative mass change over the AIS with the estimated 1σ uncertainty in shaded colours (from Shepherd *et al.*, 2018)

1.2.4. Surface Mass Balance

The surface mass balance (SMB) is the net accumulation of snow/ice on the ice sheet surface. It is the sum of accumulation (snowfall (SF), rainfall (RF), surface deposition and condensation (DE)) and ablation (erosion (ER), surface sublimation (Fig. 1.8b) and evaporation (SU), and runoff (RU)).

$$SMB = SF + RF + DE - ER - SU - RU,$$

A good assessment of the evolution of the SMB over a longer period is dependent on good data coverage, both spatially and temporally. While field observation methods exist, they only capture the SMB at one point and are thus not representative of the entire AIS. Satellite radar observations provide a better spatial coverage, however, without knowing the density or composition retrieving SMB from satellite observations still bears many uncertainties. To make

up for this lack of data, dynamic modelling is a useful tool. Since General Climate Models (GCMs) often have difficulties in accurately representing dynamic processes, due to their coarse resolution, the use of polar-oriented regional climate models (RCMs) for evaluating SMB has become very prominent alternative to remote or *in situ* observations (Agosta *et al.,* 2019).
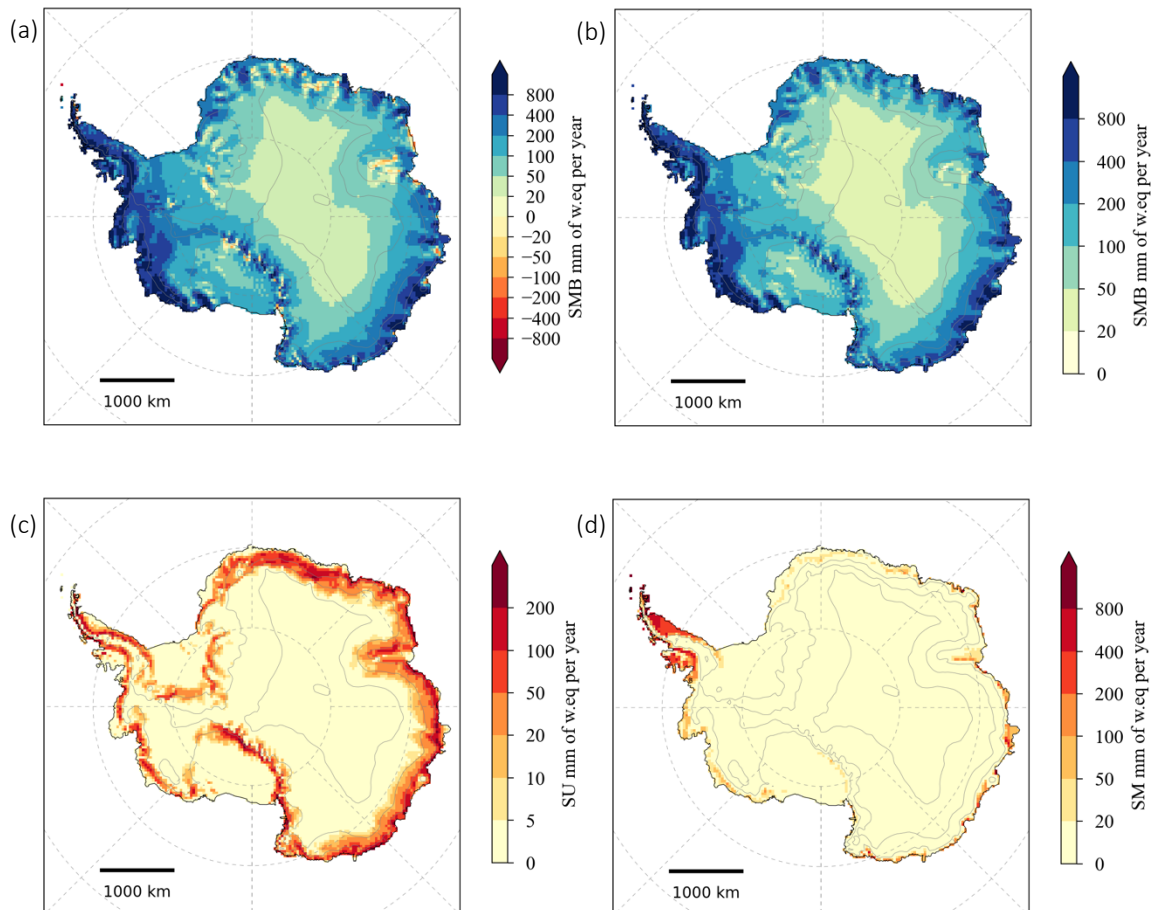
Figure 12.8: Annual sum of the surface mass balance **(a)**, precipitation **(b)**, sublimation **(c)** and surface melt **(d)** simulated by MAR over 1981–2010

Between 1987 and 2015, using model simulations, the surface mass balance of the AIS was found to be around 2300 Gt yr^{-1} (Agosta *et al*., 2019). SMB is generally the lowest inland, on the Antarctic Plateau, with values between 20 kg m-2 yr-1 and 100 kg m^{-2} yr^{-1}. Along the coast, SMB is significantly higher, resulting in a strong gradient. This is primarily a consequence of the spatial distribution of precipitation. In some areas, referred to as blue-ice areas, the surface mass balance is negative (Fig. 1.8a). The net mass loss of snow over these areas is generally due to the erosion of snow from wind and sublimation. Integrated over the entire ice sheet, there are no recent trends regarding precipitation. However, regionally, statistically significant trends with opposing signs have been found (Monaghan *et al.*, 2008).

1.2.5. Ice shelves and the surrounding ocean

The Ross and Ronne-Filchner ice shelves are the two largest Antarctic ice shelves with surface areas above 400 000 km^2. Larsen C is the largest ice shelf of the Antarctic Peninsula and one of the two remaining segments of the Larsen ice shelf, after the collapse of Larsen A and B in 1995 and 2002 respectively. Through their buttressing effect, ice shelves play a crucial role in governing the quantity of ice flowing into the ocean. The gradual disappearance of ice shelves and the subsequent reduction of their buttressing effect results in the acceleration of the flow of ice streams, which, on the one hand, contributes to sea-level rise but also promotes an increase of the width and thickness of the ice stream beds (Dupont & Alley, 2005).

The Antarctic Ice Sheet is surrounded by the Southern Ocean (SO), which in the west is separated into the Weddell, the Bellingshausen, the Amundsen, and the Ross Sea. Over recent decades, the SO has exhibited an insignificant increase in temperature, contrary to the rapidly warming Arctic Ocean (Amour *et al.*, 2016). Katabatic winds favour the formation of sea ice close to the margins of the AIS, which in turn promotes a decrease in costal near-surface temperatures as the air is cooled when moving over the ice. The extent of ice over the ocean is lower in austral summer and the highest during winter months, ranging from 3.1 10^6 km^2 in February to a surface as large as 18.5 10^6 km^2 in September 1979–2010 (Fig. 1.9; Parkinson and Cavalieri, 2012).
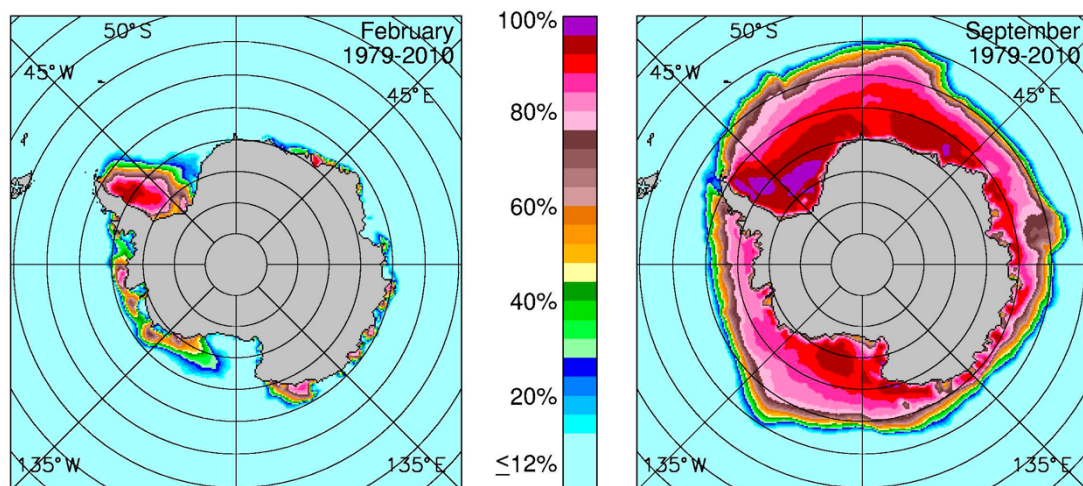
Figure 13.9: Mean sea-ice concentration around the AIS in February (left) and September (right) from satellite observations over 1979–2010 (from Parkinson & Cavalieri, 2012)

Although the interannual variability of sea-ice remains relatively insignificant, satellite data revels that the Amundsen and Bellingshausen Sea displayed a negative trend in sea ice cover (-8200 ± 1200 km^2 yr^{-1}) between 1978 and 2010, while the Ross Sea experienced an increase

(17 100 ± 2300 km^2 yr^{-1}) (Parkinson and Cavalieri, 2012). Overall, Antarcticc sea-ice extent has increased between 1979 and 2010, however, recent observations show that since 2016, sea-ice has been retreating (e.g., Meehl *et al.*, 2019). Interestingly, the expansion of Antarctic sea-ice has been attributed to the increased ice-shelf melt. Cool surface water created through basal ice-shelf melting (e.g., Rintoul *et al.*, 2016) acts a protective layer that shields sea-ice from the warmer deep water, thus favouring the expansion of sea ice (Bintanja *et al.*, 2013).

1.3. Thesis objective

The objective of this thesis is twofold. The first section of this study is dedicated to evaluating the outputs from forcing MAR$_{v3.12}$ with the ERA5 back extension. Forcing MAR $_{v3.12}$ with the new reanalysis data set produces a dataset over a longer time step than previously possible. Thus, the second part of this study is dedicated to examining the simulated climate over the AIS, in particular, during the 29-year period of the ERA5 back extension from 1950 to 1978. The variability of the climate is also assessed in conjunction with several atmospheric features (e.g., SAM, ENSO). Hence, the aim of this study is to provide, on the one hand, a look at future possibilities of extending the modelling period, using a longer reanalysis dataset and, on the other hand, an addition to the literature on the relationship of the Antarctic climate and the Atmospheric circulation in the SH.

1.4. Thesis Outline

This first chapter provided the basic characteristics of the Antarctic Ice Sheet, necessary for understanding the content of the following chapters. Chapter 2 provides a brief description of the methodology used, including the data used for evaluating the model output. In Chapter 3, the near-surface climate and surface mass balance simulated by MAR $_{v3.12}$ forced by ERA5 are evaluated. Finally, in Chapter 4 the results of the model simulation are presented in addition to an assessment of the relationship between the climate and large-scale atmospheric and oceanic circulation patterns between 1950 and 2020, followed by a general conclusion of the results of this study.

2. Methodology

2.1. The regional climate model MAR

The Antarctic Ice Sheet has been subject to numerous studies involving model simulations of the climate (e.g., Lenaerts *et al.*, 2019; Agosta *et al.*, 2019; Mottram *et al.*, 2020). The advantage of modelling as opposed to using observations for assessing past climates is the better spatial and temporal coverage. Nevertheless, model accuracy may vary a lot depending on the location and the low resolution used by GCMs and ESMs may cause difficulties in capturing small-scale local processes. Lenaerts *et al.* (2012) found that using a higher resolution, climate models can better represent local processes, such as katabatic winds and the related drifting snow erosion. This can be explained by the role topography, which is smoothed by low resolution modelling, plays regarding these processes, including orographic precipitation (Bromwich, 1998). Thus, a higher model resolution yields a higher local spatial variability of surface mass balance because local processes are resolved more accurately. Nevertheless, since SMB is mostly governed by precipitation, when integrated over the entire ice sheet, further increasing model resolution has little effect when already relatively high (~ 30 km). The climate data evaluated and examined in this study are simulated by the "Modèle Atmosphérique Régional" (hereafter MAR), which is a polar-oriented regional climate model used for studying both Antarctica (e.g., Kittel *et al.,* 2018; Agosta *et al.,* 2019) and the Greenland Ice Sheet (e.g., Fettweis *et al*., 2017) and is based on the hydrostatic approximation (Gallée & Schayes, 1994). The aim of this chapter is to provide a brief overview of characteristics of the model used in this study.

For the representation of the variability of both snow and ice layer properties, MAR uses the 1-D multi-layer surface module SISVAT (Soil Ice Snow Vegetation Atmosphere Transfer; De Ridder & Gallée, 1998). Ice and snow properties represented by the SISVAT scheme are based on the CORCUS model (Brun *et al*., 1992). Furthermore, the topography and fraction of ice and rock are inherited from the digital elevation model Bedmap2 (Fretwell *et al.,* 2013), which are available at a 1 km resolution. Finally, for modelling the large Antarctic continent, the general atmospheric circulation is constrained using an upper air boundary relaxation (van de Berg & Medley, 2016), which is applied to temperature and wind components.

For the simulations made for this study, MAR uses 24 vertical atmospheric levels with a horizontal resolution of 35 km. Moreover, although drifting-snow processes have been included in the previous model version (Amory *et al*., 2020), the module was not activated for this study. Improvements of the model version used in this study (MAR$_{v3.12}$) compared to the previous version (MAR$_{v3.11}$) used in recent studies (e.g., Kittel *et al*., 2021; Kittel *et al*., 2022) include the correction of a bug regarding the temperature of deep snowpack layers and a more efficient processing of the model calculations.

2.2.   Reanalyzes

Since MAR is a regional model, it only covers a certain region, in this case, the Antarctic continent. Thus, it must be forced at its boundaries, i.e. the model needs climatic input data based on which it can make its calculations. Meteorological records in polar regions, especially Antarctica are relatively rare, especially before satellite observations began in the late 1970s. This is mostly due to the remote location of the continent and its harsh weather conditions. Additionally, the use of satellites is complicated by the difficulty of separating cloud cover from snow cover and the polar night. The sparse network of data measurements over the AIS is not sufficient for forcing a regional climate model such as the MAR. In order to "fill the gaps" and create a continuous data record for Antarctica, global reanalyzes were constructed. Through the assimilation of observations into a general circulation model, a dataset of climatological variables with a uniform grid resolution is produced (Bromwich *et al.,* 2007).

The data provided to the model is part of the ERA5 reanalysis, the successor of the ERA-Interim reanalysis. It is the fifth-generation reanalysis produced by the European Centre for Medium-Range Weather Forecasts (ECMWF). At the time of writing, the ERA5 dataset covers the period of 1950 to 2020. Compared to the 0.75° horizontal resolution of the ERA-Interim reanalysis, ERA5 uses a horizontal resolution of about 0.3 °. Another improvement regarding the resolution is the increase in the number of vertical levels from 60 to 137. Moreover, the ERA5 dataset is produced using a 4D-Var assimilation scheme, with a spin-up period of 1 year (which may differ in practice due to some anomalies, which require different spin-up durations) (Hersbach *et al.,* 2020). The model is forced at an interval of 6 hours and uses sea-surface temperature (SST), sea-ice concentration (SIC), surface pressure, air temperature, humidity, and wind from the ERA5 dataset.

A back extension of the dataset, extending the start of the covered period from 1979 to 1950 has been made public very recently and is still under review. This back extension was produced using of both conventional observations and early satellite records. Both the quantity and quality of observations fed into the ERA5 assimilation system steadily increase from 1950 to 1978, hence resulting in a gradual improvement in the quality of the dataset. For instance, in January 1950, only around 53,000 observations (conventional only) were used by the 4D-Var assimilation scheme, whereas in December 1978, a total of approximately 570,000 observations, originating from conventional sources but also from satellites and ozone observations. To a large degree, the conventional observations assimilated for the ERA5[79→] dataset are those that had originally been assembled for ERA-40. Additional data from the ECMWF archive, as well as the International Surface Pressure Databank (ISPD) and the International Comprehensive Ocean Atmosphere Data Set (ICOADS) were added in order to cover the entire 1950–1978 period. Figure A.2 illustrates the gradual increase in available data. Satellite observations began in November 1972 with the use of vertical temperature profiling radiometers (VTPR), which were carried on board of NOAA platforms. Ozone measurements began no earlier than 1970, with the launch of the Nimbus-4 satellite carrying a backscatter ultraviolet spectrometer. Generally, ERA5 is in accordance with other climatological records and reproduces surface temperature anomalies quite well, with some regional differences. The reliability of the dataset was in part validated by properly reproducing the North Sea storm of 1953 and the warming of the stratosphere in the early 50s (Bell *et al*., 2021).

2.3. Observational Data

2.3.1. Near-surface climate observation database

To validate the model performance, the results are compared with long climatological records from *in situ* observations. These observations are very rare across the continent. Although an effort has been made to install automatic weather stations (AWS) post 1979, they are often subject to a lack of data continuity, rendering them less than optimal for evaluating the long-term model performance (Turner *et al*., 2020). The better alternative to the data from AWS are the long quality-controlled climate records from staffed weather stations that often cover many years prior to 1979. However, their primary shortcoming is the spatial disparity; most staffed stations are located along the coast, Amundsen Scott and Vostok being the only stations on the Antarctic Plateau with significantly long records.

The near-surface observation data used for evaluating $MAR_{v3.12}$ forced by ERA5 are part of several collections of climate records from (automatic) weather stations (AWS) and has been used in previous model evaluations (e.g., Mottram *et al.*, 2020). These climate records are assembled from sources including the Alfred-Wegner-Institut (AWI), the Antarctic Meteorological Research Center (AMRC), the Australian Antarctic Division Glaciology Program (AAD). Moreover, some of the data used in this evaluation is part of the READER database compiled by Turner, 2004. The AWS data was quality (re-)controlled to remove suspicious discontinuities abnormal values (e.g., wind-speed values of 0 ms^{-1} throughout an entire day), thus rendering the database reliable for the following model evaluation. Although an effort has been made to limit measurement biases, the AWS database may still contain erroneous values, for instance caused by empty batteries or equipment being trapped under the snow. A grid size of 35 km was used for the simulation run by MAR, meaning, one pixel contains the mean value of an area of around 35 km^2. Automatic weather stations, on the other hand, measure at a point scale. Thus, there is an inherent bias, when comparing the simulated value of a pixel to the observed value of an AWS**.** Moreover, modelled values are interpolated to the AWS location using a four-nearest inverse-distance-weighted method. Finally, in order to have enough points of comparison for the 1950–1978 period, a maximum difference of 250 m between the height of the measuring station and the mean height of the pixel was considered. Thus, a further bias is created due to this height difference. After removing dubious data and stations with a height difference above 250 m, 16 comparison pairs remain for 1950–1978 and 170 pairs for 1979–2020.

2.3.2. Surface mass balance observation database

Modelled surface mass balance was evaluated using the GLACIO-CLIM SAMBA database at the highest confidence level (Favier *et al.* 2013). The database does not include radar measurements and primarily contains data from stake networks. Moreover, only observations that are included in a pixel corresponding to the ice sheet were used for the evaluation. As for the AWS data used for evaluating the near-surface climate, a four-nearest inverse-distance-weighted method allowed an interpolation of the simulated SMB values to the location of the observed values. Finally, whenever several observations from more than one location are included within the same grid cell, their common average is used, resulting in 278 remaining comparison pairs for 1950–1978 and 358 pairs for 1979–2020.

3. Model Evaluation

3.1. Near-surface climate

The issue with reanalyzes is that they often produce their own climate change due to changes in the quality and quantity of assimilated data. A good example of this is the introduction of satellite sounder data from the Television InfraRed Observation Satellite in 1979. Thus, this chapter is dedicated to examining the performance of $MAR_{v3.12}$ forced by the ECMWF reanalysis (ERA5), including its back extension. The results from both periods, 1950–1978 and 1979–2020 are separately compared to a climatological record produced by a network of weather stations as explained in Chapter 2.

As a result of the limited availability of data records prior to the 1970s, there is a significant difference regarding the number of stations for evaluating the two periods. It is also worth noting that for the 1950–1978 the evaluation considers mostly the period of 1957–1978 because most Antarctic weather stations started their measuring campaign in the International Geographical Year in 1957 (Turner *et al*., 2004). Despite this shortcoming, a proper assessment could be made. Finally, only near-surface pressure, temperature, and wind speed, as well as surface mass balance are evaluated. Relative humidity and surface fluxes were not recorded by climate stations prior to the late 1970s.

The austral seasons discussed in this, and the succeeding chapter are described as follows: spring as September-October-November, summer as December-January-February, autumn as March-April-May and winter as June-July-August. It is also worth noting that, since summer months fall into two separate years, summer corresponds to the year that contains the December month.

3.1.1. Near-surface pressure

Near-surface pressure serves as a great indicator of model performance. Comparing model outputs to several local measurements allows us to assess the accuracy of the model across the Antarctic Ice Sheet. From an annual perspective, modelled surface pressure for ERA5$^{\rightarrow 79}$ performs decently, with a correlation of 0.88. While this is lower than the value found for ERA5$^{79\rightarrow}$ (0.96), it indicates that MAR appears to properly reproduce near-surface pressure.

Annually, the mean bias for ERA5$^{\rightarrow 79}$ (-17.15 hPa) appears to be significantly higher than for ERA5$^{79\rightarrow}$ (-6.52 hPa) by about a factor of three. However, relative to the high absolute values of near-surface pressures, this bias remains less significant. Moreover, since the mean surface height of the MAR pixel may differ from the station height by up to 250 m, an inherent mean bias is to be expected. This also becomes clear when comparing the root-mean-square error (RMSE) to the centred root-mean-square error (CRMSE). When corrected for systematic errors (e.g., altitude differences), the RMSE drops by a factor of around 4. Thus, MAR may even be able to represent near-surface pressure better than may be exhibited by the statistics. A denser observation dataset with more measuring points per MAR pixel would be required in order to make a more accurate evaluation. Alternatively, a higher model resolution should be able to better represent the near-surface pressure of a given station, especially in areas of fluctuating surface height. The RMSE being lower than the standard deviation of the observation dataset is also a good sign. Moreover, surprisingly in summer (0.93), the model functions significantly better than in winter (0.85). This could be the result of a lack of sufficient data fed to the model during winter by the ERA5 reanalysis.

Table 3.1: Statistics for near-surface pressure (hPa) (mean, standard deviation, bias, RMSE, CRMSE, correlation) describing model performance over 1950–1978 and 1979–2020, annually and for summer and winter

	Annual				Summer				Winter			
	Mean Bias (hPa)	RMSE	CRMSE	Correlation	Mean Bias (hPa)	RMSE	CRMSE	Correlation	Mean Bias (hPa)	RMSE	CRMSE	Correlation
1950 - 1978	-17.15	20.01	4.82	0.88	-18.39	20.05	2.91	0.93	-16.61	20.27	5.99	0.85
Mean obs	926.14				929.33				927.16			
Standard obs	10.34				7.73				11.64			
1979 - 2020	-6.52	12.62	2.68	0.96	-7.85	12.68	2.18	0.96	-5.8	12.42	2.32	0.98
Mean obs	883.71				885.55				883.67			
Standard obs	10.07				7,68				11.31			

Within the 1950–1978 period, there are also slight differences in near-surface pressure performance. Correlation drops from 0.87 to 0.85 between 1950 and 1960 and 1960–1970 and increases again to 0.91 for 1970–1978. Parallelly, the mean bias increases first and finally slightly decreases again. The initial decrease in correlation is reflected in several stations (e.g., McMurdo, Vostok, Belgrano I, Wilkes). This is most likely due to the model having more difficulties reproducing near-surface pressure in that period and can probably not be attributed to the stations themselves unless instruments were exchanged. The apparent increase in model performance is partly due to a station with poor correlation (Wilkes) ending its measurements in 1969 and the fact that new measurements with above average correlation were introduced into the evaluation (e.g., Rothera, Marambio). However, the model output is probably also more accurate, since observations used by the ERA5 reanalysis gradually increase as we approach 1978. This assumption is supported by the fact that some stations see a significant

jump in correlation (e.g., Halley, Dumon d'Urville, Esperanza). Additionally, for 1970 – 1978, the seasonal discrepancy is less marked, which supports the assumption made.

The performance of the model can also be assessed spatially. Comparing the model output to stations at different locations across the continent uncovers a spatial pattern. For this, looking at the correlation or mean bias can be misleading because the non-spatially constant height difference is not accounted for. Thus, we use the CRMSE to portray this spatial pattern. Lower (higher) CRMSE values indicate better (worse) model performance. The model appears to perform surprisingly well across the Antarctic Peninsula (e.g., Rothera, Marambio). This is unexpected because MAR should have difficulties representing near-surface pressure considering the steep terrain of the Antarctic Peninsula. However, hidden behind these low CRMSE values is the fact that measurements for these two stations began in 1976 and 1971 respectively. Thus, it is normal to find better values at these sites. Other stations at the Antarctic Peninsula with a higher temporal coverage (e.g., Esperanza, Deception, Adelaide) display lower CRMSE values. MAR appears to perform best on the Antarctic Plateau, as shown by low CRMSE values for Vostok and Amundsen Scott. This is probably a result of the area being flatter, thus easier for the model to represent accurately. The highest values are observed in coastal areas in East Antarctica (e.g., McMurdo, Dumont d'Urville, Casey). The poor values for McMurdo could be explained by its unique location. The station is located at the edge of the Ross Ice Shelf, right at the foot of the Transantarctic Mountain range.

Table 3.2: Same as Table 3.1 but for each station

	Temporel coverage	Mean Bias	RMSE	CRMSE	Correlation	Std obs	Std mod
Adelaide	1962 - 1976	-31.36	31.8	5.27	0.91	12.53	11.1
	/	/	/	/	/	/	/
Amundsen Scott	1957 - 1978	4.41	5.88	3.89	0.91	9.2	8.61
	1978 - 2018	4.64	5.15	2.23	0.97	9.07	8.79
Belgrano I	1957 - 1978	-5.15	7.25	5.1	0.86	9.8	9.11
	1979	-7.81	8.27	2.72	0.95	8.38	8
Casey (old)	1969 - 1978	-40.68	41.02	5.28	0.87	10.63	9.19
	1979 - 1990	-41.14	41.23	2.75	0.97	10.58	9.76
Deception	1959 - 1967	-15.94	16.53	4.36	0.93	12.22	11.3
	/	/	/	/	/	/	/
Dumont_Durville	1956 - 1978	-45.55	45.94	5.94	0.83	10.63	9.39
	1979 - 2017	-46.04	46.11	2.55	0.97	10.45	9.91
Esperanza	1957 - 1978	-24.81	25.24	4.67	0.92	11.71	10.99
	1979 - 2016	-24.79	25.01	3.31	0.96	11.84	11.4
Halley	1957 - 1978	-3.16	5.86	4.93	0.86	9.74	8.86
	1979 - 2018	-3.96	4.53	2.2	0.97	9.53	9.11
Leningradskaja	1971 - 1978	-13.79	14.51	4.51	0.89	9.86	9.13
	1979 - 1991	-13.1	13.37	2.67	0.97	10.19	9.76
Marambio	1971 - 1978	8.86	9.58	3.66	0.95	11.55	11.32
	1979 - 2016	7.44	7.87	2.56	0.98	11.57	11.44
McMudro	1956 - 1978	-5.04	7.77	5.92	0.83	10.35	9.65
	1979 - 2015	-3.58	5.13	3.67	0.94	10.29	10.02
Molodeznaja	1963 - 1978	-22.58	23.03	4.52	0.87	9.29	8.2
	1979 - 1999	-23.31	23.43	2.33	0.97	9.31	8.72
Novolazarevskaya	1961 - 1978	-35.33	35.57	4.1	0.9	9.32	8.3
	1979 - 2009	-32.28	32.35	2.25	0.97	9.25	8.63
Rothera	1976 - 1978	-44.6	44.77	3.95	0.96	14.24	12.77
	1979 - 2018	-45.61	45.66	2.22	0.99	13.02	11.98
Vostok	1958 - 1978	1.3	3.41	3.15	0.95	9.73	9.1
	1979 - 2017	1.84	3.14	2.55	0.96	9.57	9.47
Wilkes	1959 - 1969	-40.62	41.22	6.99	0.75	10.33	9.16
	/	/	/	/	/	/	/

3.1.2. Near-surface temperature

Unsurprisingly, modelled near-surface temperature correlates more poorly with observations than near-surface pressure. Temperature is affected by a large array of phenomena (e.g., precipitation, wind, topography, snow thickness and properties), thus it is more complex, rendering it difficult for models to properly represent. Moreover, these variables often fluctuate at a much higher resolution than the coarse 35 km resolution used by the model. Averaged over the entire 1950–1978 period, we find a correlation and mean bias of 0.86 °C and -1.04 °C respectively, compared to 0.94 °C and 0.70 °C for 1979–2020. Using ERA5[→79], MAR appears to slightly underestimate near-surface temperatures, compared to ERA5[79→,] where we find a slightly positive mean bias. Moreover, as for near-surface pressure, there is a large, but gradually weakening summer-winter discrepancy. The underestimation of near-surface temperature is less marked in winter (-0.71 °C) than in summer (-1.38 °C), while the CREMSE is significantly lower in summer (2.25 °C) than in winter (5.78 °C), when the root mean

squared error is also equal to around 95% of the observed variability. Prior to 1979, we find a similar seasonal contrast for correlation, with values of 0.77 and 0.60 respectively for summer and winter. Significant seasonal differences in performance are identified at Vostok and Amundsen Scott station, with substantially higher (lower) correlation (CRMSE) in summer (0.91/3.05 °C and 0.93/2.45 °C) than in winter (0.58/6.33 °C and 0.59/6.25 °C) (table appendix). As for near-surface pressure, this could be attributed to the ERA5 data deficiency in winter. Since both stations are located on the Antarctic Plateau, poor model performance is unlikely linked to orography. Another suggestion could be the model's inability to properly represent some local processes like surface temperature inversions, which are observed with lower frequency and magnitude in summer (Hudson and Brandt, 2005). Surprisingly, in the 1979–2020 period, the model is more yields a higher correlation in winter (0.86) than in summer (0.84), although the opposite is found for CRMSE values (3.59 °C and 2.31 °C).

Table 3.3: Same as Table 3.1 but for near-surface temperature (°C)

	Annual				Summer				Winter			
	Mean Bias (°C)	RMSE	CRMSE	Correlation	Mean Bias (°C)	RMSE	CRMSE	Correlation	Mean Bias (°C)	RMSE	CRMSE	Correlation
1950 - 1978	-1.04	5.28	4.52	0.86	-1.38	3.26	2.25	0.77	-0.71	6.42	5.78	0.60
Mean obs		-19.09				-8.32				-26.60		
Standard obs		9.33				3.74				6.81		
1979 - 2020	0.70	4.23	3.34	0.94	-0.07	2.95	2.31	0.84	1.31	4.82	3.69	0.86
Mean obs		-23.32				-12.05				-31.21		
Standard obs		9.77				4.40				7.04		

Furthermore, the succession of decrease and increase (increase-decrease) for 1950–1960 to 1960-70 to 1970–1978, although less pronounced, is still present for near-surface temperature. For 1970–1978, we find a lower CRMSE (4.23 °C), and higher correlation (0.88) compared to the 1950–1960 period (4.66 °C and 0.87). Spatial disparities regarding the mean bias can mostly be observed between inland and coastal regions, the latter generally displaying a negative bias and the former displaying a positive bias. There is no apparent spatial pattern regarding the evolution in time of the mean bias. For Halley and Dumont Durville Station the gap between observed and modelled values seem to tighten, whereas, for Vostock and Amundsen Scott Station, the gap appears to widen. However, due to the difference in altitude between each station and its corresponding MAR pixel, it is unclear, whether this change in bias refers to a better or worse performance of the model. Nevertheless, MAR is generally able to replicate the variability of the near-surface temperature on an annual scale. In some locations (e.g., Amundsen Scott, Dumont Durville) the variability displayed by the model is more pronounced than the actual measured variability. MAR also seems to reproduce most significant changes in yearly near-surface temperatures. Nonetheless, ERA5[79→] yields a more accurate representation of the near-surface temperature fluctuations than ERA5[→79].
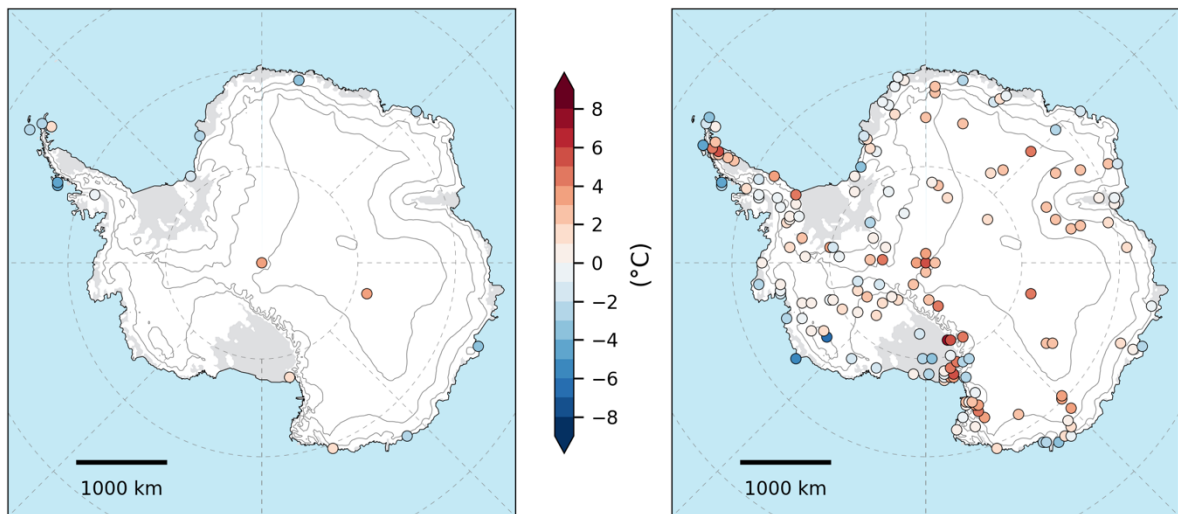
Figure 3.1: Mean annual near-surface temperature (°C) biases for MAR$_{v3.12}$ forced by ERA5 over 1950–1978 (left) and 1979–2020 (right)
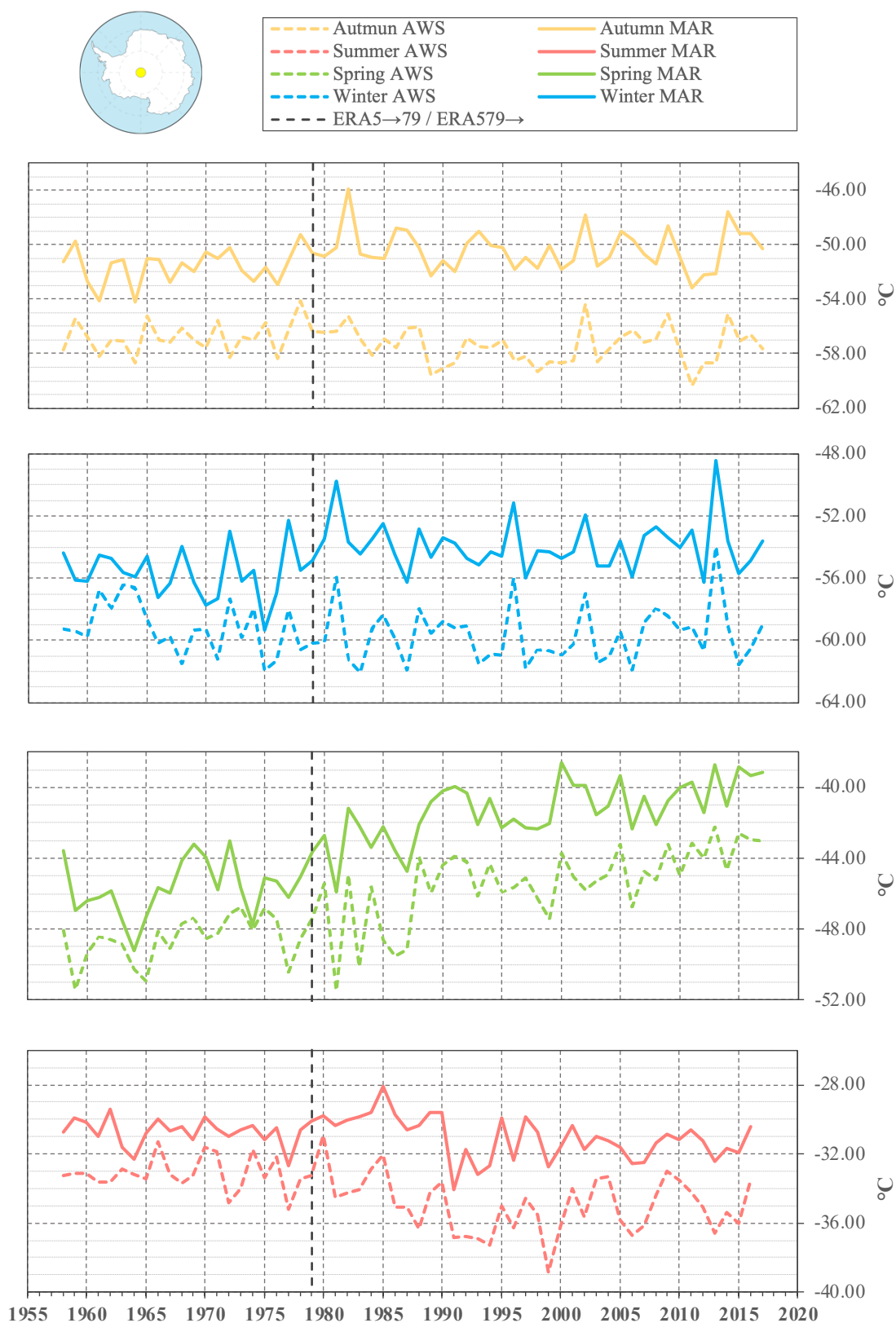
Figure 3.2: Time series of the observed (dashed line) and simulated (MAR$_{v3.12}$ forced by ERA5) (straight line) mean annual near-surface temperature (°C) for all four austral seasons at Amundsen Scott
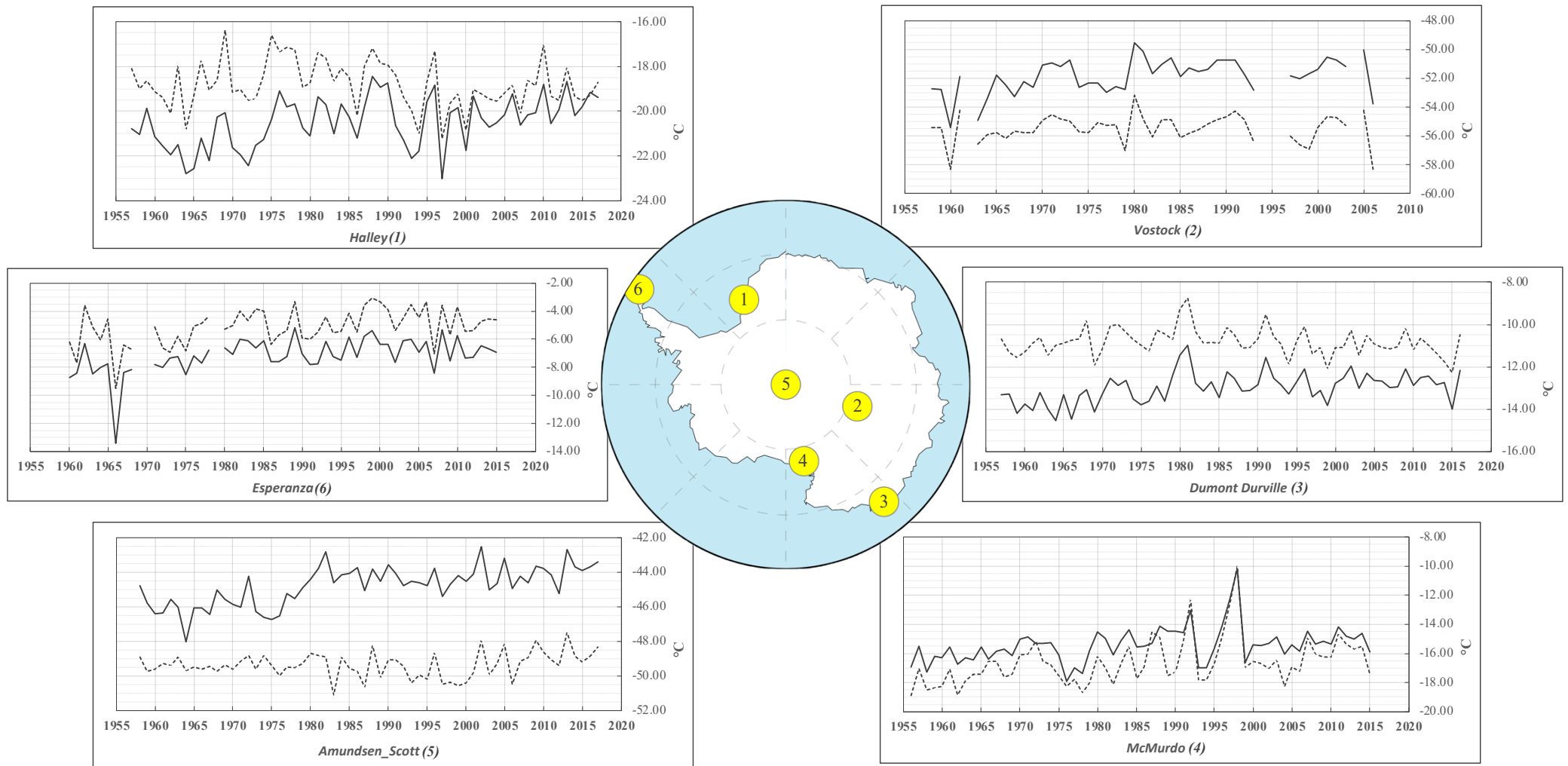
Figure 3.3: Time series of the observed (dashed line) and simulated (MAR$_{v3.12}$ forced by ERA5) (straight line) mean annual near-surface temperature (°C) at six station locations

Looking at Amundsen Scott Station, there are slight seasonal differences. For both autumn (MMA) and spring (SON), MAR produces a good representation of the climate variability for 1957–1978. While this is still the case for summer and winter, in 1968 the model displays a peak at opposite sign compared to the observations. This agrees with the reduction in model accuracy, previously observed for the 1960–1970 period.

Table 3.4: Same as Table 3.2 but for near-surface temperature (°C)

	Temporel coverage	Mean bias	RMSE	CRMSE	Correlation	Std obs	Std mod
Adelaide	1962 - 1976	-4.05	6.11	4.57	0.75	6.45	6.36
	/	/	/	/	/	/	/
Amundsen Scott	1957 - 1978	3.41	6.27	5.26	0.92	13.28	12.36
	1978 - 2018	5.18	6.37	3.72	0.96	13.61	12.25
Belgrano I	1957 - 1978	-1.69	7.01	6.8	0.85	12.89	12.14
	1979	0.44	4.87	4.85	0.93	13.29	11.33
Casey (old)	1969 - 1978	-3.4	4.95	3.6	0.88	7.39	7.01
	1979 - 1990	-3.34	4.07	2.33	0.95	7.21	7.04
Deception	1959 - 1967	-2.62	4.22	3.31	0.76	4.78	4.77
	/	/	/	/	/	/	/
Dumont_Durville	1956 - 1978	-2.71	4.23	3.25	0.89	7.09	6.95
	1979 - 2017	-1.86	2.64	1.88	0.96	7.08	6.65
Esperanza	1957 - 1978	-2.12	5.02	4.55	0.78	7.14	6.48
	1979 - 2016	-1.99	3.77	3.2	0.89	6.9	6.06
Fossil Bluff	1961 - 1978	-0.08	5.43	5.43	0.77	8.55	6.85
	1979 - 2005	-0.26	2.85	2.84	0.93	7.63	6.62
Halley	1957 - 1978	-2.57	6.39	5.85	0.85	10.53	11.03
	1979 - 2018	-1.21	3.82	3.62	0.94	10.74	10.73
Leningradskaja	1971 - 1978	1.03	3.77	3.63	0.88	7.62	7.16
	1979 - 1991	1.67	3.09	2.6	0.94	7.47	6.89
Marambio	1971 - 1978	1.02	4.94	4.84	0.81	8.3	7.21
	1979 - 2016	0.5	3.9	3.87	0.88	8.23	7.27
McMudro	1956 - 1978	1.29	4.5	4.31	0.9	9.89	8.45
	1979 - 2015	1.18	3.65	3.45	0.94	9.7	8.24
Molodeznaja	1963 - 1978	-2.27	4.12	3.44	0.9	7.67	7.3
	1979 - 1999	-1.8	2.68	1.99	0.96	7.56	7.19
Novolazarevskaya	1961 - 1978	-3.06	4.37	3.12	0.91	7.53	6.74
	1979 - 2009	-2.73	3.31	1.88	0.97	7.23	6.39
Rothera	1976 - 1978	-4.19	5.99	4.28	0.84	7.49	7.58
	1979 - 2018	-4.56	5.18	2.46	0.92	6.02	6.41
Vostok	1958 - 1978	3.06	5.8	4.93	0.94	14.3	13.08
	1979 - 2017	4.11	5.48	3.63	0.97	14.69	13.05
Wilkes	1959 - 1969	-3.75	5.62	4.18	0.84	7.51	7.09
	/	/	/	/	/	/	/

3.1.3. Near-surface wind speed

Compared to both near-surface pressure and temperature, wind speed is represented more poorly by the model with a correlation and CRMSE of 0.5 and 4.34 ms^{-1} respectively. As for the other two variables, the model performs more accurately in summer (r = 0.5) than in winter (r = 0.4). This seasonal contrast is less pronounced for ERA5[79→], with correlations of 0.68 and 0.7 respectively. The model slightly underestimates mean near-surface wind speed, especially in coastal regions and on the Antarctic Peninsula. Good representations of the wind are observed on the Antarctic Plateau, probably as a result of the flat topography (e.g., Vostok and Amundsen Scott). Since wind speed can fluctuate at a very small scale, this poor performance is not astonishing, especially in areas with steep terrain. With a resolution of 35 km, the model has difficulties capturing the small-scale changes in wind speed, which explains the large disparities compared to the measurements. Moreover, the quality of early wind measurements is also questionable, thus introducing another uncertainty.
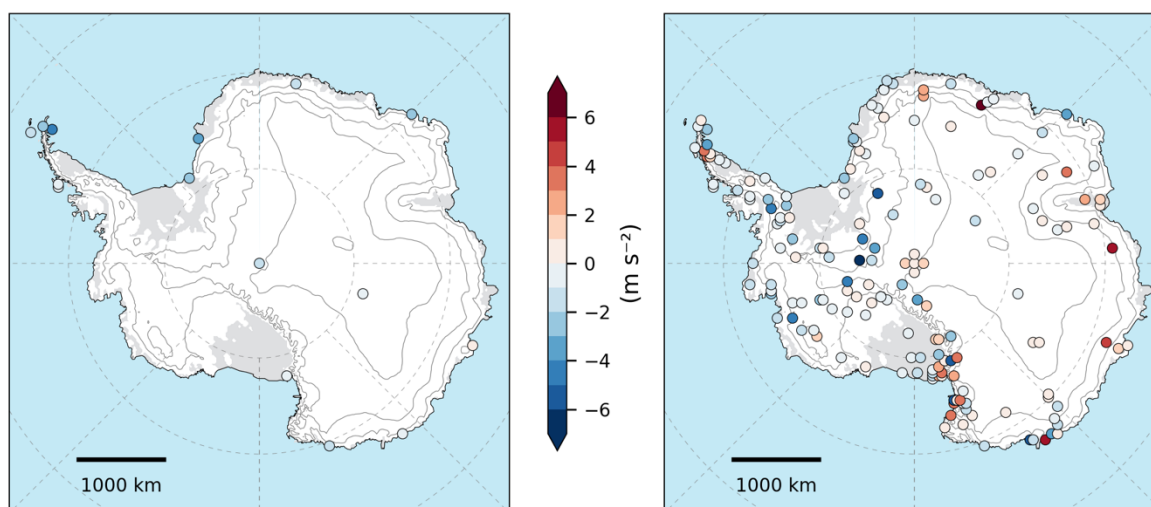
Figure 3.4: Same as figure 3.1 but for near-surface wind speed (ms^{-1})

Table 3.5: Same as Table 3.1 but for near-surface wind speed (ms^{-1})

	Annual				Summer				Winter			
	Mean Bias (m s^{-1})	RMSE	CRMSE	Correlation	Mean Bias (m s^{-1})	RMSE	CRMSE	Correlation	Mean Bias (m s^{-1})	RMSE	CRMSE	Correlation
1950 - 1978	-1.47	4.73	4.34	0.46	-1.61	3.74	3.24	0.50	-1.14	5.31	4.91	0.40
Mean obs		7.41				5.94				8.05		
Standard obs		4.82				3.74				5.28		
1979 - 2020	-0.22	3.05	2.63	0.69	-0.73	2.52	2.11	0.68	0.29	3.4	2.83	0.7
Mean obs		6.49				5.43				7.09		
Standard obs		3.59				2.87				3.90		

Table 3.6: Same as Table 3.2 but for near-surface wind speed (ms^{-1})

	Temporel coverage	Mean bias	RMSE	CRMSE	Correlation	Std obs	Std mod
Adelaide	1962 - 1976	-0.77	4.93	4.87	0.36	5.01	3.13
	/	/	/	/	/	/	/
Amundsen Scott	1957 - 1978	-1.31	2.41	2.03	0.54	2.32	1.78
	1978 - 2018	-0.33	1.57	1.54	0.7	2.1	1.85
Belgrano I	1957 - 1978	-2.29	5.61	5.13	0.41	5.62	2.06
	1979	-2.75	5.61	4.89	0.63	6	2.25
Casey (old)	1969 - 1978	0.71	5.26	5.21	0.55	6.21	3.8
	1979 - 1990	1.12	4.14	3.99	0.73	5.83	3.99
Deception	1959 - 1967	-1.31	3.95	3.73	0.33	3.76	2.39
	/	/	/	/	/	/	/
Dumont_Durville	1956 - 1978	-0.44	6.04	6.03	0.4	6.53	3.4
	1979 - 2017	0.88	4.47	4.38	0.6	5.5	3.55
Esperanza	1957 - 1978	-2.03	7.85	7.59	0.41	8.26	2.56
	1979 - 2016	-0.65	4.5	4.45	0.62	5.58	2.69
Halley	1957 - 1978	-3.24	4.67	3.36	0.6	4.18	2.54
	1979 - 2018	-2.43	3.27	2.18	0.86	4.02	2.75
Leningradskaja	1971 - 1978	-1.79	5.71	5.42	0.35	5.75	2.63
	1979 - 1991	-1.63	4.88	4.61	0.51	5.37	2.78
Marambio	1971 - 1978	-4.71	7.33	5.62	0.43	6.2	2.25
	1979 - 2016	-2.92	5.06	4.13	0.66	5.31	2.44
McMudro	1956 - 1978	-0.69	3.59	3.52	0.3	3.26	2.61
	1979 - 2015	0.16	2.88	2.87	0.42	2.72	2.62
Molodeznaja	1963 - 1978	-2.94	5.17	4.26	0.65	5.49	2.73
	1979 - 1999	-3.14	4.75	3.56	0.82	5.5	2.85
Novolazarevskaya	1961 - 1978	-1.48	4.59	4.35	0.66	5.74	3.24
	1979 - 2009	-1.63	3.99	3.65	0.8	5.69	3.32
Rothera	1976 - 1978	-0.73	3.67	3.59	0.6	4.51	2.83
	1979 - 2018	-0.12	2.89	2.89	0.69	3.89	3.24
Vostok	1958 - 1978	-0.74	1.88	1.73	0.45	1.8	1.44
	1979 - 2017	-0.62	1.43	1.29	0.67	1.65	1.52
Wilkes	1959 - 1969	0.94	5.32	5.24	0.35	5.28	3.58
	/	/	/	/	/	/	/

3.2. Surface Mass Balance

MAR SMB during the period excluding the recently released ERA5 back extension has been evaluated in the past (Agosta *et al*., 2019, Mottram *et al*., 2020) with the conclusion that MAR performs well. Agosta *et al*. (2019) found that when performing a simulation using MAR$_{v3.6.4}$ forced by ERA5-Interim over the 1979–2015 period, no systematic spatial bias stands out. Moreover, they found a mean bias of around 6 kg m^{-2} yr^{-1}, in addition to a correlation coefficient of 0.83, significant at the 1% level. Using MAR$_{v3.11}$ forced by ERA5, Kittel (2021) found a mean bias of only -1 kg m^{-2} yr^{-1} and as for MAR$_{v3.6.4}$ forced by ERA-Interim, no systematic spatial biases were detected. Using different elevation classes, Kittel (2021) found that for all levels, MAR has a tendency to underestimate high SMB values, whereas low values are generally overestimated. He found high biases, indicating weaker model performance for the 1200 masl – 2200 masl range (14 kg m^{-2} yr^{-1}) and for the 2800 masl and 3400 masl range (23 kg m^{-2} yr^{-1}, r = 0.57 and rlog = 0.55).

As for near-surface pressure, temperature, and wind speed, surface mass balance is evaluated in two different periods, (1) 1950–1978 and (2) 1979–2020. Contrary to the previously assessed variables, the number and location of observations used for the evaluation are to a certain degree different between both periods. Thus, the statistics for the two periods must be analysed separately and are not directly comparable. Since the distribution of SMB values is log-normal, their logarithmic values as well as the correlation coefficient of the latter are plotted below. The other statistical indicators, given in table 3.7, are based on the original values. Using ERA$^{\rightarrow 79}$, MAR$_{v3.12}$ produces SMB values with a mean bias of -8.5 kg m^{-2} yr^{-1} and a correlation of 0.85 with observed values. Between 1950 and 1978, MAR forced by ERA5 tends to underestimate high and overestimate low values. As done by Kittel (2020), SMB values are evaluated in elevation classes in order to make better conclusions regarding the mean bias (Fig. 3.5a-f). Across the ice shelves, the mean bias is relatively low (-4 kg m^{-2} yr^{-1}) with high correlations ($rlog$ = 0.85, r = 0.81). For levels between 0 and 2800 masl, the model yields slightly worse results, especially for the 2200 – 2800 masl range (-37 kg m^{-2} yr^{-1}, $rlog$ = 0.77, r = 0.80), where the RMSE is equal to around 78% of the observed variability.

Table 3.7: Same as Table 3.1 but for surface mass balance (Gt/year) and different elevation classes

	Mean				Bias		RMSE		Corr		SD obs	
	Obs	Mar	Obs	Mar								
	1950-1978		1979-2020		1950-1978	1979-2020	1950-1978	1979-2020	1950-1978	1979-2020	1950-1978	1979-2020
Shelf	0.158	0.154	0.359	0.181	-0.004	-0.178	0.062	0.191	0.806	0.502	0.105	0.083
0-1200 m	0.279	0.254	0.354	0.211	-0.025	-0.144	0.155	0.221	0.827	0.091	0.275	0.160
1200-2200 m	0.228	0.243	0.239	0.191	0.015	-0.049	0.110	0.088	0.799	0.759	0.160	0.112
2200-2800 m	0.118	0.080	0.090	0.069	-0.037	-0.021	0.061	0.042	0.532	0.559	0.078	0.044
2800-3400 m	0.052	0.045	0.066	0.051	-0.008	-0.015	0.015	0.028	0.900	0.092	0.028	0.024
3400m-top	0.033	0.029	0.039	0.034	-0.005	-0.004	0.008	0.010	0.734	0.720	0.010	0.012

In the 1979–2020 period, the model when forced by ERA5 produces SMB values with a mean bias of -37.8 kg m^{-2} yr^{-1} and a correlation coefficient of 0.85. The mean bias is also quite significant for the ice shelves (-178 kg m^{-2} yr^{-1}), however, for the period in question only 9 ice shelf observations are used for the evaluation, compared to 84 observations used for the years between 1950 and 1978. Similarly, for the 0 – 1200 masl range, there are large discrepancies between the modelled and observed SMB for 1979–2020, the RMSE (221 kg m^{-2} yr^{-1}) being higher than the variability of the observed SMB (160 kg m^{-2} yr^{-1}). For 1200 – 2200 masl, 2200 – 2800 masl and 3400 masl and above the mean biases are lower (-49, -21 and -4 kg m^{-2} yr^{-1}) and relatively good correlations ($rlog$ = 0.80, 0.49 and 0.75), although as for 1950–1979, MAR tends to underestimate high SMB values. Between 2800 masl and 3400 masl, the model exhibits a low mean bias (-15 kg m^{-2} yr^{-1}), it does, however, correspond to almost 30% of the

observed SMB for that elevation range. Moreover, for that elevation class, there is no correlation between observed and modelled SMB (*rlog* = 0.11 and r = 0.09).

The surface mass balance biases highlighted in this chapter could be the result of MAR not including drifting snow processes, especially for the 1200 masl – 2200 masl range, where surface erosion and atmospheric sublimation are more frequent (e.g., Lenaerts & van den Broeke, 2012). However, the primary component driving the SMB variability is precipitation, which is significantly larger (more than 10 times) than the other components that govern surface mass balance (e.g., runoff, sublimation). Moreover, despite RACMO2 integrating drifting snow processes, Agosta *et al.* (2019) found that both models are in good agreement. They did, however, find that RACMO2, which includes the sublimation of drifting snow, produces sublimation values that are larger by about 50 % than in MAR, which only considers the sublimation at the surface. Kittel (2020) also highlighted the fact that using a resolution of 50 km versus the 35 km resolution used by MAR$_{v3.11}$, biases for modelled surface mass balance increase over the ice shelves. This could be attributed to the coarser resolution having difficulties in accurately capturing processes such as local katabatic winds and precipitation. Finally, the fact that the older period from 1950 to 1978 yields better results than the recent 1979–2020 period is not necessarily evidence for the reanalysis being more reliable in the former period. The second period is a lot longer and observations that were used for the evaluating the years prior to 1979 do not always extend over the entire period, thus not capturing the entire bias. Moreover, stake measurements which were used for the comparison can be subject to small-scale accumulations (e.g., sastrugi) as a result of the local wind patterns, a process that regional climate models cannot reproduce with a resolution of several kilometres. Nevertheless, the evaluation shows that overall, MAR forced by ERA5 is able to properly reproduce surface mass balance across the Antarctic continent.
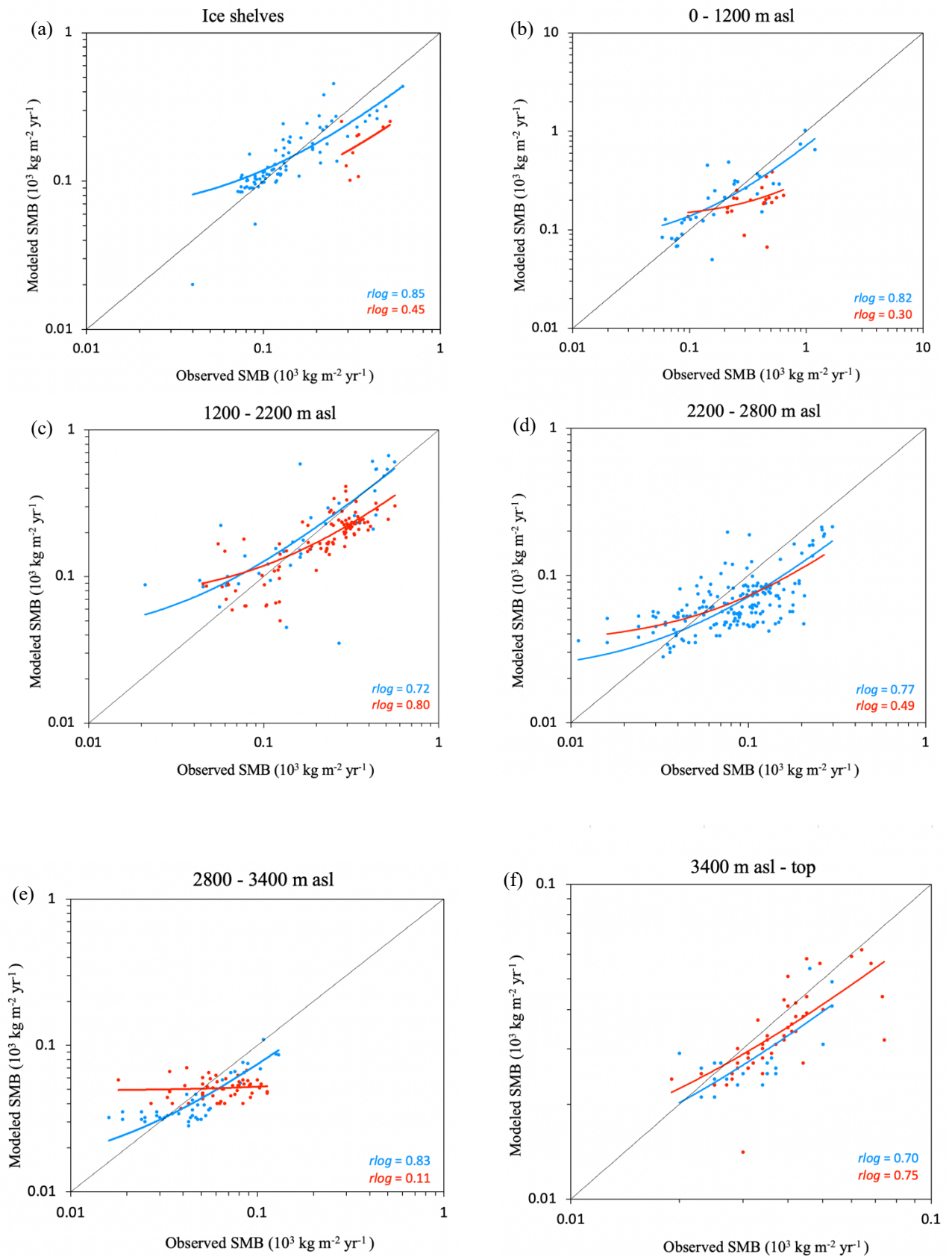
Figure 3.5 (a-f): Scatter plots showing the correlation between observed and modelled surface mass balance for six elevation classes over 1950–1978 and 1979–2020

3.3. Reanalysis

In the past it has been demonstrated that reanalysis perform better in areas where observations are available, whereas data-sparse regions are less accurately represented (e.g., Cullather *et al.*, 1996; Bromwich *et al.*, 2000). Bromwich & Fogt (2004) found significant differences between the NCEP1 and ERA-40 in the South Pacific, where data is rare, especially prior to the 1980s. In addition to the average difference, there are also important fluctuations of these differences. For instance, when regarding differences in 500 hPa geopotential height between two regions in the South Pacific, differences reached values above 200 gpm (compared to the mean differences of around 50 gpm). Moreover, in these regions where observation-based data is limited, it is nearly impossible to know which reanalysis produces more satisfactory results. This may as well be the case for Antarctica, especially the interior of the continent, where hardly any observations exist. Even after the introduction of satellite data, reanalysis can produce significant uncertainties over the AIS. For instance, discerning snow cover from cloud cover is not always evident. Moreover, during winter months, there is no solar radiation. Nevertheless, overall, it has been shown that reanalysis produces significantly better results after the late 1970s. It is also worth mentioning that in the past reanalysis have displayed better results during the summer months, whereas winter months need to be considered with prudence (e.g., Bromwich & Fogt, 2004). Also worth mentioning is the fact that changes in the assimilation scheme used by reanalysis, as well as the quality and quantity of assimilated data can produce artificial climate changes that are not captured by Antarctic stations (e.g., Hines et al., 2000; Bromwich *et al.*, 2011), indicating the importance of using reanalysis with caution. For a detailed evaluation of the ERA5 reanalysis, we refer to Marshall *et al.* (2022). In short, they found that ERA5 reproduces Antarctic near-surface temperature the best, compared to the 20CRv3 and JRA-55 reanalysis, in both the 1950–1979 and 1980–2020 period. They also found a significant improvement for all reanalyzes in the more recent period.

3.4. Chapter Discussion

While MAR yields better results using ERA5$^{79\rightarrow}$ compared to ERA5$^{\rightarrow79}$, overall, the evaluation displays a satisfactory performance of the model (except for near-surface wind speed). Near-surface pressure is generally simulated with good accuracy, with some expectations due to unique local configurations (proximity to the coast, topography). While early modelled near-surface temperature values need to be treated with care, the accuracy of

the model appears to improve, as it approaches the 80s. Finally, for all three variables, there is a large but slowly dissipating winter-summer contrast. Because the improvement over the entire 1950–2020 period is more pronounced in summer, the model data can be deemed more homogenous in that season. This is in accordance with previous reanalysis evaluation studies (e.g., Bromwich & Fogt, 2004). Marshall *et al.* (2022) found similar results when assessing the accuracy of portraying changes in SAM structure before 1979 using three different reanalyzes, including ERA5. While all three reanalyzes were able to display changes over time in the SAM-SAT relationship, they found ERA5 to be the most homogenous across both sub-periods and to have the best representation of near-surface temperature. Along with the 20CRv3 reanalysis, ERA5 also produced the closest SAM index to the observation-based index of Marshall (2003) (good RMSE, correlation and bias), with the highest homogeneity over the entire studied period (Fig. 3.6). These remarks need to be taken into consideration when discussing the climate over the Antarctic Ice Sheet prior to 1979.
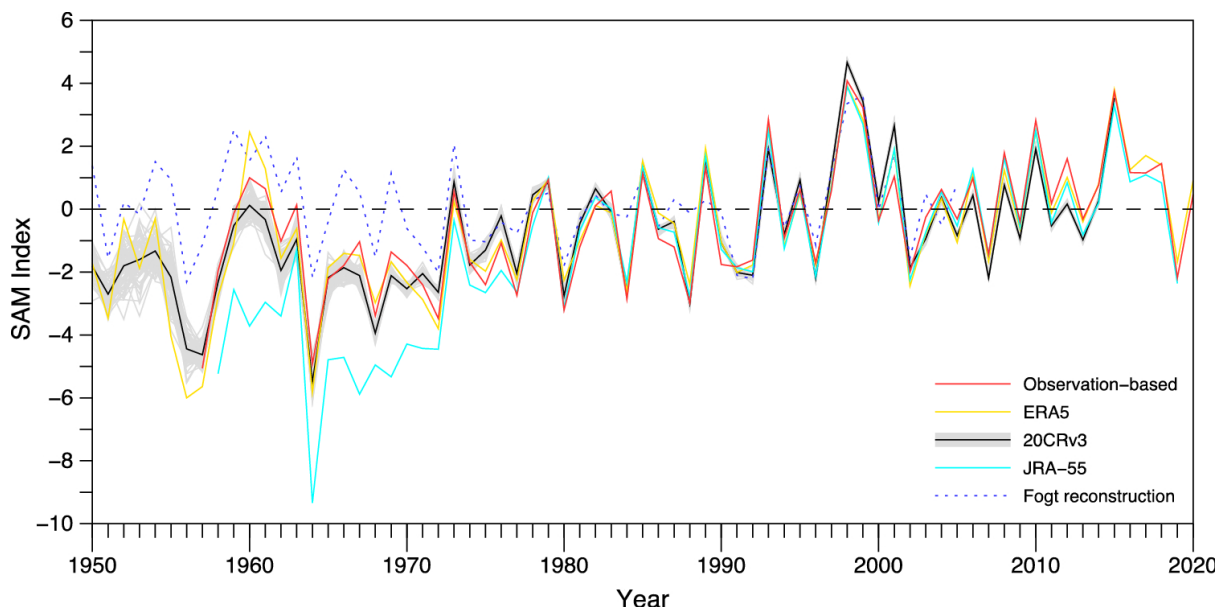
Figure 3.6: Time series of the SAM indices (normalized over 1981–2010) from observations, reanalyzes and a statistical reconstruction (from Marshall *et al.*, 2022)

4. Results

The following chapter includes an in-depth description of the spatio-temporal evolution of the modelled climate over the AIS, using climatic variables such as near-surface temperature and wind speed but also surface mass balance, surface melt and sublimation. The aim of this chapter is to provide a portrait of the climate prior to 1979, using the results from MAR forced by the ERA5 back extension and compare it to previously published results.

4.1. Near-surface climate

4.1.1. Near-surface temperature (SAT)

In this chapter, modelled near-surface temperature (SAT) is compared for two distinct periods. As a reference we use the 1981–2010 period, as recommended by the WMO, a period that has been simulated previously. Using ERA5[→79], which allows us to compute values further over a longer time span, the second period used extends from 1951 to 1980, a period of equal duration as the reference period (30 years). The aim of this chapter is to describe the near-surface temperature in 1951–1980 and address any major changes compared to the reference period, both spatially and seasonally. Moreover, the results are then compared to similar studies. (e.g., Turner *et al.,* 2020). For the sake of simplicity, for the remainder of this study, we refer to the 1951–1980 as the EARLY period, while addressing the 1981–2010 period as the REF period.
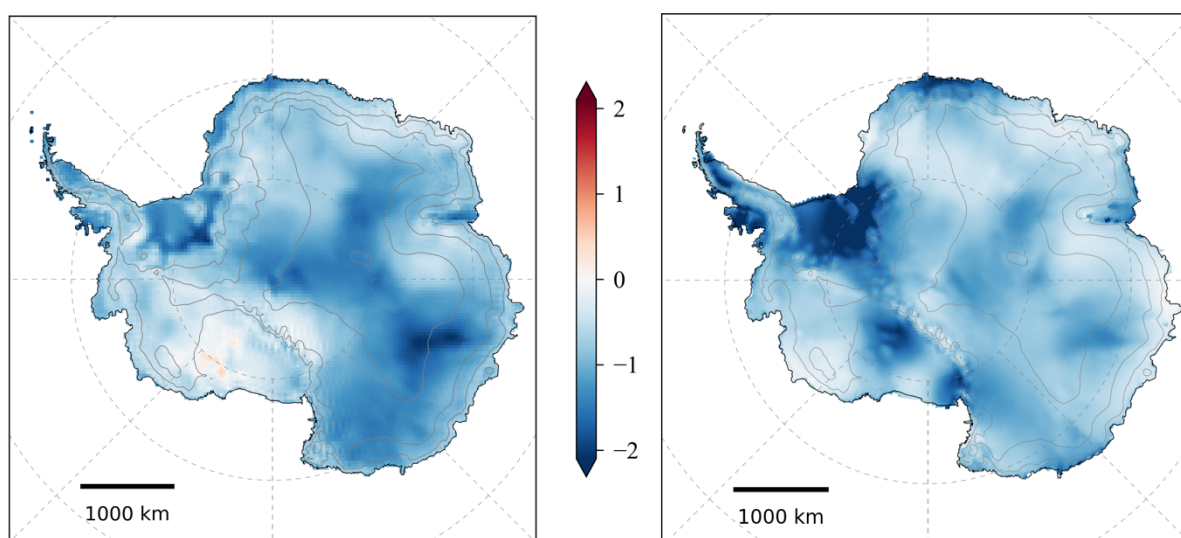
Figure 4.1: Near-surface temperature anomalies (°C) for 1951–1980 compared to the 1981–2010 reference period from MAR$_{v3.12}$ forced by ERA5 (left) and from ERA5 (right)

For both periods, modelled near-surface temperatures are the lowest in East Antarctica (-36.9 °C & -35.9 °C). In West Antarctica, the mean temperature hovers around -23 °C, while the highest temperatures are produced across the Peninsula. Overall, among the highest interannual variabilities are those observed for the Antarctic Peninsula (0.7 °C) and West Antarctica (0.5 - 0.7 °C) (Tab. 4.1). Moreover, high *SD* values can be a result of the North-South movement along the coast of the western side of the Peninsula of sea ice during a year. High positive and negative anomalies and the resultant high interannual variability might also be linked to an enhanced foehn effect by stronger westerly winds associated with a positive SAM phase. The periods of warmer or colder than usual near-surface temperature could also be linked to a change in the deepening and location of the ASL or other large-scale atmospheric anomalies (e.g., ENSO).
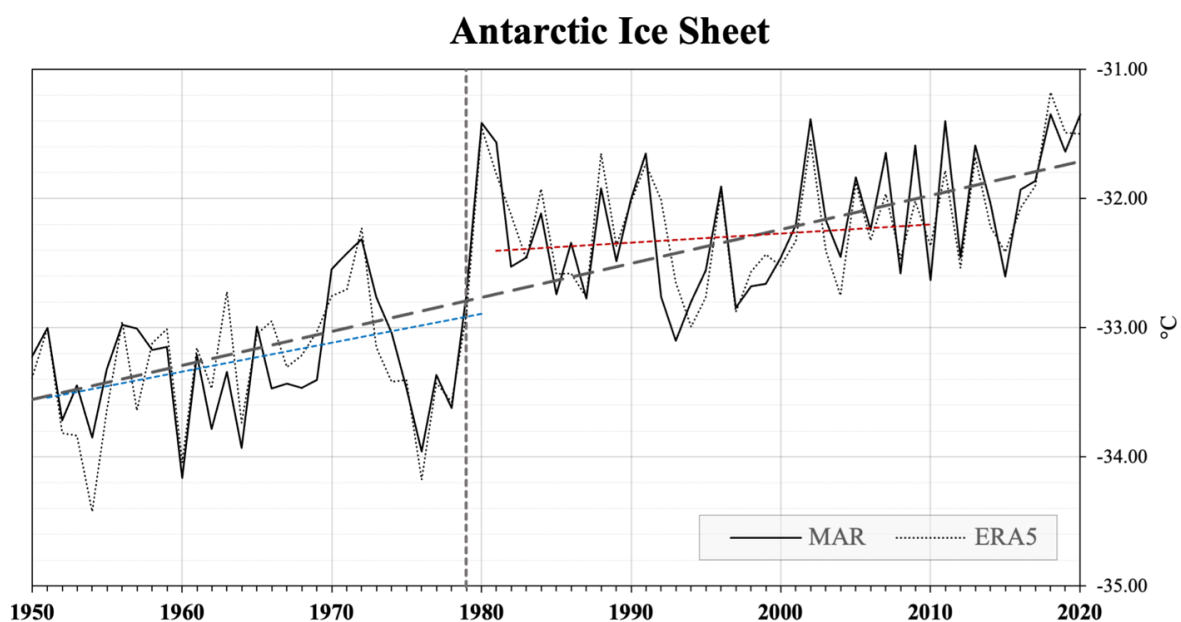
Figure 4.2: Mean annual near-surface temperature (°C) from MAR$_{v3.12}$ forced by ERA5 and from ERA5 over the AIS. The blue (1951–1980) and red (1981–2010) dashed line represents the temperature trend
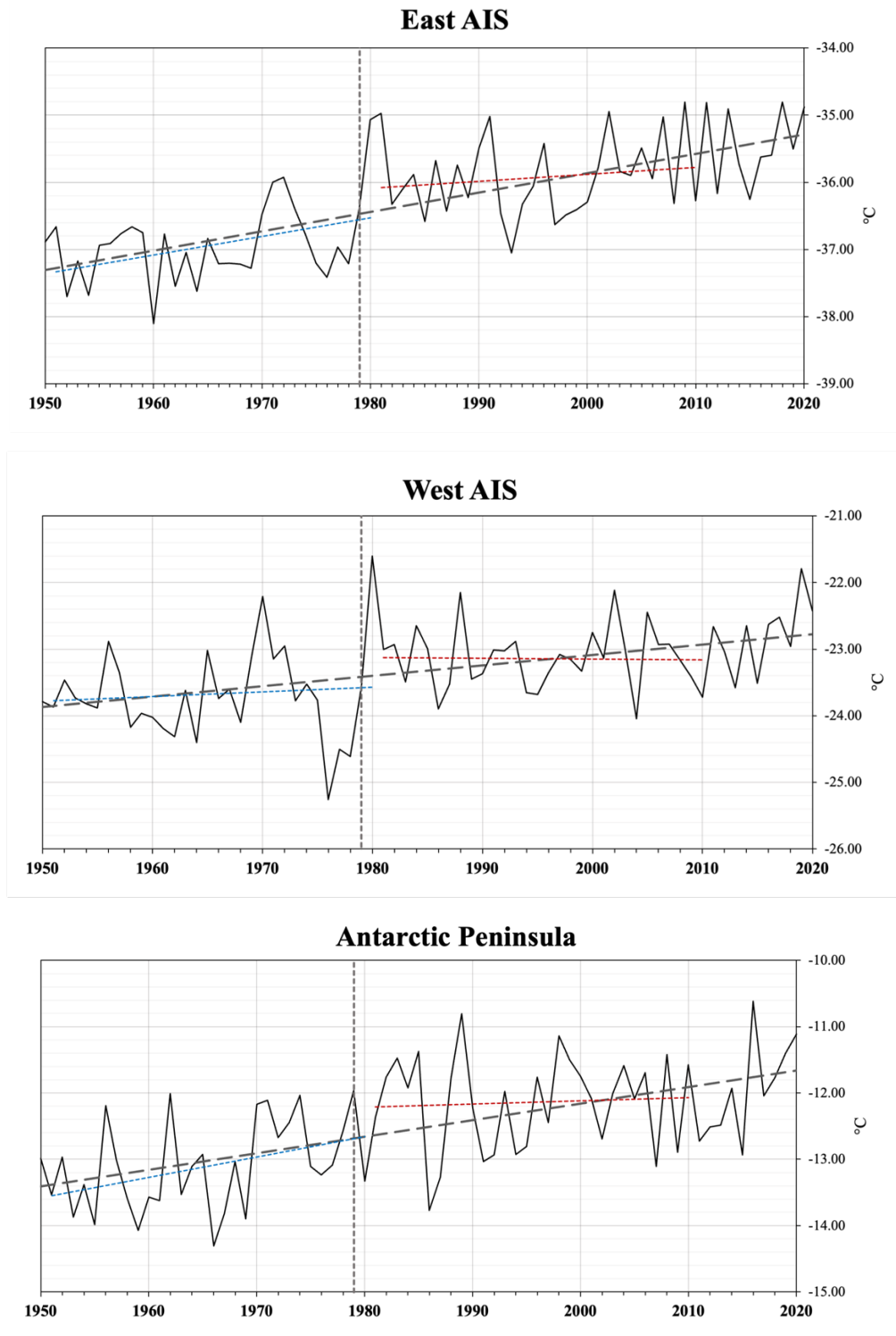
Figure 4.3: Same as figure 4.2 but for East Antarctica, West Antarctica, and the Antarctic Peninsula

Over the entire Ice Sheet, there is a slight mean difference of around 1 °C between the EARLY period (-33.2 °C) and the REF period (-32.3 °C), while the interannual variability remains mostly the same. What stands out when regarding the time series of annual means, spanning over both periods (Fig. 4.2), is that there appears to be a significant jump in temperature when switching from the original ERA5[79→] to the back extension, with a temperature difference above 2°C between 1978 and 1980. The fact that this inconsistency was not observed when comparing modelled values to station values is likely since observations from the stations in question were assimilated in the ERA5 dataset, thus reducing the bias of the reanalysis at these sites. Also interesting to mention is the fact that there is an initial jump in temperature of about 1 °C from 1978 to 1979, followed by another jump in temperature from 1979 to 1980 of 1 °C, before finally stabilizing. Thus, the major jump in temperature is slightly carried over into the POST-79 period. When looking at the data assimilated into the ERA5 reanalysis over time, there is an increase in the number of daily assimilated observations for brightness temperature and ozone around 1980, which might explain the modelled temperature. The jump in near-surface temperature between the PRE-79 and the POST-79 periods might also be attributed to a natural phenomenon (e.g., the onset of the ozone layer destruction, greenhouse gases) but this needs to be analysed further.
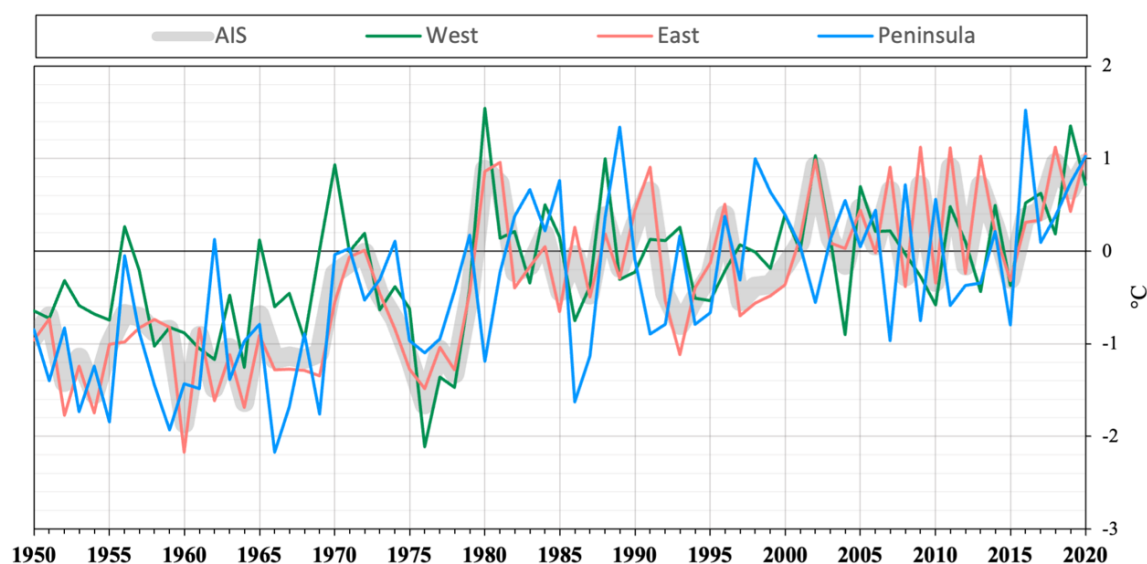
Figure 4.4: Near-surface temperature anomalies (normalized over 1981–2010) simulated by MAR$_{v3.12}$ forced by ERA5

Annually, near-surface temperature anomalies over the AIS are mostly negative, reaching values -2 °C lower than during the REF period (Fig. 4.4). The lowest anomalies, indicating significantly colder temperatures in the EARLY period, are found in East Antarctica, especially in Wilkes Land and a few coastal regions in the western part, but also around the Ronne Ice

Shelf. Similarly, a mean change of 1 °C between both periods is exhibited across the Peninsula. In West Antarctica, anomalies remain low with some slightly positive anomalies (< 1 °C) observed at the eastern edge of the Ross Ice Shelf (Fig. 4.2). Despite the little deviation from the mean temperatures, there is a slight change in interannual variability between the EARLY and the REF period, while for the Peninsula and East Antarctica, this is not the case (Tab. 4.1).

Within the EARLY period, there appears to be a period (1970–1973) during which near-surface temperatures are especially high. This trend is observed across all three Antarctic regions, with the most anomalous 1970–1973 values found over West Antarctica. Moreover, across the REF period and onwards, there is a clear rise in mean annual temperature in East Antarctica, starting in the early 2000s, which explains the higher temperature difference in that region. For both other regions, this trend is only found from 2015 to 2020. Additionally, for West Antarctica, the trend in the REF period is even slightly negative indicating an overall decrease in mean temperature (Fig. 4.3).

Table 4.1: Mean annual and seasonal Antarctic near-surface temperature (°C) over 1951–1980 and 1981–2010. Standard deviations are given in brackets

Region	Year	Near-surface temperature (°C)				
		Annual	Spring	Summer	Autumn	Winter
AIS	1951-1980	-33.2 (0.6)	-33.8 (0.9)	-20.5 (0.5)	-37.1 (0.9)	-41.4 (1)
	1981-2010	-32.3 (0.5)	-32.8 (0.6)	-20.1 (0.6)	-36.3 (0.9)	-40 (1)
West	1951-1980	-23.7 (0.7)	-24.7 (1.2)	-13.1 (0.6)	-26.5 (1.1)	-30.4 (1.3)
	1981-2010	-23.1 (0.5)	-23.6 (1.2)	-13.2 (0.6)	-25.8 (1)	-30 (1.2)
East	1951-1980	-36.9 (0.6)	-37.5 (1)	-23.8 (0.6)	-41.1 (1.1)	-45.3 (1.2)
	1981-2010	-35.9 (0.6)	-36.4 (0.6)	-23.3 (0.8)	-40.2 (1)	-43.7 (1.4)
Peninsula	1951-1980	-13.1 (0.7)	-12.9 (0.9)	-5.5 (0.5)	-14.8 (1.4)	-19.2 (1.4)
	1981-2010	-12.1 (0.7)	-12.1 (1.2)	-4.9 (0.5)	-13.3 (1.3)	-18.2 (1.6)
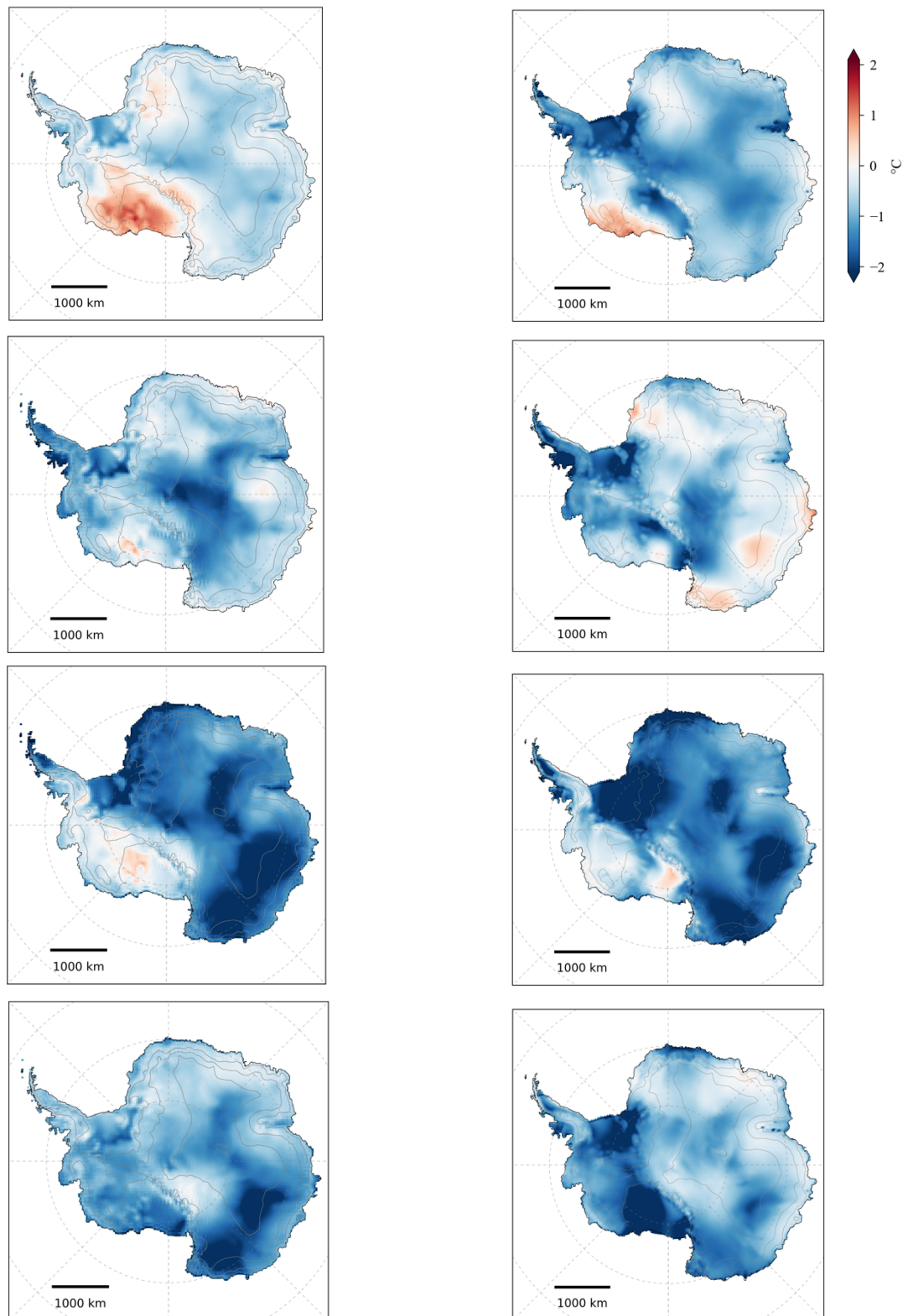
Figure 4.5: Same as figure 4.1 but for all four austral seasons from summer (top) to spring (bottom) for MAR$_{v3.12}$ forced by ERA5 (left) and from ERA5 (right)

In summer, almost no difference in mean annual temperature (except the Antarctic Peninsula) or the associated interannual variability (except East Antarctica) is observed across the AIS. During summer, the shift in near-surface temperature between PRE-79 and POST-79 is less noticeable. This might be a result of the model being more homogenous in summer, as found in the previous chapter. Moreover, summer mostly yields the lowest interannual variability across all regions and by definition, the highest mean temperatures, when compared to the other seasons. The negative anomalies found over the Ronne Ice Shelf and Wilkes Land are less noticeable in summer and a large patch of positive anomalies appears over the Ross Ice Shelf. During autumn, when forced by ERA5, the model produces a mean difference of 0.8 °C between both periods. At the regional scale this gap widens, with very low negative anomalies over the Antarctic Peninsula. Additional areas of negative anomalies are found over the Ronne Ice Shelf and on the Antarctic Plateau. Moreover, there is no significant change in interannual variability in any of the regions. In winter, mean annual temperatures appear to fluctuate the most, between both periods but also from year to year. The more pronounced temperature difference in East Antarctica (1.6 °C) is linked to negative temperature anomalies over the eastern part of that region (Wilkes Land and Victoria Land) with additional negative anomalies along the coast in the western part. Interestingly, the highest interannual variability is observed in winter, across both periods. Very noticeable changes in near-surface temperature between the two periods are also observed in spring. The model results exhibit large areas of negative anomalies in the EARLY period in the eastern part of East Antarctica (e.g., Wilkes Land and Victoria Land). Significant negative anomalies are also found over parts of the Ronne Ice Shelf (Fig. 4.5).

Figure 4.6: Same as figure 4.1 but for austral summer and winter

Figure 4.6 also displays interesting results regarding the jump in temperature found around 1979. From an annual point of view, the jump covers three years, 1978, 1979 and 1980. However, time series of winter temperatures only show a jump between 1979 and 1980, whereas during summer months, the pronounced rise mostly occurs between 1978 and 1979. Moreover, the temperature jump is more i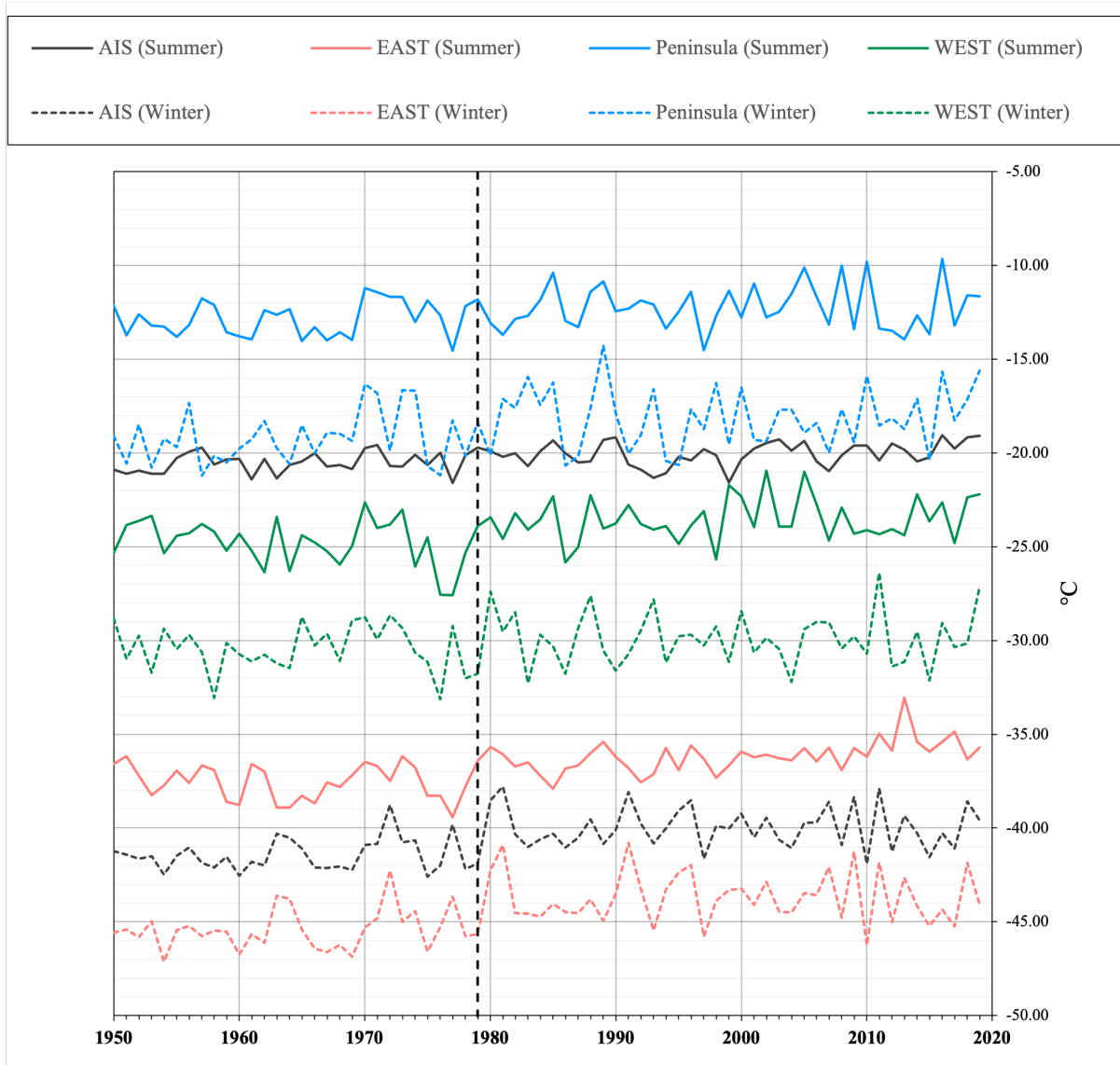mportant during winter months, which once again points to the already observed seasonal discrepancy in reanalysis performance.

To assess whether the modelled changes, especially the troubling temperature upsurge, are caused by the reanalysis or the model itself, MAR values are also mapped against ERA5 values. Mean annual AIS temperatures of both the model and the reanalysis match to the extent that we can conclude that the variability exhibited by the model is steered by the variability of the ERA5 dataset. This is especially true after the 70s, with a near-perfect overlap of both time series (fig. x). In the EARLY period, the overlap is weaker and temperature differences of around 0.5 °C occur during 1954 and 1963. Nevertheless, the overall variability remains consistently similar and more importantly, figure 4.2 highlights the fact that the 1978–1980 temperature upsurge originates in the ERA5 dataset and can thus not be attributed to a faulty behaviour of the model.

Overall, anomalies are consistent between the reanalysis and model. The negative anomalies found in eastern East Antarctica are less pronounced when using ERA5, while the reanalysis produces even lower negative anomalies across the Peninsula and in the Ronne Ice Shelf area (Fig. 4.1). During summer, MAR produces a larger area of positive anomalies around the Ross Ice Shelf than ERA5. Moreover, the negative ERA5 temperature anomalies on the Ronne Ice Shelf are more noticeable. During autumn and winter months, anomalies produced by the model and reanalysis exhibit a very similar spatial distribution, especially regarding the very low anomalies around -2 °C in East Antarctica. Finally, in spring, the marked negative anomalies found in Wilkes and Victoria Land only appear when using MAR, whereas ERA5 delivers such anomalies over the Ronne and Ross Ice Shelves. To conclude, the modelled temperature evolution is very similar to the situation displayed by the reanalysis, which indicates that the model behaves as it should. The primary differences include the striking negative ERA5 temperature anomalies found in the Ronne Ice Shelf area in during all seasons, which is not the case for the modelled temperature (Fig. 4.5).

4.1.2. Near-surface wind speed

As for the REF period, wind during the EARLY period is generally low inside the continent and reaches high values above 10 ms^{-1} in coastal areas, especially in East Antarctica. Generally, there is a flow from inside the continent, outwards towards the margins, following the slope and accelerating over time, due to the absence of obstacles (Fig. 1.4). The highest mean wind is generated in East Antarctica (7 ms^{-1}), with slightly lower values in West Antarctica (6 ms^{-1}) and the lowest values across the Peninsula (4 ms^{-1}). There is also a seasonal discrepancy, wind being the highest during winter and the lowest during summer for both periods. Moreover, interannual variability is relatively low, with little to no local or seasonal contrast (Tab. 4.2).
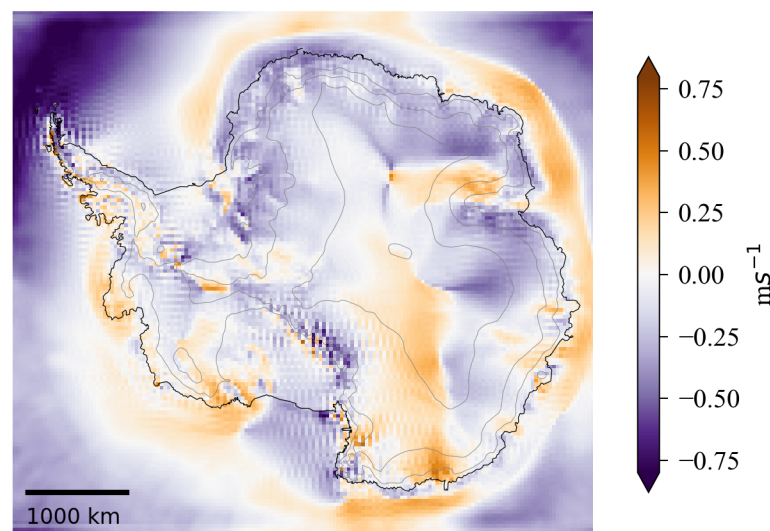
Figure 4.7: Near-surface wind speed anomalies (ms^{-1}) for 1951–1980 compared to the 1981–2010 reference period for MARv3.12 forced by ERA5

Across the entire continent, there is a slight increase in mean wind speed between both periods of about 0.1 ms^{-1}. This increase is not attributed to a sudden jump in values around 1980, as was observed for temperature and SMB, but is the result of a steady increase over time. At a regional scale the mean differences remain low, although they are slightly higher in winter and across East Antarctica and no mean change at all is produced in autumn (Fig. 4.7).

Again, on a yearly basis, the most anomalous behaviour is observed in West Antarctica, with mean annual wind speeds being more than 0.3 ms^{-1} above the 1981–2010 mean in 1956, 1970, 1971 and 1974 and 0.5 ms^{-1} below the reference value in 1976. There is also a period between

approximately 1950 and 1960 when mean wind speeds across East Antarctica are anomalously low (Fig. 4.9).

Annually, the margins of the continent are mainly dominated by negative anomalies, whereas some areas inside the continent (e.g., Wilkes land) display values higher than during the REFERENCE period. Moreover, there appears to be a ring of positive anomalies around the continent, especially in the eastern parts (Fig. 4.7).
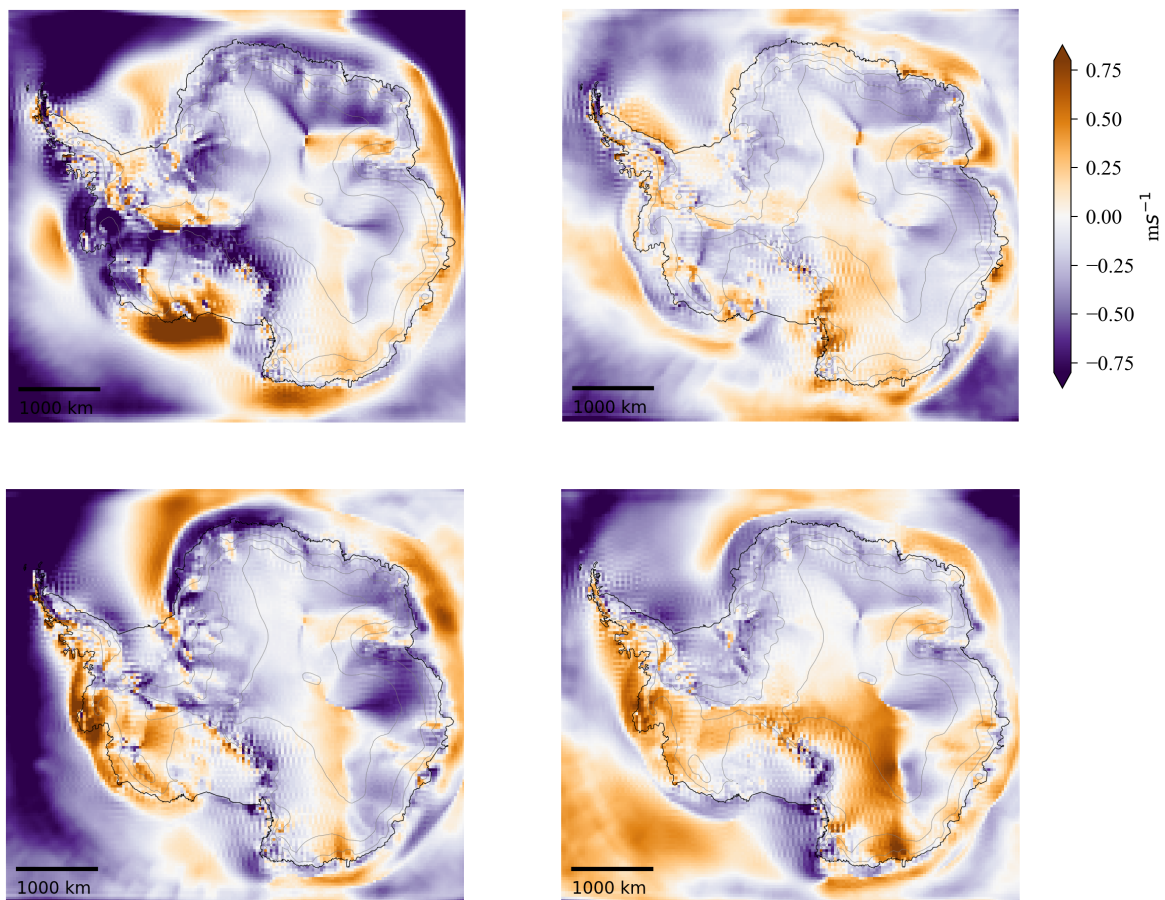
Figure 4.8: Same as figure 4.7 but for austral summer (upper-left), autumn (upper-right), winter (lower-left) and spring (lower-right) for MARv3.12 forced by ERA5

Across the Peninsula, there is an unorganized mix of both positive and negative wind speed anomalies. MAR may have difficulties representing the steep topography and thus portraying differences in mean wind speed with the resolution we used. Figure 4.8 indicates that seasonally, differences in mean wind speed between both periods can be very local. Thus, instead of commenting on every minor change, I will focus on the general pattern and the areas where anomalies are substantial.

In autumn, wind anomalies follow the general pattern already described for annual anomalies. Moreover, anomalies during autumn are the lowest among all four seasons. During the spring months, positive anomalies are more dominant than during the other seasons, with a stretch of positively anomalous values from East Antarctica to the Peninsula and a large patch in the parts of the Ross and Amundsen Sea. In summer and winter, there are local areas of very high/low anomalies. For instance, in summer, there is a large area of higher-than-normal mean wind speed above the Ross Sea, near the coast. Moreover, the stretch of positive anomalies observed in spring changes sign during the summer months. In winter, there is a large area of negative anomalies, reaching values lower than -0.75 ms^{-1} along the coastline in East Antarctica and opposite anomalies in West Antarctica (Fig. 4.8).

In the Evaluation chapter, we found that large biases exist for modelled wind speed. Thus, the statements made above need to be considered with great care. Nevertheless, it is important to examine the evolution strength and direction of the wind. Although implications are less direct as for temperatures or snowfall changes, wind also plays a role regarding the mass balance of the ice sheet.

Table 4.2: Mean annual and seasonal Antarctic near-surface wind speed (ms^{-1}) over 1951–1980 and 1981–2010. Standard deviations are given in brackets

Region	Year	ms-1				
		Annual	Spring	Summer	Autumn	Winter
AIS	1951-1980	6.4 (0.1)	6.7 (0.2)	4.9 (0.2)	7.1 (0.2)	7.5 (0.2)
	1981-2010	6.5 (0.1)	6.7 (0.2)	5 (0.2)	7.1 (0.2)	7.6 (0.3)
West	1951-1980	5.9 (0.2)	6.5 (0.4)	4.3 (0.2)	6.6 (0.3)	6.9 (0.4)
	1981-2010	5.9 (0.2)	6.4 (0.4)	4.5 (0.3)	6.6 (0.3)	6.8 (0.3)
East	1951-1980	7 (0.1)	7.2 (0.2)	5.3 (0.3)	7.7 (0.2)	8.1 (0.2)
	1981-2010	7.1 (0.1)	7.2 (0.2)	5.5 (0.3)	7.7 (0.2)	8.3 (0.3)
Peninsula	1951-1980	3.9 (0.1)	4.5 (0.3)	3 (0.2)	4.5 (0.2)	4.9 (0.2)
	1981-2010	4 (0.1)	4.4 (0.3)	3.1 (0.2)	4.5 (0.2)	5.1 (0.2)

There are for instance threshold wind speeds for snow transport that depend on the properties of the surface snowpack (e.g., cohesion). For instance, for wet snow transport, Li and Pomeroy (1996) estimated threshold 10 m wind speeds ranging from 7 to 14 ms^{-1}, whereas for dry snow, values lie between 4 and 11 ms^{-1}. Although, we only found a change in mean wind speed of around 0.1-0.2 ms^{-1}, that is only the mean change and obscures areas where wind may change to a greater extent at a lower spatiotemporal scale, thus reaching the thresholds for snow transport. An increase in snow transport can reduce or even prevent any accumulation. Moreover, higher katabatic winds can create favourable conditions for sublimation (e.g.,

Grazioli *et al*., 2017), as described in the previous chapter, thereby further reducing accumulation over the AIS. This can lead to the creation of blue ice areas or glaze surfaces that are primarily found on the plateau in East Antarctica (e.g., Scambos *et al*., 2012), thereby reducing the local albedo (and increasing absorption of short-wave solar radiation and encouraging surface melt. The eroded snow is either redeposited downslope or in depressions (Das *et al*., 2013). This is often a source of overestimation for SMB, which can reach values above 50 Gt for the AIS. Thus, properly integrating these complex processes into climate models is important for ameliorating SMB estimates. In addition to the changes to the mass balance, changes in the direction and strength of the wind also affect sea-ice drift, thus creating local differences in near-surface temperature (Holland & Kwok, 2012).
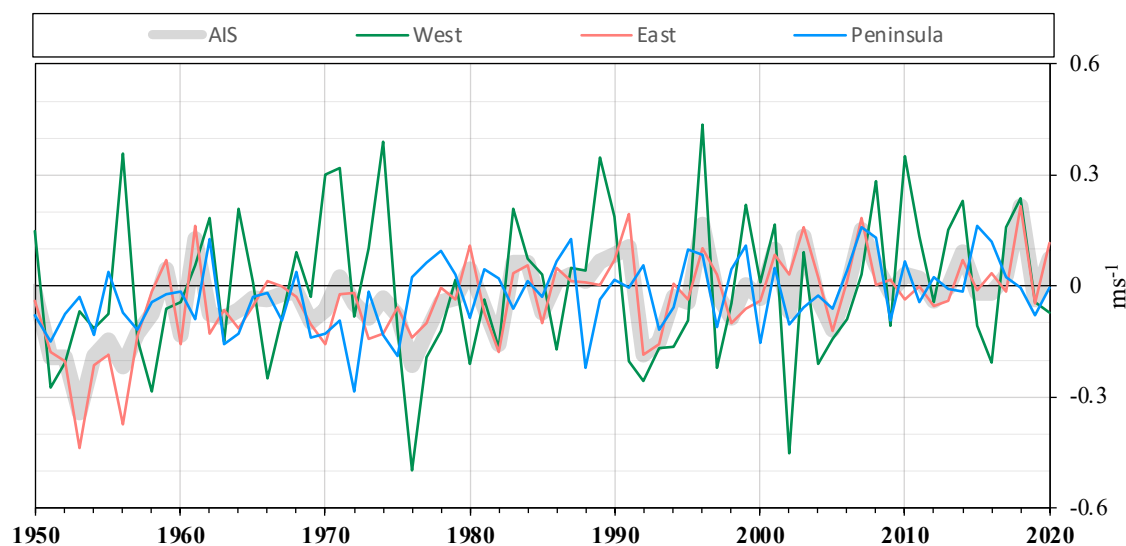
Figure 4.9: Near-surface wind speed anomalies (ms^{-1}) (normalized over 1981–2010) simulated by MARv3.12 forced by ERA5

4.2. Surface mass balance

As for near-surface temperature, there are marked changes in the Antarctic surface mass balance between the EARLY period and the REF period. The pronounced jump between 1978 and 1980 remains visible, with values of around 2460 Gt/year and 2760 Gt/year respectively for both periods. The 300 Gt difference is primarily produced at the transition from ERA$^{\rightarrow 79}$ and ERA$^{79 \rightarrow}$. After the jump in SMB, there is a slight decrease until around 2007 with a successive positive trend until 2020. Moreover, in the EARLY period, very low SMB values were found in 1961 (2210 Gt) and 1967 (2180 Gt). Overall, there are no noticeable periods of prolonged positive or negative anomalies (Fig, 4.10).
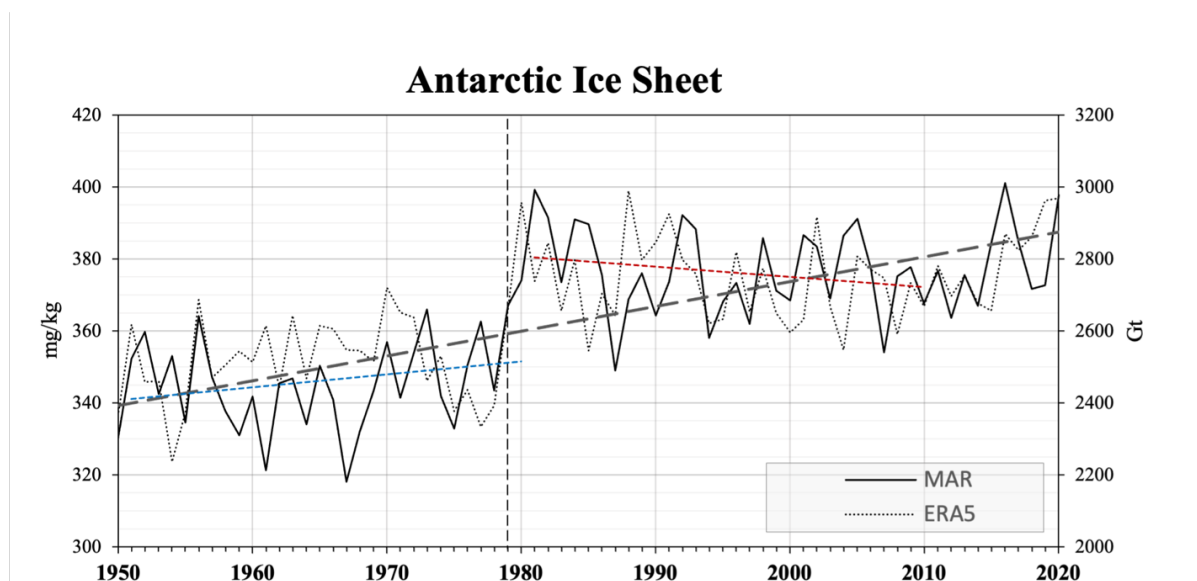
Figure 4.10: Annual surface mass balance (Gt) from MAR$_{v3.12}$ forced by ERA5 and specific humidity at the 700 hPa level from ERA5 over the AIS. The blue (1951–1980) and red (1981–2010) dashed line represents the SMB trend.

As for near-surface temperature, in order to assess if the SMB variability (especially the 1978–1980 jump) produced by MAR is driven by the variability in the ERA5 dataset, modelled SMB is plotted against ERA5 700 hPa specific humidity. The ERA5 reanalysis does not provide a SMB dataset, but since surface mass balance is primarily steered by precipitation, the humidity at 700 hPa is a good proxy for the former. Overall, the variability of the humidity resembles the SMB variability, especially during the REF period. Most importantly, the discrepancy between the PRE-79 and POST-79 period is displayed by the humidity time series. In the EARLY period, the variability of both variables is also similar, with a few exceptions between 1957 and 1963 when humidity and SMB exhibit opposite behaviours (Fig. 4.10).

Table 4.3: Annual and seasonal Antarctic surface mass balance (Gt/year) over 1951–1980 and 1981–2010. Standard deviations are given in brackets

Region	Year	Annual	Spring	Summer	Autumn	Winter
		Gt/year				
AIS	1951-1980	2462.5 (133.4)	580 (45.5)	419.3 (43.3)	739.4 (63.3)	725.8 (68.6)
	1981-2010	2763.2 (123.4)	668.2 (58.9)	464.6 (53.8)	813.2 (65.1)	816.2 (71.6)
West	1951-1980	753.3 (62.9)	181.1 (32.7)	108.5 (24.1)	224.4 (35.1)	239.4 (39.5)
	1981-2010	801.1 (74.6)	201.6 (40.3)	112.9 (23.6)	240.6 (42)	246 (45.7)
East	1951-1980	1244.3 (86)	276.9 (27.6)	223.1 (30.6)	378.5 (35.2)	365.7 (52.4)
	1981-2010	1422.9 (100.9)	329 (29.4)	255.6 (36.9)	415.7 (36.4)	422.6 (56.2)
Peninsula	1951-1980	314.2 (42.1)	90.8 (12.7)	49 (11.9)	91.5 (20.7)	83 (15.7)
	1981-2010	383.2 (42.7)	103.2 (22.3)	64.3 (11.5)	109.8 (22.6)	105.8 (19.7)

For both periods, SMB is the highest in winter and autumn, with values of around 730 and 815 Gt/year respectively. In spring, SMB is slightly lower and during summer, we find the lowest values for SMB. The value for describing interannual variability, expressed through the standard deviation is dependent on the absolute SMB values, which in turn depend on the region, season, and period. Generally, higher mean SMB values can produce higher standard deviations. Thus, it is worth noting that despite the increase in mean SMB from the EARLY to the REFERENCE period, surface mass balance shows slightly higher standard deviations in the former period than the latter. For the seasons, however, this is not the case, and we observe an increase in SMB accompanied by an increase in interannual variability (Tab. 4.3).

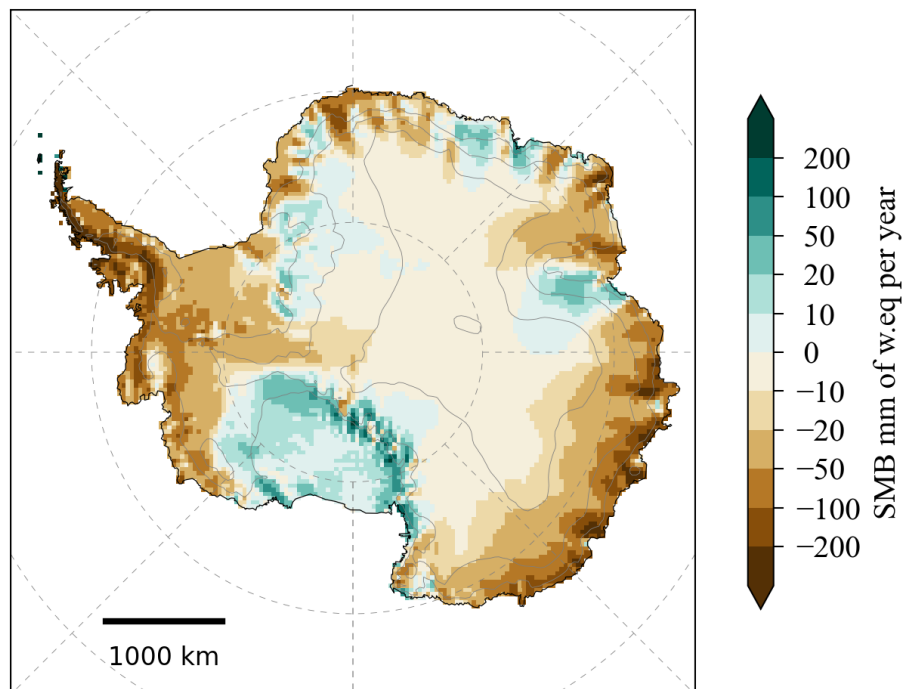**Figure 4.11:** Surface mass balance anomalies (mm of water equivalent per year) for 1951-1980 compared to the 1981-2010 reference period for MAR$_{v3.12}$ forced by ERA5
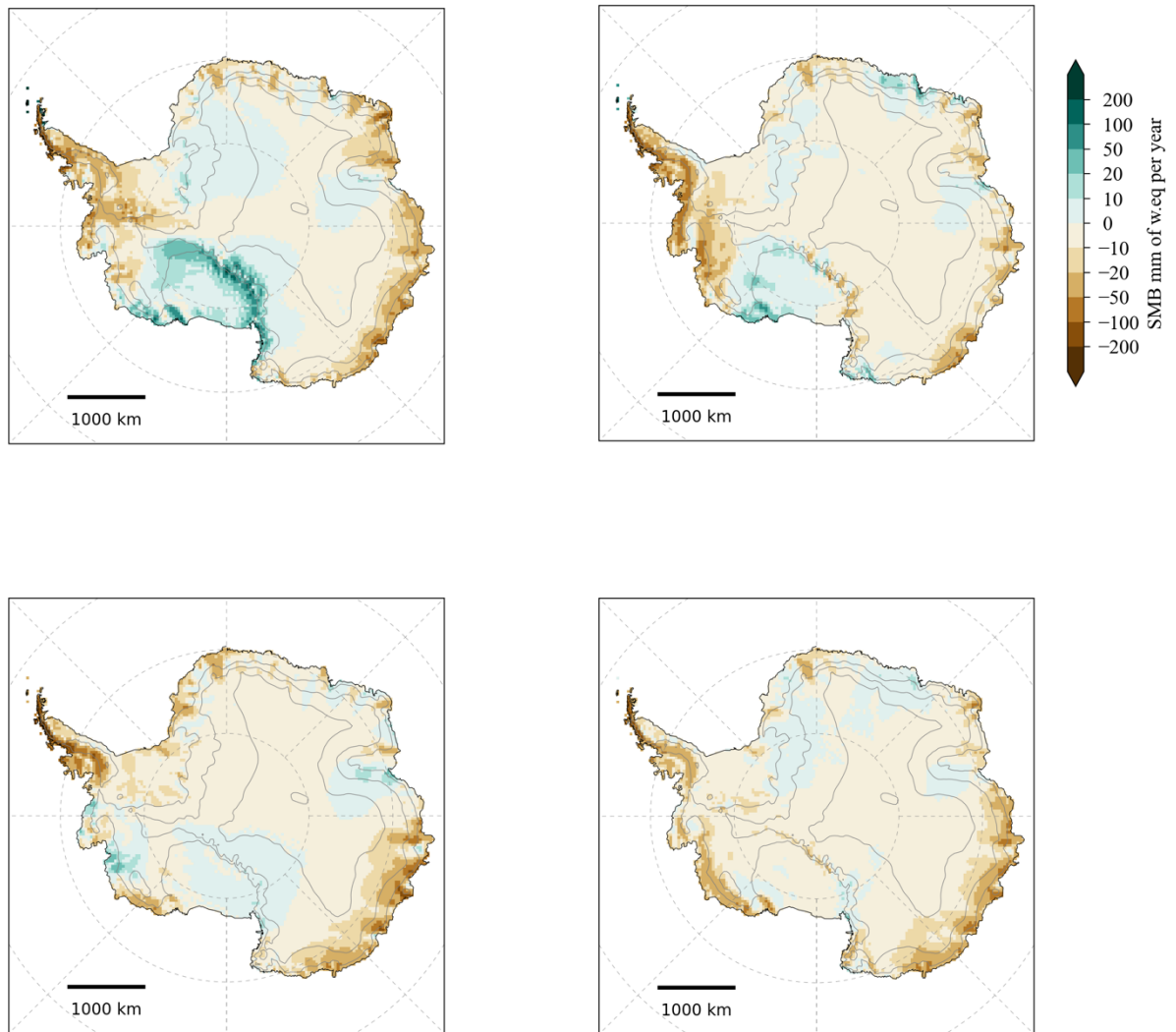
Figure 4.12: Same as figure 4.11 but for austral summer (upper-left), autumn (upper-right), winter (lower-left) and spring (lower-right)
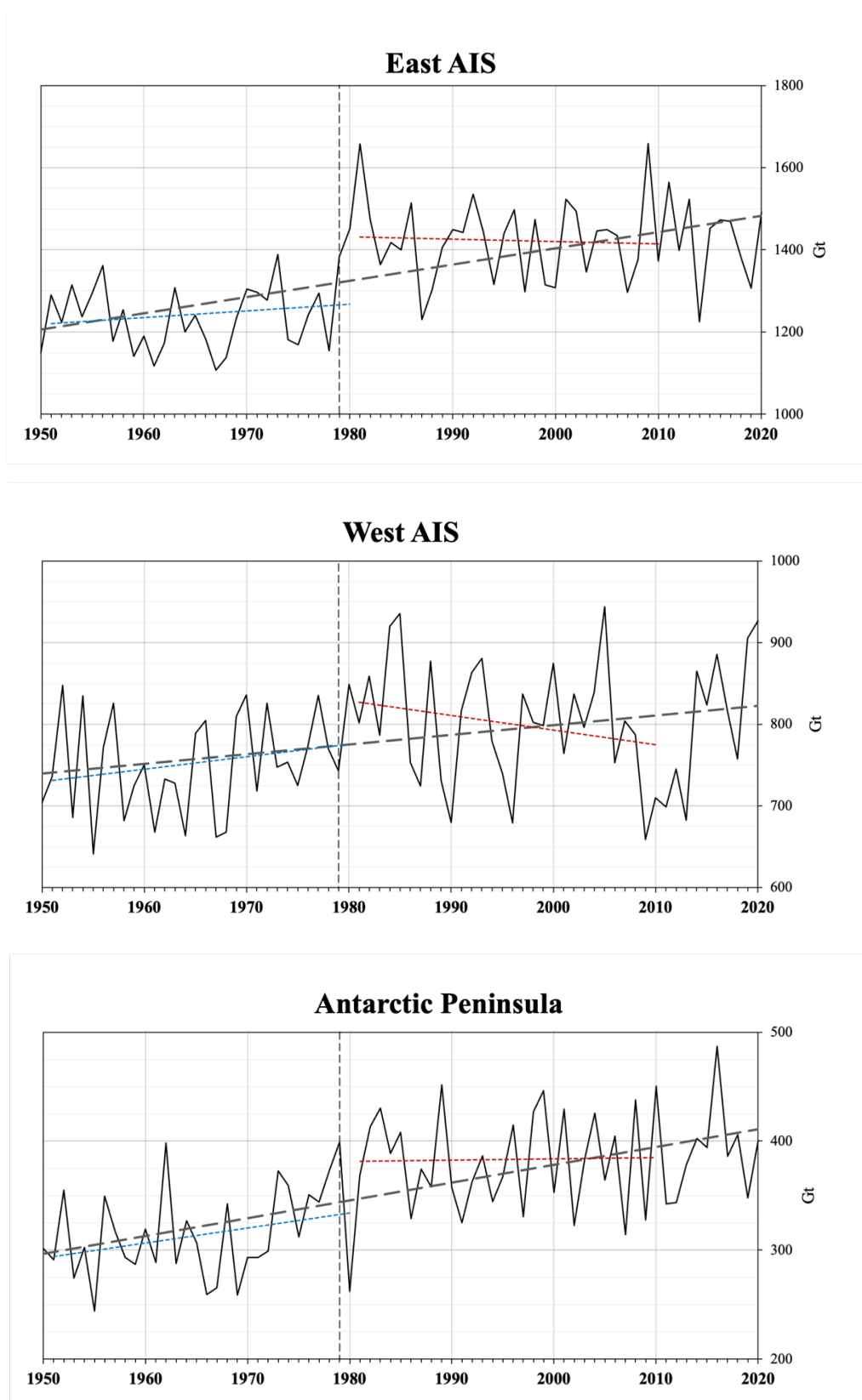
Figure 4.13: Same as figure 4.10 but for East Antarctica, West Antarctica, and the Antarctic Peninsula

The highest negative SMB anomalies in the EARLY period are found along the western side of the Antarctic Peninsula and the eastern part of East Antarctica, along the coast, with values higher than 200 mm of water equivalent per year. Over the entire Antarctic Peninsula, the annual SMB experiences an increase of around 70 Gt/year between both periods. A few areas display positive SMB anomalies, the most marked region being the Ross Ice Shelf, especially along the Transantarctic Mountains. On the Antarctic Plateau, little to no changes in SMB are observed between both periods. Moreover, although East Antarctica displays the highest SMB, the mass is spread across a significantly larger surface, and only displays total SMB values less than twice as high as the values simulated for West Antarctica (Fig. 4.11 & 4.13).

Over the Antarctic Peninsula, the highest negative anomalies are witnessed in spring and autumn. Across all four seasons SMB values remain positively anomalous over the Peninsula. This is also the case over the Ronne Ice Shelf, where SMB is slightly lower than normal throughout the entire year. In 1955, 1966 and 1980, MAR produced very low surface mass balance values across the Peninsula, with peaks opposite to West Antarctica (and East Antarctica to a certain extent). From a relative point of view, Antarctic Peninsula SMB also appears to be the most variable from year to year, compared to the other regions. Finally, there is a steady increase in SMB throughout the EARLY period, whereas values remain quite constant between 1981 and 2010 (Fig. 4.11 & 4.13).

Figure 4.14: Surface mass balance anomalies (%) (normalized over 1981–2010) simulated by MARv3.12 forced by ERA5

In East Antarctica, in summer, SMB anomalies are mostly negative along the coast. Along the Transantarctic Mountains, the model produces higher SMB in the EARLY than in the REF period. During the other seasons, anomalies along the coast are of both signs and remain low during spring. In spring, there is also a change in sign of the positive anomalies found along the Transantarctic Mountain Range. Over East Antarctica, SMB is st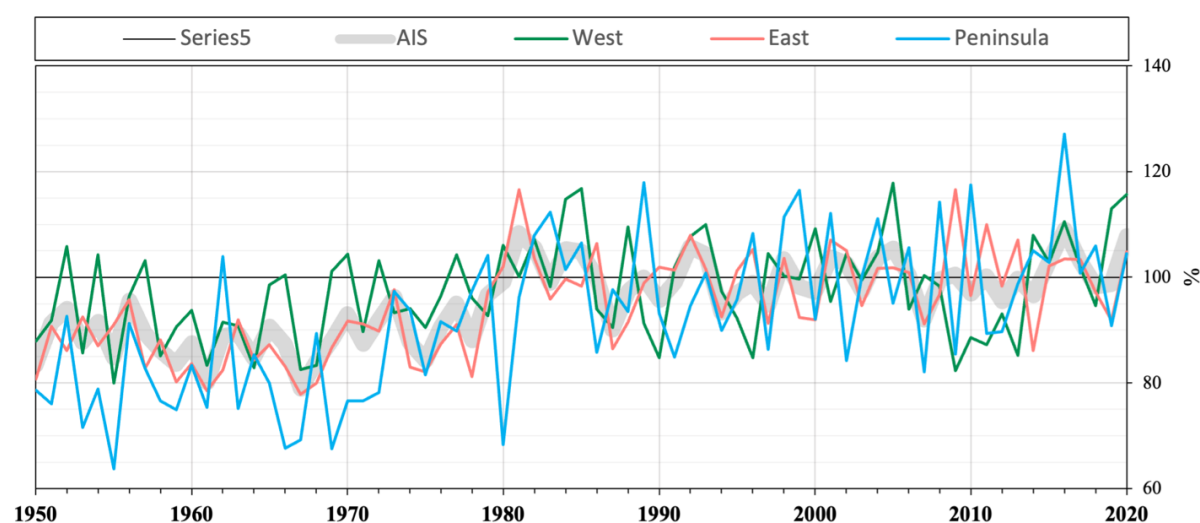ill highest during autumn and winter but the gap between the other seasons is less noticeable than for the other regions. Moreover, in the EARLY period, the amplitude of the anomalies across East Antarctica is not very pronounced compared to the other regions. Interestingly, we observe a slightly positive trend during the EARLY period and a steady negative trend during the second period. From 1951 onwards there was an increase until 1978, followed by a jump in temperature until 1980 and finally a steady decrease until 2010 (Fig. 4.11 & 4.13).

Finally, West Antarctica displays a large range of different anomalies, from being almost entirely negative in autumn and spring to a mix of both in summer and winter. Furthermore, MAR produces the same seasonal differences as for the other regions. In West Antarctica the difference between both periods is also the lowest. This might be due to the decreasing trend line in the REF period.

It is also worth mentioning that generally, the difference between surface mass balance in autumn, winter and spring and surface mass balance in summer is less pronounced in the REF period. In other words, during summer, the increase in SMB across both periods is less sharp than for the other three seasons (Tab. 4.3).

The jump in SMB between 1978 and 1980 that is visible on the chart displaying the entire AIS is less noticeable in West Antarctica and, as already mentioned, of opposite sign for the Antarctic Peninsula. In East Antarctica, however, the jump is substantially higher. Thus, the reanalysis might have more difficulties reproducing SMB over the eastern part of the continent (Fig. 4.14).

Surface mass balance over the Antarctic Ice Sheet corresponds largely to snowfall. Thus, the temporal and spatial patterns regarding SMB that were discussed above are also reflected in the snowfall trends. As a result, in order to better understand the behaviour of the surface mass balance and the changes between both periods, it is necessary to analyse the precipitation patterns, which in turn, are largely governed by large-scale atmospheric features.

4.2.1. Surface Melt

Antarctic surface melt has generally been attributed to the summer season, when melt energy is contributed by solar radiation (e.g., Munneke *et al*., 2018). Ice and snow at the surface of the AIS melts almost exclusively during summer (95%) (table x). Thus, any significant changes in surface melt between both periods occur during that season. However, during winter months, there are occurrences of surface melt on the Larsen C Ice Shelf as a result of the foehn winds bringing dry and warm air to the eastern part of the Antarctic Peninsula. At an Antarctic Peninsula station, Munneke *et al*. (2018) found that during austral winter, temperatures could reach beyond the melting point, thus contributing to around 23% of surface melt fluxes between 2014 and 2017.

Despite its modest size, the Antarctic Peninsula contributes to about 59% (61%) of the total surface melt over the AIS during the EARLY (REF) period (Tab. 4.4). The dominant surface melting in this region is linked to the higher near-surface temperature. This coincides with recent results, which reveal that the melt potential (based on air temperature) is the highest for the Antarctic Peninsula (Orr *et al.*, 2022). Surface melt happens in particular over the Larsen C Ice Shelf, on the eastern flank of the Peninsula and on its western flank, across the Wilkins and George VI Ice Shelf. To a certain extent, surface melt takes place along the coastline in other regions, notably in the eastern part of East Antarctica. MAR produces some surface melt at the western and eastern edge of the Ross Ice Shelf and none on the Antarctic Plateau, where temperatures are the lowest and tropical maritime air cannot penetrate.
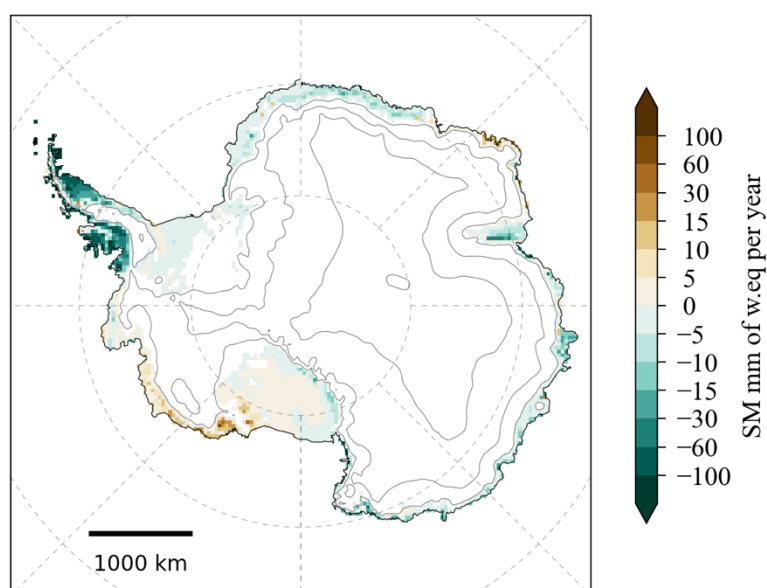
Figure 4.15: Summer surface melt anomalies (mm of water equivalent per year) for 1951–1980 compared to the 1981–2010 reference period for MAR$_{v3.12}$ forced by ERA5. Anomalies are only shown when surface melt is higher than 1 mm of w. eq. per year

Because surface melt is primarily observed across the Peninsula, this is where any substantial anomalies are found during the EARLY period. Across the three largest Peninsula ice shelves, we observe negative anomalies, thus an increase in surface melt over time. This is also highlighted by figure 4.16., where Peninsula surface melt anomalies are almost exclusively negative until 1979. Interestingly, the jump that was found for both surface mass balance and temperature occurs only from 1978 to 1979 and is not carried over into 1980. After the jump in 1979, surface melt dropped back down to the area of the PRE-79 mean. This could be attributed to the fact that for summertime near-surface temperatures, the jump also occurs only between 1978 and 1979. Nevertheless, between the EARLY and the REF period, there is an increase of about 20% in annual surface melt over the Peninsula. The negative SM anomalies across the Peninsula are congruent with the negative SMB and SAT anomalies found in that region. Moreover, the increase (decrease) between both periods in summertime near-surface temperature on the Antarctic Peninsula (Ross Ice Shelf) is also reflected by an increase (decrease) in surface melting. Although no significant change in surface melt has been found in between 1979 and 2010 (Munneke *et al.*, 2011) and our model produces a negative trend between 1981 and 2010, in 2019 and 2020, surface melt was anomalously high, with values reaching well above 100 Gt. With the increasing greenhouse gas concentration, both summer and winter melting are expected to increase in the coming years. Independent of the emission scenario, Trusel *et al.* (2015) predict a doubling of surface melt across the entire continent. The

likely cause of this increase in surface melt rates is twofold; (1) higher humidity and the resultant increase in downward radiation and (2) the reduction of the albedo (Donat-Magnin *et al.,* 2021). Moreover, meltwater almost exclusively refreezes in Antarctica, however, in some instances, it may lead to the formation of large ponds. These meltwater ponds exert a pressure on the ice shelves which may result in the (partial) collapse of the later (e.g., Munneke *et al*., 2018), especially in areas where ice shelves are more vulnerable to hydrofracture (e.g., Wilkins and Larsen C Ice Shelves) (Lai *et al*., 2020). This is relevant because ice shelves regulate the Antarctic contribution to sea-level rise by preventing ice flow into the ocean through their buttressing effect. Thus, a destabilization of the ice shelves caused by intensified melting, may have severe implications for the sea level.
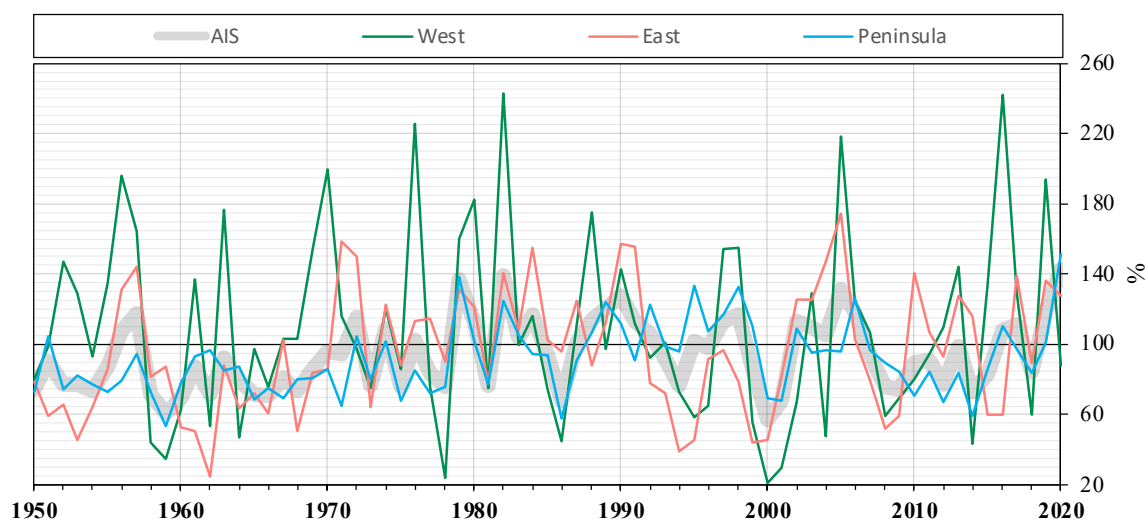
Figure 4.16: Surface melt anomalies (%) (normalized over 1981–2010) simulated by MARv3.12 forced by ERA5

Furthermore, while SM increases slightly during the EARLY period, there is a decrease of similar magnitude during the second period, with very low values found in 1986 (55 Gt) and in 2014 (56.5 Gt). After 2014, the model produced a sharp increase in melting, with record values in 2020 (144 Gt). In addition, to the mean annual SM increasing over time, interannual variability also experiences an increase, the REFERENCE period displaying more extremes.

Table 4.4: Annual and seasonal Antarctic surface melt (Gt/year) over 1951–1980 and 1981–2010. Standard deviations are given in brackets

Region	Year	Gt/year				
		Annual	Spring	Summer	Autumn	Winter
AIS	1951-1980	134.7 (27.4)	6 (3.8)	126.6 (28.1)	2.3 (1.7)	0.2 (0.1)
	1981-2010	154 (31.6)	6.8 (3.1)	143 (38.2)	3.9 (1.8)	0.3 (0.1)
West	1951-1980	12.7 (5.9)	0.1 (0.1)	12.6 (7)	0 (0)	0 (0)
	1981-2010	11.1 (5.8)	0.2 (0.3)	11 (6.8)	0 (0)	0 (0)
East	1951-1980	37.3 (14.3)	0.4 (0.5)	37.2 (16.8)	0 (0)	0 (0)
	1981-2010	42.2 (16.2)	0.6 (0.8)	41.8 (18.9)	0 (0)	0 (0)
Peninsula	1951-1980	79.6 (15.4)	5.4 (3.5)	71.7 (13.6)	2.3 (1.7)	0.2 (0.1)
	1981-2010	95.4 (18.7)	6 (3.1)	85 (22.3)	3.9 (1.8)	0.3 (0.1)

Across East Antarctica, we find a slight increase in surface melt (4.6 Gt/year) and interannual variability (2.1 Gt/year), which is illustrated by negative anomalies along the coastline. Finally, MAR produces positive anomalies for the EARLY period in the western part of West Antarctica, along the shore and to a certain extent at the edge of the Ross Ice Shelf. In this area, positive SAT anomalies are also found during summer, which could explain the higher-than-normal SM. This is also highlighted by the fact that mean summer surface melt in West Antarctica decreases between the EARLY (12.6 Gt/year) and the REF period (11 Gt/year). The amplitude of year-to-year surface melt in West Antarctica is also substantially higher than for the other regions, resulting in high amplitudes of anomalies (Fig. 4.16). This behaviour might be influenced by the position and strength of the Amundsen Sea Low and should be investigated further. Scott *et al.* (2018) found that extreme events of surface melt in the Ross-Amundsen sector are linked to prolonged periods of blocking anticyclones in the Amundsen Sea. They identified the advection of warm moist air from the ocean, cloud cover and the resultant increase in downwelling LW radiation, a reduction in offshore sea ice cover and Foehn winds as the main drivers of surface melting in West Antarctica.

4.2.2. Sublimation

Sublimation refers to the (generally direct) transition of a substance from the solid to the vapour phase. The opposite would be deposition and is by definition the transition from the vapour to the solid phase (van den Broeke, 1997). Although sublimation is more prevalent over temperate glaciers or even the Greenland Ice Sheet, sublimation over the AIS should not be discarded when considering the mass balance. Good conditions for sublimation include low relative humidity, dry and strong winds, strong sunlight, and high air pressures. Sublimation over the

ice sheet can either happen directly from the deposited snow at the surface or from snow particles that are suspended into the air as a result of high wind speeds (e.g., katabatic winds) (King *et al*., 2001). In addition, recent studies have highlighted the presence of a third type of sublimation, the low-level sublimation of precipitation, thus significantly reducing snowfall accumulation, especially on the margins of East Antarctica (e.g., Grazioli *et al*., 2017). Although the rate of mass losses through the second mechanism should be very high, the conditions for drifting snow are often linked to high relative humidity, thus hindering effective sublimation (King *et al.,* 2001). Nevertheless, Amory and Kittel (2019) found that in Adélie Land, an area where strong katabatic winds and the subsequent drifting snow occur frequently, saturation is mostly confined to a thin layer no higher than 1 m above ground. Earlier papers (e.g., Loewe, 1962) suggested that the contribution of sublimation and deposition to the mass balance is negligible. However, while sublimation remains low in areas such as the Antarctic Plateau, in coastal areas on the AIS, sublimation is enhanced by the strong katabatic winds (van den Broeke, 1997). Dry air advection is strengthened by these katabatic winds that are especially strong in coastal regions where the plateau encounters a sharp drop, thereby favouring sublimation.
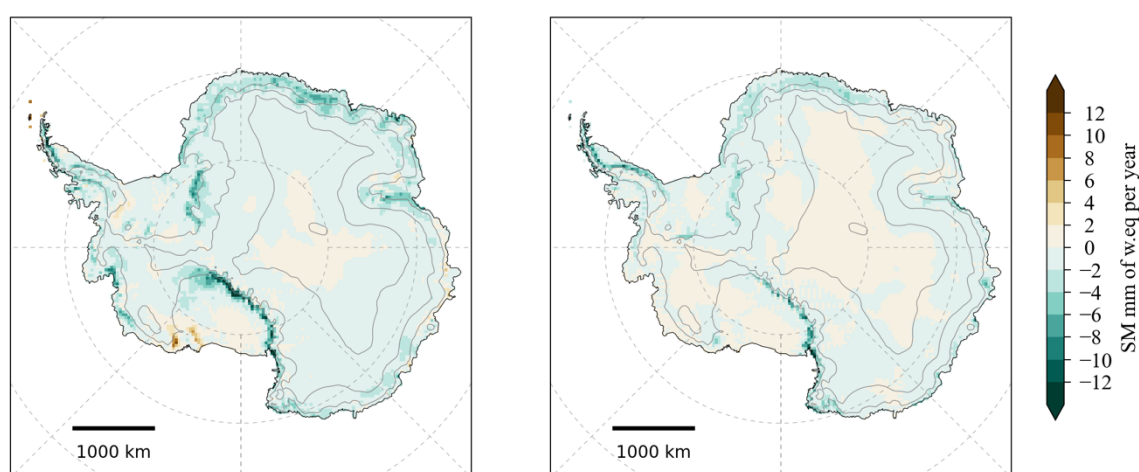
Figure 4.17: Sublimation anomalies (mm of water equivalent per year) for 1951–1980 compared to the 1981–2010 reference period for austral summer (left) and spring (right) from MAR$_{v3.12}$ forced by ERA5

Sublimation occurs almost exclusively along the coastline, with values surpassing 100 mm of w.eq. per year in some areas (Fig. 1.8). The total sublimation is the highest in East Antarctica (119/136 Gt) (Tab. 4.5). Spatial differences in sublimation along the East Antarctica coast can be explained by dry air advection discrepancies. On the Antarctic Plateau, the criteria for sublimation (low relative humidity, strong wind and sunlight, high air pressure) are not met, thus hardly any to none occurs. On the large Ross and Ronne Ice Shelves and inland in West Antarctica, negative sublimation (deposition) takes place. Over the Antarctic Peninsula, we

also find contrasting values between inland and coastal regions. Although the coarse resolution may have difficulties in reproducing small-scale processes over the Peninsula, sublimation appears to be consistent, with high values along the coast and deposition along the ridges (Fig. 1.8).
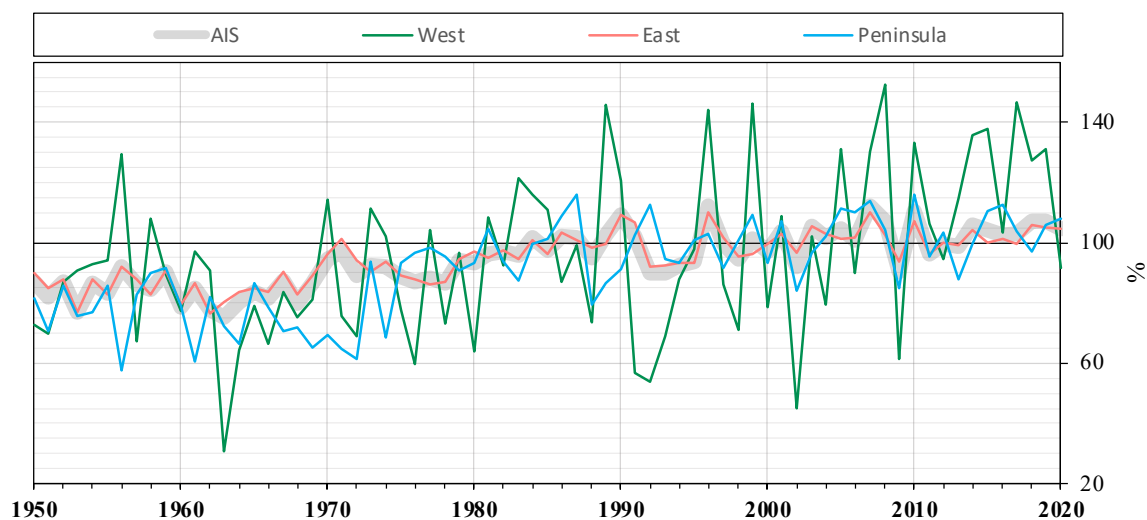
Figure 4.18: Sublimation anomalies (%) (normalized over 1981–2010) simulated by $MAR_{v3.12}$ forced by ERA5

In addition to the spatial distribution, as already determined by previous studies (e.g., van den Broeke, 1997; King *et al*., 2001), sublimation in Antarctica develops primarily during summer and is negligible during winter months. During winter, sublimation is either very low (East Antarctica) or negative (West Antarctica, Peninsula).

Differences in mean annual sublimation between the two periods in question are mainly found close to the coastline in East Antarctica, over parts of the Peninsula and along the Transantarctic Mountains, at the edge of the Ross Ice Shelf (Fig. 4.17). As for surface melt, in relative terms, the highest amplitude in anomalies is observed for West Antarctica as displayed by figure 4.18. Moreover, from the EARLY period to the REF period, there is an increase of around 17 Gt/year, while interannual variability displays a slight decrease (Tab. 4.5).

Table 4.5: Annual and seasonal Antarctic sublimation (Gt/year) over 1951–1980 and 1981–2010. Standard deviations are given in brackets

		Gt/year				
Region	Year	Annual	Spring	Summer	Autumn	Winter
AIS	1951-1980	139.1 (9.1)	39.1 (5.6)	99.2 (7.5)	3.1 (2.4)	-1.9 (1.8)
	1981-2010	161.2 (10.3)	44.9 (4.9)	111.8 (7.2)	4.9 (2.7)	-0.4 (2.4)
West	1951-1980	9.8 (2.3)	4.5 (1.4)	14.8 (1.5)	-5.1 (1.1)	-4.3 (0.8)
	1981-2010	11.6 (3.5)	4.9 (1.3)	16.7 (2.2)	-5.2 (1.1)	-4.8 (0.9)
East	1951-1980	119.4 (8)	31.3 (4.5)	73 (6.5)	10.6 (1.8)	4.8 (1.6)
	1981-2010	136.2 (7.3)	35.5 (4)	82.1 (6.2)	12.1 (2.2)	6.5 (2.1)
Peninsula	1951-1980	9.3 (1.4)	3.2 (0.7)	8.4 (0.7)	-0.9 (0.5)	-1.4 (0.5)
	1981-2010	11.7 (1.2)	4.1 (0.7)	9.3 (0.8)	-0.6 (0.6)	-1.1 (0.4)

It is also worth mentioning that surface sublimation reduces accumulation by snowfall by about 15%. Van den Broeke (1997) found that surface sublimation may remove 10–15% of accumulation by snowfall, while King *et al.* (2001) found even higher rates (25%) when taking into account sublimation of blowing snow. Moreover, despite an increase in snowfall, the ratio of sublimation to snowfall does not decrease and even shows signs of slightly increasing (Fig. 4.19). This indicates that growing precipitation over the AIS might not result in equal amounts of accumulation due to other processes that are involved.
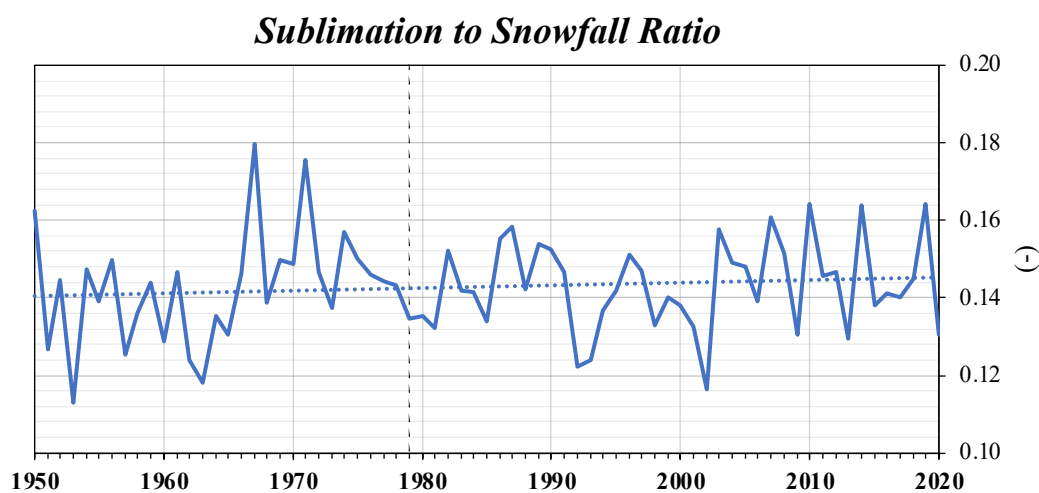

Figure 4.19: Sublimation to snowfall ratio simulated by MAR$_{v3.12}$ forced by ERA5

4.3. Climate response to large-scale atmospheric features

4.3.1. SAM-SAT relationship

The relationship between the Southern Annular Mode and Antarctic near-surface temperature has been thoroughly assessed in past studies (e.g., Thompson & Solomon, 2002; Marshall, 2007). The generally observed relationship which was identified in these studies are higher near-surface temperatures across the Peninsula when the SAM is in its positive phase, while the rest of the continent experiences colder than usual temperatures. Until recently, the analysis has been restricted either spatially, when observation-based temperatures were used, or temporally, when reanalysis data were used. Using the newly released ERA5 back extension, it has become possible to benefit from the spatial coverage of a reanalysis dataset, while using a longer period than in the past was only accessible with observations.
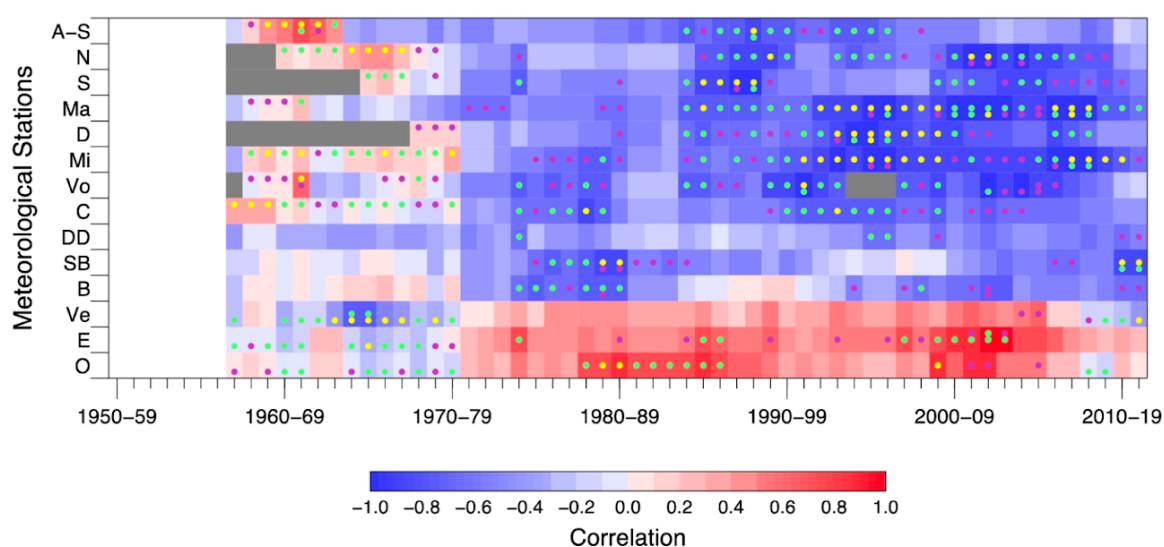
Figure 4.20: Correlations between the decadal running observation-based annual SAM index and annual mean SAT (°C) at 14 Antarctic meteorological stations (from Marshall *et al.*, 2022)

Although the SAM-SAT relationship described could be observed in past few decades, a clear switch in the relationship in the late 70s has been spotted in recent studies (e.g., Turner et al., 2020; Marshall et al., 2022). This change is highlighted by figure 4.20, representing the decadal correlation between observed near-surface temperature and the observation-based SAM index. The switch appears to happen a few years earlier in some areas (e.g., Amundsen Scott) and not at all for others (e.g., Durmont d'Urville). In addition to the sudden shift in the correlation sign, the magnitude of the latter is also lower in the EARLY period. Marshall et al. (2022) reproduced that same figure using 3 different reanalyzes (ERA5, 20CRv3 & JRA-55)

(Fig. 4.21). They found that ERA5 performs the best among all 3 reanalyzes. Thus, it would be interesting to see whether MAR produces satisfactory results when forced by ERA5.
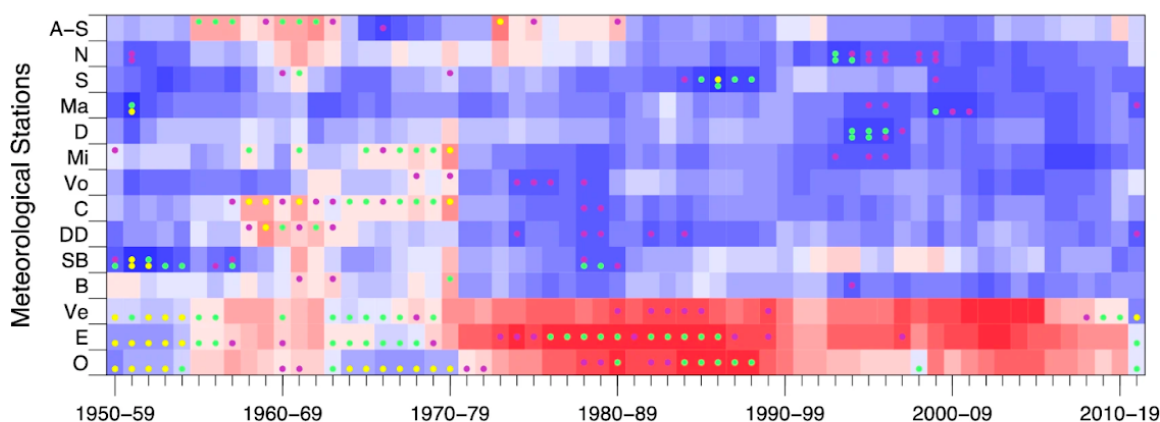
Figure 4.21: Same as figure 4.20 but using ERA5 generated SAT and SAM values (from Marshall *et al.*, 2022)

Using detrended data, the correlation coefficient between the SAM index and Antarctic near-surface temperature was determined. In order to minimize uncertainties, the observation-based SAM index as defined by Marshall (2003) was used. The SAM index is defined as the difference in normalized mean zonal pressure at 40 °S and 65 °S. For near-surface temperature, the values produced by MAR (forced by ERA5) were used. In both cases, detrended data was used, based on the assumption that the linear trend of the predictor (SAM) and predictand (SAT) are not directly linked. Figure 4.23 highlights the fact that after 1979, MAR properly reproduces the spatial correlation observed in figure 4.20, i.e. a positive SAM-SAT correlation is found over the Peninsula, while the rest of the continent (especially East Antarctica) displays negative correlation values.
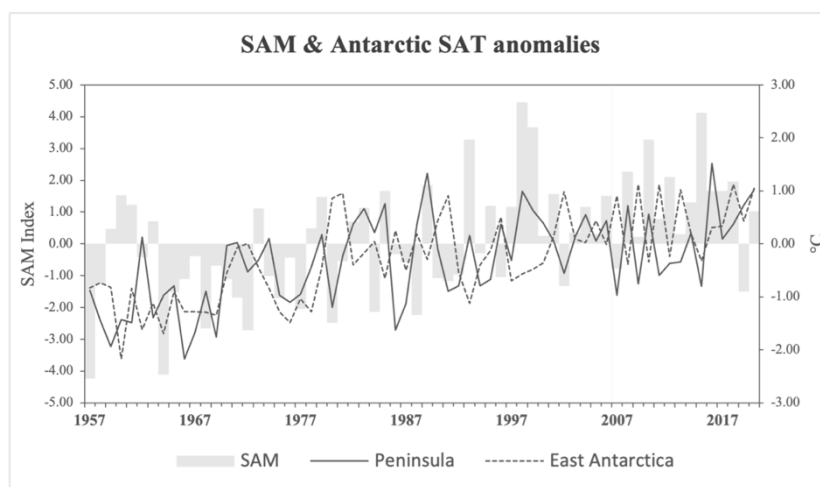
Figure 4.22: Observation-based SAM index (from Marshall, 2003) and mean annual near-surface temperature (°C) in East Antarctica (dashed line) and over the Antarctic Peninsula (straight line)

The same was then established for the ERA5 back-extension period (prior to 1979) (Fig. 4.24). Since the observation-based SAM started in 1957, years before 1957 were not included. Overall, the SAM-SAT relationship is a lot weaker in the years prior to 1979, a fact already observed by Marshall *et al.* (2022). Over parts of the eastern side of the Peninsula, the observed reversal in sign of the SAM-SAT relationship appears to be present. Moreover, for most West Antarctic stations, the reversal is also properly reproduced by MAR (e.g., Mirny, Davis, Casey). However, for some stations MAR produces a reversal, although none was observed (e.g., Mawson, Dumont d'Urville) or does not reproduce the observed switch (e.g., Byrd). Interestingly, MAR produces the reversal in the SAM-SAT observed in East Antarctica almost exclusively in coastal areas, except for a region on the Antarctic Plateau between Amundsen Scott and Vostok. Because most stations are located along the coast, it is difficult to evaluate whether this pattern is correct or a result of the model failing to properly represent the SAM-SAT relationship inside the continent. When mapping the SAM-SAT relationship using ERA5 near-surface temperature, the same spatial pattern is revealed. Only the positive correlations in the eastern part of the Peninsula are not produced by ERA5 and correlations are slightly more significant in East Antarctica, whereas the opposite is true in West Antarctica.

Figure 4.23: Correlation Coefficient between the detrended observation-based SAM index and near-surface temperature (°C) from MARv3.12 forced by ERA5 (left) and from ERA5 (right) over 1979-2010. Black circles indicate the locations of the stations used in figure 4.20

Moreover, the fact that hardly any observations from the Antarctic Plateau, nor any satellite data is available before the late 70s suggests that the reanalysis itself and as a result the model produces large uncertainties in that area. At the same time, the Antarctic Plateau is relatively flat, making it easier to both predict and reproduce dynamic processes, thus suggesting that the model results may be trusted. Either way, both figures yield interesting results and open new pathways towards further research.
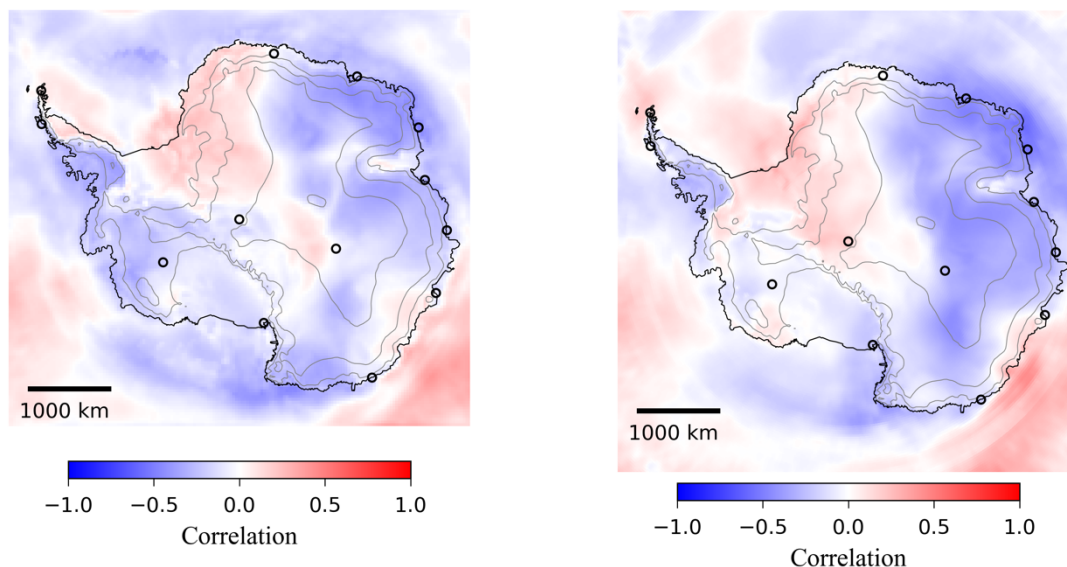
Figure 4.24: Same as figure 4.23 but for 1957–1978

In addition to the switch observed in the late 70s, figure 4.20 also displays a recent weakening and to some extent, a reversal in the sign of the SAM-SAT relationship across the Antarctic Peninsula and possibly on the Antarctic Plateau (Amundsen Scott). Interestingly, MAR is able to reproduce this evolution over the Antarctic Peninsula (in particular on the western side) (Fig. 4.25). The weakening of the relationship and even reversal in the area around Amundsen Scott is also visible. Moreover, in East Antarctica, just west of the Peninsula, there is a large area, partly covering the Ronne Ice Shelf, where correlations have turned slightly positive. Although this period is very recent and the reanalysis is more reliable, it's a fairly short period for analysing the response of the climate to large-scale variability features. The results need to be considered with prudence because this may just be a temporal feature with little effect when integrated over the entire period.
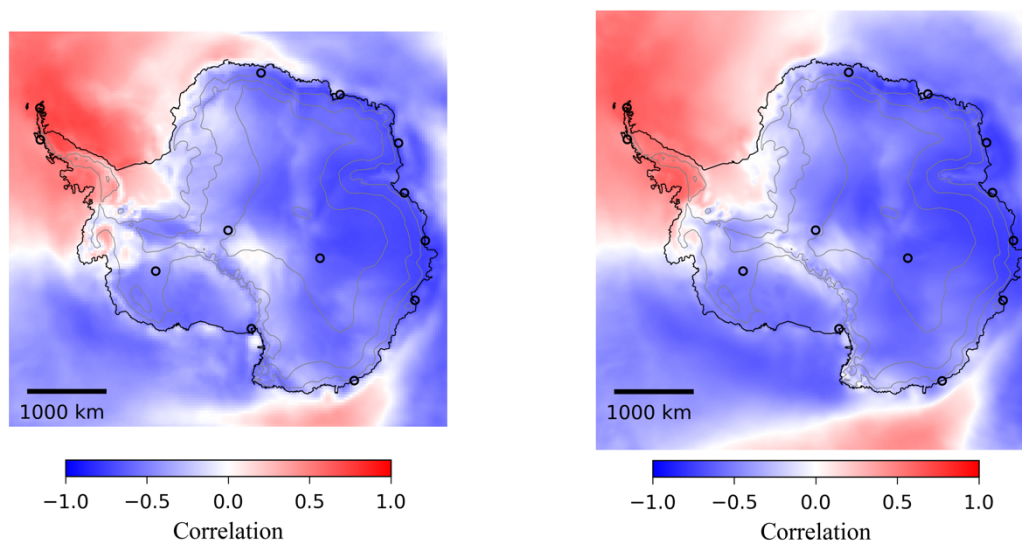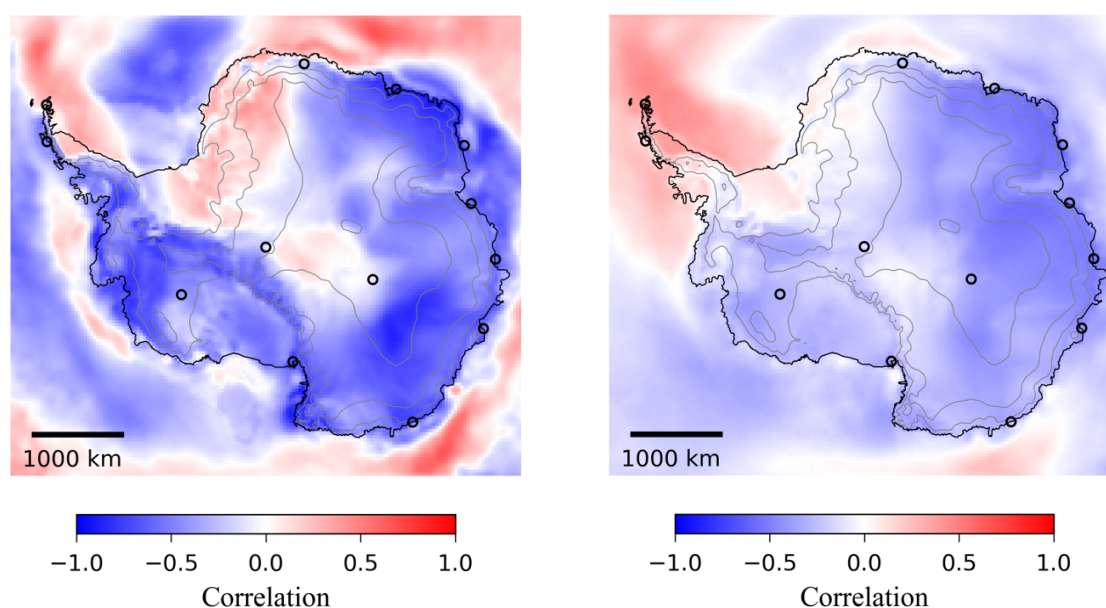
Figure 4.25: Correlation Coefficient between the detrended observation-based SAM index and near-surface temperature (°C) MARv3.12 forced by ERA5 over 1957–2019 (right) and 2010–2020 (left). Black circles indicate the locations of the stations used in figure 4.20

When simulating the seasonal SAM-SAT relationship for 1957–2019 with MAR, we find that in terms of size, seasonal correlations are similar to annual correlations (Fig. 2.25). MAR also generally reproduces the seasonal characteristics that were found in past studies (e.g., Marshall, 2007). In general, the spatial pattern (negative correlation across East Antarctica and positive correlation across the Peninsula) is also observed in all four austral seasons. Marshall (2007) did, however, find some seasonal differences in the magnitude, significance and even sign of the observed correlations. Correlations in autumn are close to the annual situation (same for winter but slightly weaker correlations and significance). In spring, Marshall (2007) found a slightly weaker correlation over the Peninsula, while during summer, the correlation for Esperanza (Northern Peninsula) and East Antarctic correlations are very high. The high summer correlation across the northern Antarctic Peninsula is associated with westerly warm air advection, as explained by Marshall *et al.* (2006). Moreover, during austral summer, Clem et al. (2016) found SAM-SAT correlations of opposite sign between the northeast and western Peninsula, a pattern also captured in this study. Thus, when considering the SAM-SAT relationship over the entire Antarctic Peninsula as a whole, correlations appear weak. Although the cause of this relationship is not yet entirely clear, it is most likely related to the nature of the westerly flow (associated to a positive SAM) during summer (Fig. 4.26).

Figure 4.26: Same as figure 4.25 (right) but for austral summer (upper-left), autumn (upper-right), winter (lower-left) and spring (lower-right)

4.3.2. SAM-SMB relationship

Regarding the SAM-SMB relationship, there are some conflicting results in the scientific literature. Donat-Magnin *et al.* (2020) did not find a significant relationship between the Southern Annular Mode and West Antarctic surface mass balance (nor surface melt) for 1979–2017 (during summer). Medley and Thomas (2019) on the other hand found that Antarctic accumulation rates were somewhat influenced by the sign of the SAM. However, they only considered the relationship annually and the large-scale modes of variability (including SAM) can display significant seasonal discrepancies. Thus, in order to gain some more insight on the matter, the SAM-SMB relationship was computed for the longer 1957–2020 period, annually but also separately for each season. The correlation coefficient represented in the figures below are based on the modelled SMB and the observation-based SAM index. As for near-surface temperature, detrended time series were used.
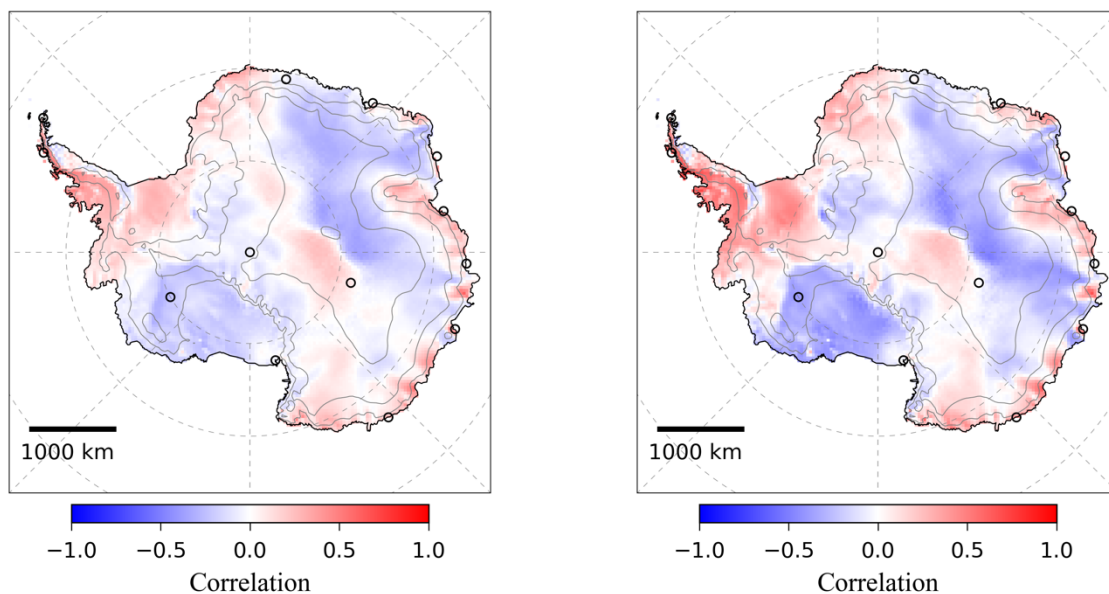
Figure 20.27: Correlation Coefficient between detrended observation-based SAM index and simulated surface mass balance for 1957–2019 (left) and 1979–2019 (right)

Interestingly, as for near-surface temperature, correlations increase when discarding the period prior to 1979. Once again, this could either be the result of unreliable reanalysis data or evidence for a change in the influence that SAM has on Antarctic climate that occurs in the late 70s. Marshall *et al.* (2017) found that a positive SAM causes an increase in precipitation, primarily over the western part of the continent. The Antarctic Peninsula is also affected by this, however, only over the western parts because stronger westerly winds encountering the

elevated terrain enhance the foehn effect, reducing moisture as air passes over the mountainous terrain. The same pattern is displayed by the figures above, although part of West Antarctica, especially in the Ross Ice Shelf area yield negative correlations.

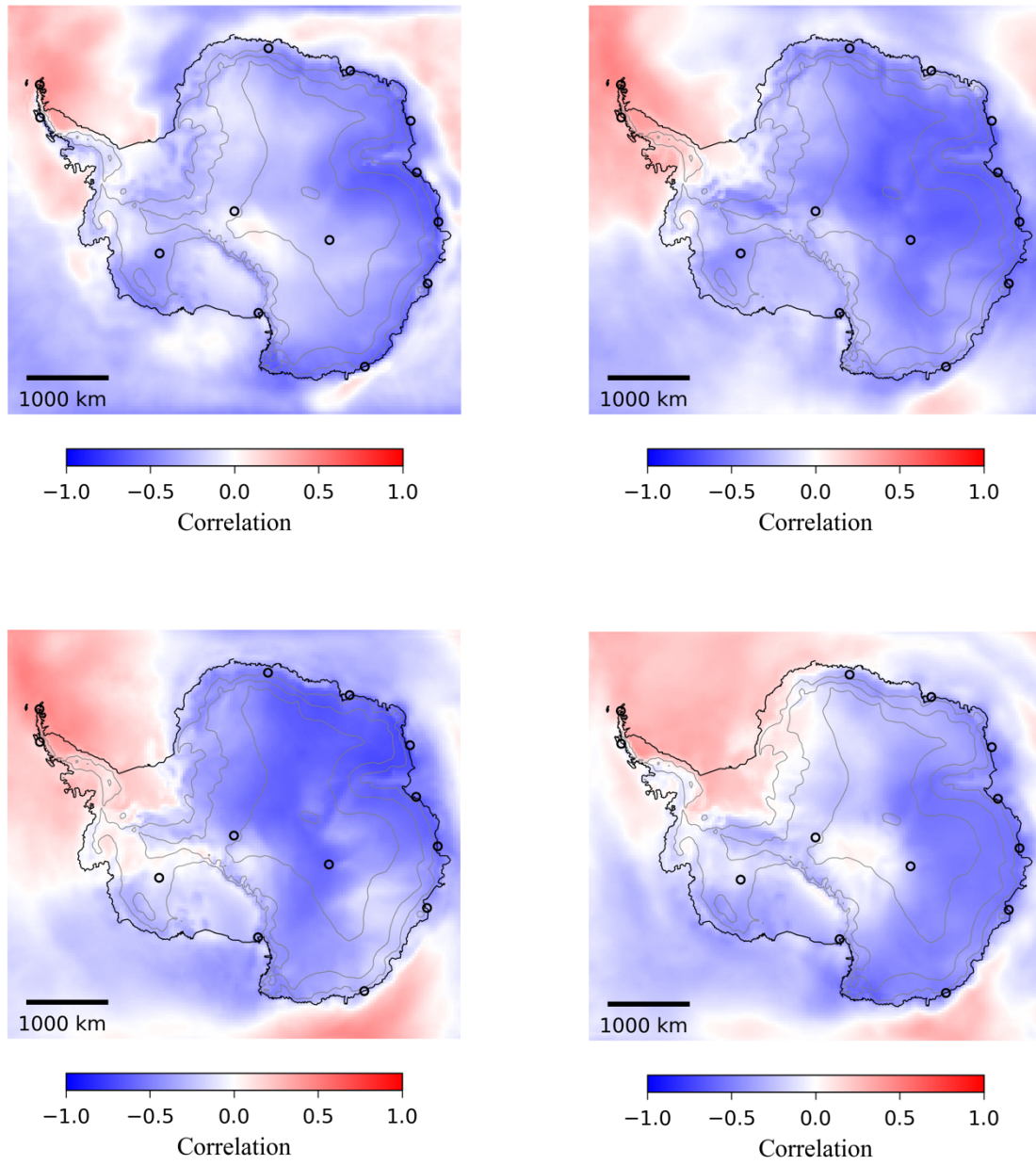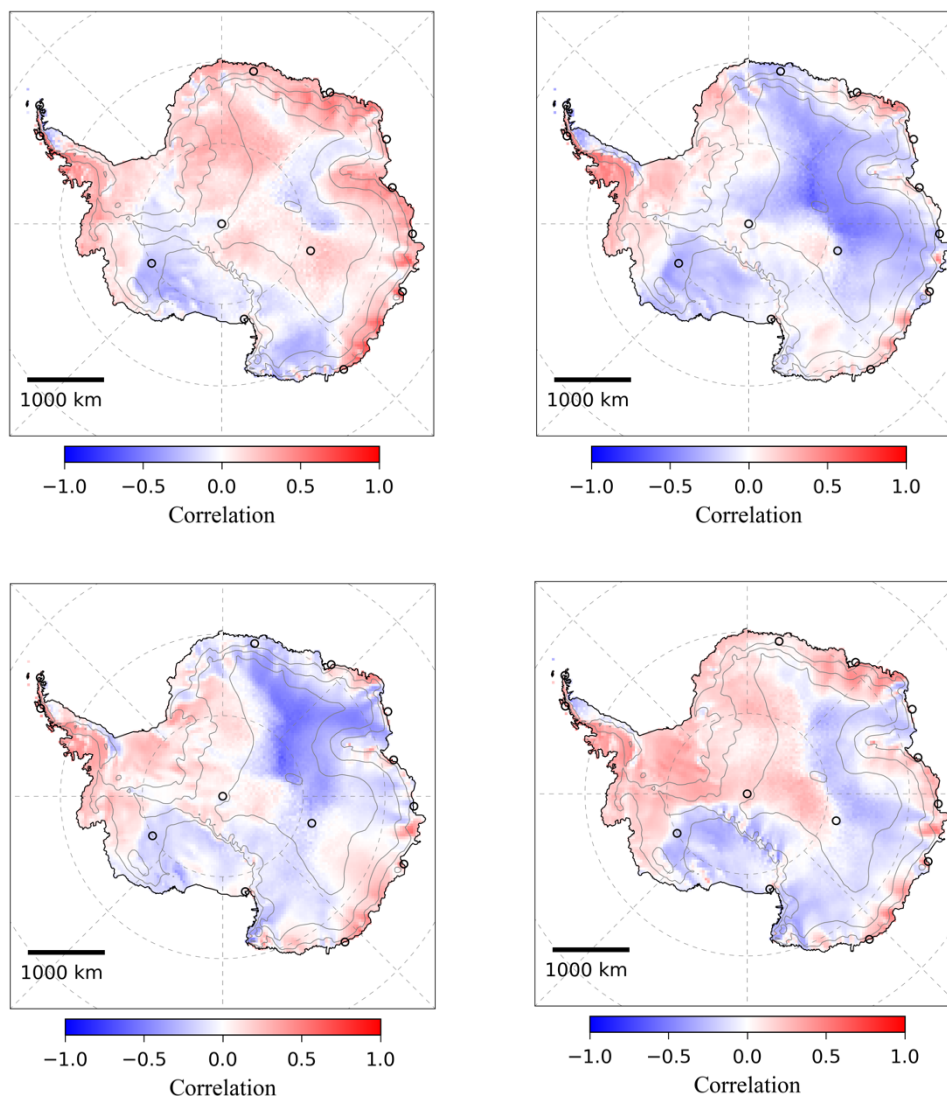**Figure 4.28:** Same as 4.27 (right) but for austral summer (upper-left), autumn (upper-right), winter (lower-left) and spring (lower-right)

There are also significant seasonal differences in the spatial correlation with the observation-based SAM index (Fig. 4.28). However, although some areas exhibit higher correlations than others, overall, the relationship is a lot less pronounced than the SAM-SAT relationship. Across the Peninsula, the situation remains consistent all year long, with positive correlations on the windward side and negative correlations on the leeward side. This contrast is especially marked during the autumn months. In West Antarctica, the relationship also remains mostly the same. In East Antarctica, however, the relationship is primarily positive along the coastline but during

autumn and winter there are large areas where a SAM in its positive phase favours lower surface mass balance.

Using ERA5 to force MAR over a longer period, some insight on the relationship between the SAM and Antarctic climate was gained, in particular on the temporal differences of the spatial patterns and the seasonal differences of the SAM influence on near-surface temperatures. Although the results are generally in agreement with the scientific literature, they need to be considered carefully. As already empathized earlier, reanalysis data is unreliable prior to the satellite area. Moreover, over large parts of the interior of the continent, no observation values exist for comparing the modelled results. Further research, with a deeper analysis of the SAM-SAT relationship may be necessary. Nevertheless, despite the gradual improvement of models (by better representing complex mechanisms and increasing the resolution), the limits regarding the past SAM-SAT relationship appear to be reached.

4.3.3. ENSO-SMB relationship

In addition to the Southern Annular Mode, the El Nino/Southern Oscillation (ENSO) has also been studied, in particular regarding its influence on variables governing the ice sheet mass balance (e.g., Paolo *et al.* (2018), Donat-Magnin *et al*. (2020). The advantage of studying the effect of ENSO compared to the SAM is the higher reliability of the observation-based index that we use, as well as the longer usable timespan (1951-present) (SOI). However, mechanisms through which both El Niño and La Niña affect Antarctica are relatively complex. Since ENSO primarily influences the weather regimes in the Pacific sector, we only consider West Antarctica for assessing the ENSO-SMB relationship. A simple representation of the relationship between the sign of ENSO and West Antarctic surface mass balance is represented by figure 4.29. Generally, we find anomalously high SMB values during years dominated by El Niño events, whereas the opposite is true for years when La Niña is dominant. This can be explained by how ENSO affects the Amundsen Sea low, a permanent area of low pressure situated across the Bellingshausen, Amundsen, and Ross Sea.

SOI & West Antarctic SMB anomalies
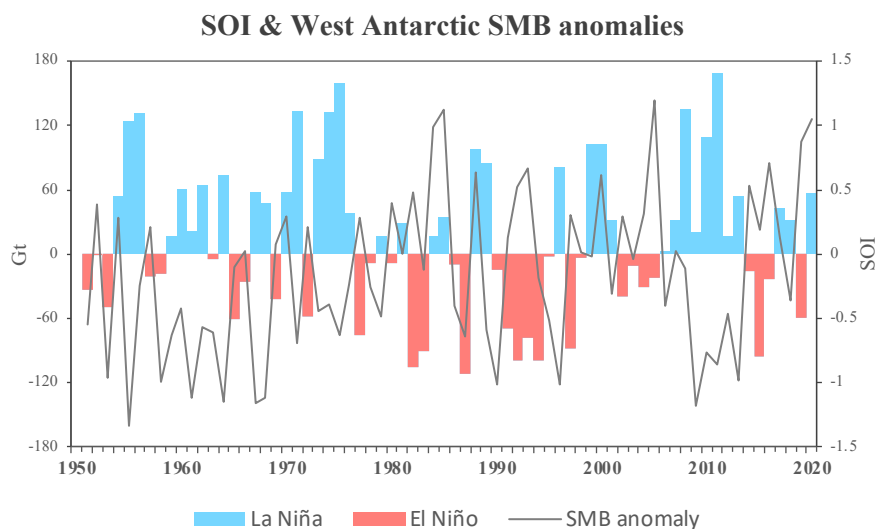
Figure 4.29: Observation-based SOI index and simulated West Antarctic surface mass balance (Gt) over 1951–2020

El Niño events favour an increase in snowfall, while La Niño is generally associated with periods of lower snowfall. Although generally, that pattern is displayed by figure 4.29, for some years, this is not the case. This should not necessarily be attributed to the MAR producing erroneous SMB values. In short, while the explanations for the ENSO-SMB relationship given above may generally apply theory, in reality the relationship is not always as straightforward and may be influenced by other factors. For instance, since SAM and ENSO display significant correlations (e.g., Scott et al., 2018; Fogt et al., 2011), some authors assessed the SAM/ENSO-Climate relationship after removing the influence of either SAM or ENSO, in order to evaluate their relative influence separately (e.g., Clem *et al.*, 2016; Donat-Magnin *et al.*, 2020).

Figure 4.30: Correlation Coefficient between the detrended observation-based SOI index and simulated surface mass balance for 1951–2020 (left), 1979–2020 (middle) and 2000–2020 (right)

Above, the ENSO-SMB relationship is also represented spatially, for three different timespans (Fig. 4.30). There appears to be no significant change in correlation when adding the PRE-79 period. A shorter but more recent period (2000–2020) is also displayed, where we can see higher rates of anticorrelation, but the positive correlations at the base of the Antarctic

Figure 4.31: Correlation Coefficient between the detrended observation-based SOI index and simulated surface mass balance for 1979–2019 (summer-autumn-winter-spring)

Peninsula also increase.

When considering the seasons separately, winter and summer months stand out as having lower absolute values of correlation. During autumn, ENSO and SMB correlate slightly better and the strongest relationship is displayed in spring. The generally lower seasonal correlations values, as well as the differences between each season highlight the complexity of the matter. Studies have highlighted the existence of a lag of several weeks to months, i.e. some of the effects of ENSO may be visible only months later across Antarctica. Looking at figure 4.31, West Antarctic anticorrelation during summer increases slightly when considering a 3–6 month-long lag (Fig. 4.32). Moreover, the propagation mechanisms through which ENSO influences the West Antarctic climate can be slowed down depending on the season, thus resulting in different correlations. In short, the ENSO-SMB relationship cannot be represented by a simple correlation and more in-depth studies, making use of the longer period simulated by regional climate models need to be carried out.
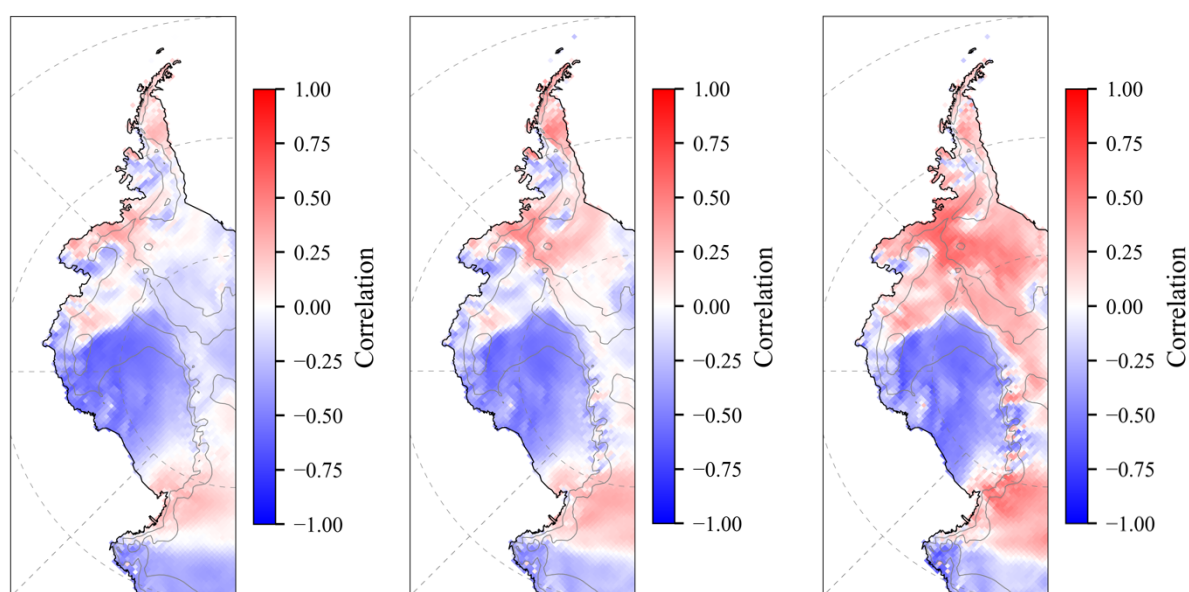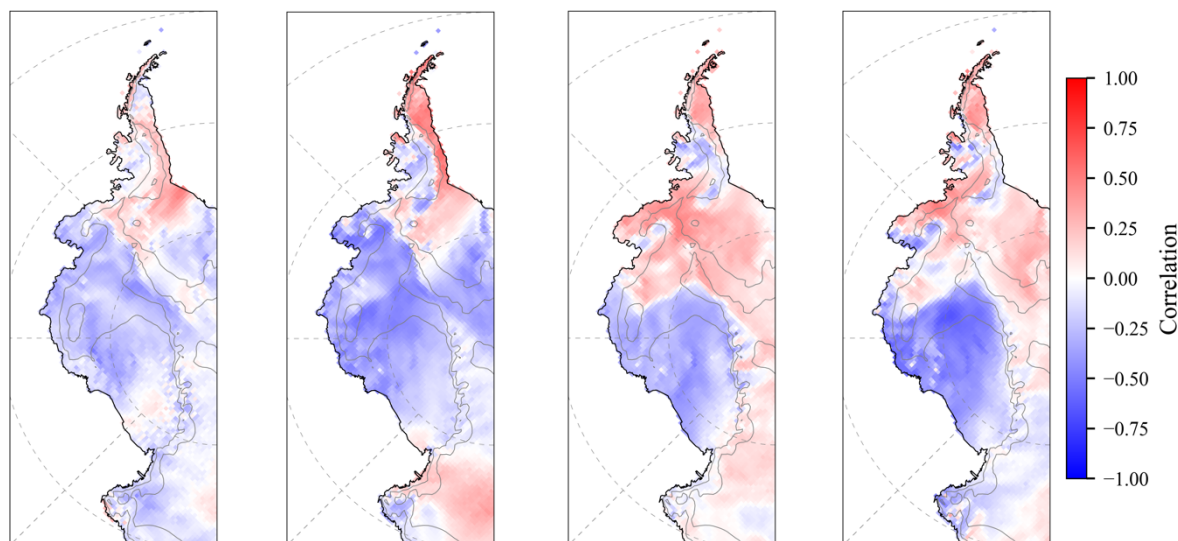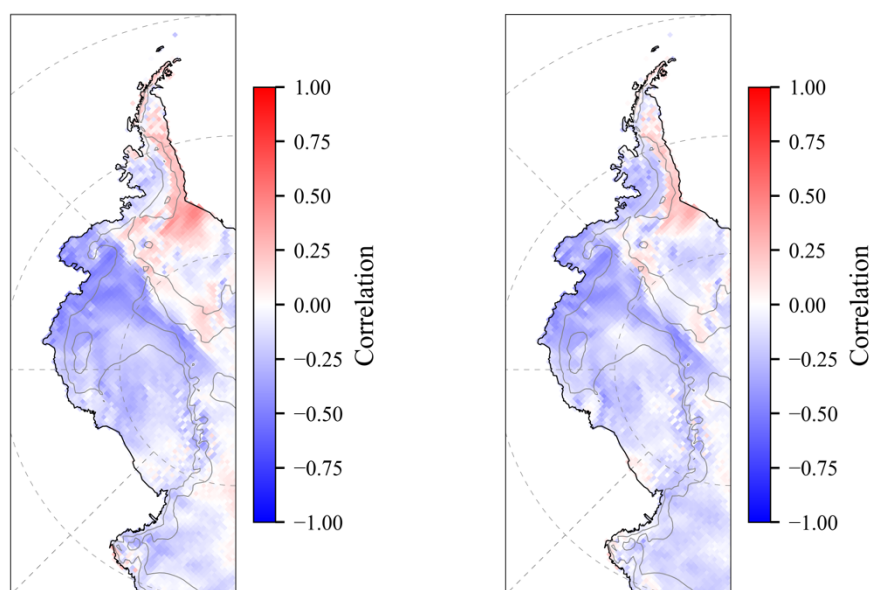
Figure 4.32: Correlation Coefficient between the detrended observation-based ENSO index and simulated surface mass balance for 1979-2019 (summer) using a 3-month (left) and 6-month (right) lag

4.4. Chapter Discussion

Few studies exist describing the evolution of the climate prior to the late 70s. Most studies spanning over longer periods either use ice cores (e.g., Medley & Thomas, 2019), which may display large uncertainties or observations from stations (e.g., Turner et al., 2020), which although being more accurate are limited spatially and can often describe the climate only locally. Nevertheless, it is valuable to compare the general trends produced by MAR when forced by ERA5 to the results of past studies.

The increasingly positive SAM should result in a decrease of temperature in East Antarctica, but this was neither displayed by annual station-based values (Turner *et al.,* 2020) nor by MAR when forced by ERA5. This may be the result of a counterbalancing effect such as increasing greenhouse gas emissions. However, seasonally, the model was able to capture this effect. The modelled cooling during autumn in parts of East Antarctica, as well as the pronounced cooling in summer (1–2 °C) in West Antarctica (notably in the Ross Sea area) and to a certain extent during autumn has been identified in past studies (e.g., Nicolas & Bromwich, 2014) and may be attributed to the increasingly positive phase of the SAM in summer and autumn.

Spring is the only season, during which an increase in near-surface temperature between 1951–1980 and 1981–2010 is found across the entire Ice Sheet. This Antarctic-wide warming during spring has also been highlighted by Turner *et al.* (2020). Moreover, some of the pronounced negative or positive anomalies are also reflected in station-based temperatures. The anomalously warm temperatures in 1956 and 1989 were also measured by all the Antarctic Peninsula stations. Interestingly, there are differences in interannual variability between the western and eastern side of the Peninsula that were not captured by the analysis that only considered values at a regional scale. Temperature variability around the Peninsula is strongly affected by sea ice concentration (e.g., Turner *et al.*, 2020), which is in turn affected by the depth and location of the Amundsen Sea Low (e.g., Hosking *et al.,* 2013). The Foehn winds associated with a stronger westerly flow also play a role, but their impact remains mostly short term. As highlighted by Turner *et al.* (2020), we also found that for the Peninsula, interannual variability of near-surface temperature is higher than for East Antarctica.

Finally, station-based values also reveal anomalously high temperatures in 1980 in East Antarctica and on the Antarctic Plateau, however, contrary to the modelled values, mean temperatures drop back down to the PRE-79 mean (Turner *et al.,* 2020). This points once again to the hypotheses that the modelled warming between 1951–1980 and 1981–2010 is (at least to a certain extent) artificial.

Monaghan *et al.* (2006) found no significant increase in snowfall accumulation between 1955 and 2004. These conclusions were made by using model simulations in conjunction with ice core observations. Between 1951–1980and 1981–2010, MAR (when forced by ERA5) produces a total increase of around 300 Gt/year of SMB, with areas where above 200 mm of w. eq. per year is found. However, the large increase our analysis exhibits are probably largely artificial, and a result of the pronounced jump observed in the late 1970s. The results from Medley and Thomas (2019) are also partially in agreement with our findings. Using ice core date, they found an accumulation rate trend up to values above 15 mm w. eq. yr^{-1} $decade^{-1}$ for the Antarctic Peninsula between 1957 and 2000, with values of opposite sign in the Ross Sea sector. In these regions we found an increase and decrease respectively in surface mass balance between 1951–1980 and 1981–2010. However, they also found a decrease in the accumulation rate along the coastline in the eastern part of East Antarctica, a pattern not found in our analysis. It is worth noting though that in that particular region, only 2 ice core measurements were used in the reconstruction.

The results presented in the section on the SAM-SAT relationship after 1979 are generally in good agreement with the scientific literature (e.g., Marshall, 2003; 2006). This is both true from an annual point of view but also when considering each season separately. For instance, as also illustrated by figure 4.23, Scott *et al.* (2018) found that high summer temperatures in West Antarctica are generally favoured by a negative phase of the SAM. We also compared the correlation between both variables before 1979 and identified a pronounced switch in the relationship that has been pointed outed out recently (e.g., Turner *et al.*, 2020; Marshall *et al.*, 2022). More recent changes in the relationship between the SAM and near-surface temperature have been attributed to changes in the SAM structure which may in turn be affected by large-scale alterations of the variability of the sea-surface temperature (e.g., Marshall *et al.*, 2009; 2013; Wachter *et al.*, 2020), which may also be the cause for the shift found in the late 1970s (Marshall *et al.*, 2022).

The results regarding the relationship between the Southern Annular Mode and the surface mass balance are in good agreement with the conclusions of Marshall *et al.* (2017). They found that a positive SAM favours higher precipitation ($\approx$ SMB) across both West Antarctica and the western side of the Antarctic Peninsula. The eastern Antarctic Peninsula, however, displays lower rates of precipitation when the SAM is in its positive phase. This is attributed to the precipitation shadow created over that area when westerly winds cross the steep orography of the Peninsula. Moreover, they found that a positive SAM also reduces precipitation on the Antarctic Plateau, a pattern MAR only captured partially.

The ENSO-SMB relationship exhibits overall positive correlations across the Bellingshausen Sea and Antarctic Peninsula region and negative correlations in the Amundsen Sea sector, a pattern highlighted in past studies (e.g., Donat-Magnin *et al.*, 2020; Paolo *et al.*, 2018)

On a large scale, the conditions that favour surface melting over West Antarctica (maritime air intrusions) are created by AS blocking, which is in turn promoted by Rossby waves which are influenced by El Niño events. This is important because extreme El Niño events are predicted to become more frequent. At the same time, the SAM, which exhibits an anticorrelation with West Antarctic surface melting, is becoming increasingly positive. If this trend relaxes, we might see a further increase in melting events (e.g., Scott *et al.*, 2018).

We also found a recent growing anticorrelation between ENSO and surface mass balance (Fig. 4.30). In addition to the expected increasing frequency of extreme El Niño events, this could lead to more accumulation over West Antarctica in the coming years. Medley and Thomas (2019) found that increasing accumulation rates could mitigate sea-level rise. In fact, El Niño-driven accumulation over West Antarctic ice shelves has led to an increase in ice shelf height. At the same time, extreme El Niño events contribute to the coastal upwelling of Circumpolar Deep Water (CDW), thereby melting the ice shelves from below and causing thinning. Thus, although satellite observations reveal an increase in ice shelf height, the melted ice is a lot denser than the accumulated snow, resulting in an overall mass loss. This affects the dynamic balance between the ice sheet and the ice shelves by reducing the buttressing effect of the latter (Paolo *et al.*, 2018).

The modelled increase in surface mass balance (e.g., Medley and Thomas, 2019) may be the direct result of stratospheric ozone depletion in the 1970s, as proposed by Lenaerts *et al.* (2018). The warming of the atmosphere as a result of increasing greenhouse gas emissions might also be responsible. Atmospheric warming results in higher moisture-holding capacity, thereby potentially increasing snowfall (Huybrechts *et al.,* 2004). However, according to Monaghan *et al.* (2006) the observed variability of snowfall should probably be attributed to the variability of the atmospheric circulation rather than the increase in the moisture-holding capacity. Another hypothesis suggests that the strengthening of the ENSO-SMB relationship accompanied by an increase in El Niño events (Cai *et al.*, 2014) could be the cause. Finally, the change in surface mass balance could be attributed to the increasingly positive phase of the SAM since the 1950s (Marshall, 2003), a trend that is driven by both ozone depletion and greenhouse gas emission (Arblaster & Meehl, 2005), thus further supporting the first two hypotheses. The most likely answer is probably a combination of the mechanisms cited above, which are all somewhat interconnected.

In addition to the SAM and ENSO, the Amundsen Sea Low is a third important climate driver of interannual variability in the Antarctic Pacific sector. Previous studies have highlighted the important role the ASL plays in governing the climate in the West Antarctic region. As a result of the changing central pressure and location of the ASL, regional wind is modified, leading to anomalies in accumulation rates, temperature, and sea ice concentration (e.g., Turner *et al.,* 2016). The connection between Antarctic precipitation and ASL longitudinal position has been described by Hosking *et al.* (2013). Donat-Magnin *et al.* (2020) found that during austral

summer, SMB is generally the highest across Thwaites and Pine Island when there is a significant westward (30°) and slight southward (3–4°) deviation of the ASL's usual location. That positioning of the ASL results in an enhanced southward flow, east of the ASL, in the direction of the ice shelves. Coupled with the convergence of moisture, this promotes precipitation and finally SMB. At the same time, with an anticyclonic anomaly, ASL promotes more surface melt, through moisture convergence over the Amundsen Sea Embayment which results in more cloud cover, ultimately leading to more LWD (Scott *et al.,* 2018).

An analysis of the evolution of the influence the ASL has on Antarctic climate was not included in this chapter. For the assessment of SAM and ENSO, observation-based indices were used. However, indices describing the ASL are derived from reanalysis data (e.g., https://scotthosking.com/asl_index, last accessed: 18/08/2022), which, as already mentioned, are relatively unreliable over the AIS before the satellite era. Nevertheless, through assessing the influence of both ENSO and SAM, we already include the effect of the ASL, at least partially. Both the variability of the Southern Hemisphere pressure and tropical Pacific ocean-atmosphere, which are represented by the SAM and ENSO respectively, greatly impact the strength and location of the ASL (e.g., Hosking *et al*., 2013; Raphael *et al*., 2016; Turner *et al*., 2017). For instance, ASL central pressure has been found to be lower when SAM is in its positive phase and during La Niña events, whereas the opposite is true during El Niño years. That being said, the ASL being a driver of regional climate variability in West Antarctica, different ENSO events can display different climatic responses depending on the ASL strength and location (which does not solely depend on ENSO) (Paolo *et al.,* 2018). Thus, our ENSO analysis is not able to entirely capture the complex mechanisms involved.

5. Concluding Discussion

The objective of this study was twofold, the first section being dedicated to the assessment of the usability of the ERA5 dataset prior to 1979. The evaluation reveals good model performance before 1979 regarding near-surface pressure with a mean bias of -17.15 hPa and a correlation of 0.88 with observed values, slightly worse than between 1979 and 2020, with respective values of -6.52 hPa and 0.96. Prior to 1979, during summer months, modelled near-surface pressure is closer to the measured near-surface pressure (r = 0.93) than during summer (0.85). This seasonal discrepancy was also found by Marshall *et al.* (2022) and could be due to the higher quantity of data assimilated into the ERA5 dataset during summer. MAR when forced by the ERA5 back extension also performs relatively well for near-surface temperature (r = 0.86). As for near-surface pressure, there is a difference in model performance between winter (r = 0.60) and summer (r = 0.77). The evaluation also highlights the fact that MAR forced by ERA5 is able to reproduce the variability of the observed near-surface temperature at different sites spread across the AIS. Near-surface wind exhibit poor performance for both 1950–1978 (r = 0.46) and 1979–2020 (r = 0.69). Thus, the slight differences in near-surface wind speed between 1951–1980 and 1981–2010 identified in Chapter 4 need to be considered carefully. Finally, a comparison of simulated SMB values to SMB values from *in situ* measurements show that generally the model results are satisfactory before 1979 (r > 0.7), except for values between 2200 masl and 2800 masl (r = 0.53). Moreover, in both periods, MAR forced by ERA5 tends to underestimate high SMB values.

The second part of this study sheds some light on the evolution of the climate prior to the late 70s, as well as the linkages to large-scale atmospheric drivers in interannual variability (e.g., ENSO, SAM). This Chapter highlighted both seasonal and spatial discrepancies found in the Antarctic climate. For instance, summer near-surface temperature displays a decrease in the Ross ice shelf sector, while during winter and spring, there is an increase in temperature in eastern East Antarctica between 1951–1980 and 1981–2010. For near-surface wind speed, the most notable changes occur during winter, but overall wind speed does not appear to increase or decrease significantly between 1950 and 2020. Surface mass balance appears to increase slightly between 1950 and 1980, whereas between 1981 and 2010 there is a negative trend. In the last two decades, however, surface mass balance has been steadily increasing. If this trend continues, it could potentially lead to the mitigation of the contribution of the AIS to sea-level

rise (Medley & Thomas, 2019). Between 1951–1980and 1981–2010, SMB has decreased significantly with values above 200 mm of water equivalent per year, especially along the coast and across the Antarctic Peninsula, while the Ross ice shelf sector displays a decrease in SMB. Surface melt, which primarily occurs on the Antarctic Peninsula, has increased by around 20 Gt/year between 1951–1980 and 1981–2010. Increasing surface melt has led to the collapse of parts of the Larsen ice shelf and could potentially result in the disappearance of the remaining parts (Larsen C & D). Finally, sublimation, which is only a minor component of the surface mass balance, has slightly decreased in summer, especially between the Ross ice shelf and the Transantarctic Mountains.

The change in surface mass balance and near-surface temperature described above is likely linked to a change of the Southern Annular Mode and the El Nino/Southern Oscillation, which both exhibit a tendency towards being increasingly positive and negative respectively. The relationship between SAM/ENSO and the Antarctic climate has been demonstrated in Chapter 4.3 and the results are in good agreement with the scientific literature. A positive SAM promotes a stronger westerly flow across the Antarctic Peninsula, thus increasing near-surface temperature and increasing precipitation on the western side. At the same time, the enhanced westerly flow inhibits meridional flow of warm maritime air, thus lowering near-surface temperatures across the rest of the AIS. This relationship is observed across all four seasons, with slight spatial differences. Moreover, MAR forced by ERA5 is able to reproduce the marked change in the SAM-SAT relationship in the late 1970s, a phenomenon that has been identified in recent studies (e.g., Turner *et al.*, 2020; Marshall *et al.*, 2022). Moreover, the past few years also reveal a change in the sign of SAM-SAT relationship. An analysis of the link between ENSO and West Antarctic SMB showed that El Niño events generally promote increasing snowfall, thus increasing surface mass balance and the height of the ice shelves. However, this effect may be counterbalanced by the upwelling of warm Circumpolar Deep Water, which is also favoured by episodes of El Niño (Paolo *et al*., 2018).

We also found a jump in near-surface temperature between 1978 and 1980, especially during winter months. Moreover, the sudden increase in temperature is less pronounced across the Antarctic Peninsula. This jump was not displayed by any of the measuring stations; thus, it is likely that this jump is artificial and might be traced back to the introduction of assimilated ozone data into the reanalysis dataset in the same period. However, these stations are mostly

located along the coastline, thereby not being representative of the entire AIS. The same jump was also found for near-surface wind speed but was identified for surface mass balance.

To interpret whether the modelled changes in climate between 1950 and 2020 are consistent with the reanalysis, ERA5 near-surface temperature and 700 hPa humidity were plotted against modelled near-surface temperature and surface mass balance. In short, the climate variability produced by MAR deviates little from the ERA5 values. Most importantly, the sudden increase in both SMB and SAT around 1978 is reflected by the reanalysis.

Reproducing the same analysis but using a different reanalysis also spanning over a longer timespan (e.g., 20CR$_{v3}$, JRA-55) could be an interesting subject for future studies, especially regarding the pronounced jump found for almost all variables in the late 1970s. Alternatively, simulated values could also be directly compared to ice core measurements to assess if the jump in surface mass balance and temperature is artificial or natural. Finally, a recently corrected version of the ERA5 back extension has been made public as a response to anomalous behaviour of the reanalysis in the tropics. In the future, it is likely that the back extension, which is still under review, will undergo further corrections, thus altering the results presented in this study. Thus, simulating the climate over the AIS with the final reviewed ERA5 dataset might reveal interesting new insights. Similarly, future model versions, with more accurate representations of physical processes (e.g., drifting snow) and higher resolutions might result in the climate being simulated even more accurately. Finally, reevaluating the relationship between the climate and both SAM and ENSO in a few years could show the impact that the disappearance of the ozone hole and increasing greenhouse gases may have on the former.

6. References

Agosta, C., Amory, C., Kittel, C., Orsi, A., Favier, V., Gallee, H., van den Broeke, M. R., Lenaerts, J. T. M., van Wessem, J. M., van de Berg, W. J., Fettweis, X., Sub Dynamics Meteorology, & Marine and Atmospheric Research. (2019). Estimation of the Antarctic surface mass balance using the regional climate model MAR (1979–2015) and identification of dominant processes. The Cryosphere, 13(1), 281–296. https://doi.org/10.5194/tc-13-281-2019

Amory, C., & Kittel, C. (2019). Brief communication: Rare ambient saturation during drifting snow occurrences at a coastal location of East Antarctica. The Cryosphere, 13(12), 3405–3412. https://doi.org/10.5194/tc-13-3405-2019

Amory, C., Kittel, C., Le Toumelin, L., Agosta, C., Delhasse, A., Favier, V., & Fettweis, X. (2021). Performance of MAR (v3.11) in simulating the drifting-snow climate and surface mass balance of Adélie Land, East Antarctica. Geoscientific Model Development, 14(6), 3487–3510. https://doi.org/10.5194/gmd-14-3487-2021

Armour, K. C., Marshall, J., Scott, J. R., Donohoe, A., & Newsom, E. R. (2016). Southern Ocean warming delayed by circumpolar upwelling and equatorward transport. Nature Geoscience, 9(7), 549–554. https://doi.org/10.1038/ngeo2731

Arblaster, J. M., & Meehl, G. A. (2006). Contributions of External Forcings to Southern Annular Mode Trends. Journal of Climate, 19(12), 2896–2905. https://doi.org/10.1175/JCLI3774.1

Bamber, J. L., Griggs, J. A., Hurkmans, R. T. W. L., Dowdeswell, J. A., Gogineni, S. P., Howat, I., Mouginot, J., Paden, J., Palmer, S., Rignot, E., & Steinhage, D. (2013). A new bed elevation dataset for Greenland. The Cryosphere, 7(2), 499–510. https://doi.org/10.5194/tc-7-499-2013

References

Bell, B., Hersbach, H., Simmons, A., Berrisford, P., Dahlgren, P., Horányi, A., Muñoz-Sabater, J., Nicolas, J., Radu, R., Schepers, D., Soci, C., Villaume, S., Bidlot, J., Haimberger, L., Woollen, J., Buontempo, C., & Thépaut, J. (2021). The ERA5 global reanalysis: Preliminary extension to 1950. Quarterly Journal of the Royal Meteorological Society, 147(741), 4186–4227. https://doi.org/10.1002/qj.4174

Bintanja, R., van Oldenborgh, G. J., Drijfhout, S. S., Wouters, B., & Katsman, C. A. (2013). Important role for ocean warming and increased ice-shelf melt in Antarctic sea-ice expansion. Nature Geoscience, 6(5), 376–379. https://doi.org/10.1038/ngeo1767

Bromwich, D. H., & FOGT, R. L. (2004). Strong Trends in the Skill of the ERA-40 and NCEP–NCAR Reanalyses in the High and Midlatitudes of the Southern Hemisphere, 1958–2001. Journal of Climate, 17(23), 4603–4619. https://doi.org/10.1175/3241.1

Bromwich, D. H., Chen, B., & Hines, K. M. (1998). Global atmospheric impacts induced by year-round open water adjacent to Antarctica. Journal of Geophysical Research: Atmospheres, 103(D10), 11173–11189. https://doi.org/10.1029/98JD00624

Bromwich, D. H., Nicolas, J. P., & Monaghan, A. J. (2011). An Assessment of Precipitation Changes over Antarctica and the Southern Ocean since 1989 in Contemporary Global Reanalyses. Journal of Climate, 24(16), 4189–4209. https://doi.org/10.1175/2011JCLI4074.1

Bromwich, D. H., Fogt, R. L., Hodges, K. I., & Walsh, J. E. (2007). A tropospheric assessment of the ERA-40, NCEP, and JRA-25 global reanalyses in the polar regions. Journal of Geophysical Research - Atmospheres, 112(D10), D10111–n/a. https://doi.org/10.1029/2006JD007859

Bromwich, D. H., Rogers, A. N., Kallberg, P., Cullather, R. I., White, J. W. C., & Kreutz, K. J. (2000). ECMWF Analyses and Reanalyses Depiction of ENSO Signal in Antarctic Precipitation. Journal of Climate, 13(8), 1406–1420. https://doi.org/10.1175/1520-0442(2000)0132.0.CO;2

References

Brun, E., David, P., Sudul, M., & Brunot, G. (1992). A numerical model to simulate snow-cover stratigraphy for operational avalanche forecasting. Journal of Glaciology, 38(128), 13–22. https://doi.org/10.3189/S0022143000009552

Cai, W., Borlace, S., England, M. H., Guojian Wang, Guilyardi, E., Jin, F.-F., Lengaigne, M., van Rensch, P., Collins, M., Vecchi, G., Timmermann, A., Santoso, A., Mcphaden, M. J., & Lixin Wu. (2014). Increasing frequency of extreme El Niño events due to greenhouse warming. Nature Climate Change, 4(2), 111–116. https://doi.org/10.1038/nclimate2100

Clem, K. R., Renwick, J. A., McGregor, J., & Fogt, R. L. (2016). The relative influence of ENSO and SAM on Antarctic Peninsula climate. Journal of Geophysical Research. Atmospheres, 121(16), 9324–9341. https://doi.org/10.1002/2016JD025305

Cullather, R. I., Bromwich, D. H., & Van Woert, M. L. (1996). Interannual variations in Antarctic precipitation related to El Niño-Southern Oscillation. Journal of Geophysical Research. D. Atmospheres, 101(D14), 19109–19118. https://doi.org/10.1029/96JD01769

Das, I., Bell, R., Lenaerts, J. T., van den Broeke, M., Marine and Atmospheric Research, & Sub Dynamics Meteorology. (2013). Influence of persistent wind scour on the surface mass balance of Antarctica. Nature Geoscience, 6(5), 367–371. https://doi.org/10.1038/ngeo1766

De Ridder, K. & Gallee, H. (1998). Land Surface–Induced Regional Climate Change in Southern Israel. Journal of Applied Meteorology (1988), 37(11), 1470–1485. https://doi.org/10.1175/1520-0450(1998)0372.0.CO;2

Donat-Magnin, M., Jourdain, N. C., Gallée, H., Amory, C., Kittel, C., Fettweis, X., Wille, J. D., Favier, V., Drira, A., & Agosta, C. (2020). Interannual variability of summer surface mass balance and surface melting in the Amundsen sector, West Antarctica. The Cryosphere, 14(1), 229–249. https://doi.org/10.5194/tc-14-229-2020

Donat-Magnin, M., Jourdain, N. C., Kittel, C., Agosta, C., Amory, C., Gallee, H., Krinner, G., & Chekki, M. (2021). Future surface mass balance and surface melt in the Amundsen sector of the West Antarctic Ice Sheet. The Cryosphere, 15(2), 571–593. https://doi.org/10.5194/tc-15-571-2021

Dupont, T. K. & Alley, R. B. (2005). Assessment of the importance of ice-shelf buttressing to ice-sheet flow. Geophysical Research Letters, 32(4), L04503–n/a. https://doi.org/10.1029/2004GL022024

Favier, V., Agosta, C., Parouty, S., Durand, G., Delaygue, G., Gallée, H., Drouet, A.-S., Trouvilliez, A., & Krinner, G. (2013). An updated and quality controlled surface mass balance dataset for Antarctica. The Cryosphere, 7(2), 583–597. https://doi.org/10.5194/tc-7-583-2013

Fettweis, X., Box, J. E., Agosta, C., Amory, C., Kittel, C., Lang, C., van As, D., Machguth, H., & Gallée, H. (2017). Reconstructions of the 1900–2015 Greenland ice sheet surface mass balance using the regional climate MAR model. The Cryosphere, 11(2), 1015–1033. https://doi.org/10.5194/tc-11-1015-2017

Fogt, R., Bromwich, D. H., & Hines, K. M. (2010). Understanding the SAM influence on the South Pacific ENSO teleconnection. Climate Dynamics, 36(7–8), 1555–1576. https://doi.org/10.1007/s00382-010-0905-0

Fretwell, P., Pritchard, H. D., Vaughan, D. G., Bamber, J. L., Barrand, N. E., Bell, R., Bianchi, C., Bingham, R. G., Blankenship, D. D., Casassa, G., Catania, G., Callens, D., Conway, H., Cook, A. J., Corr, H. F. J., Damaske, D., Damm, V., Ferraccioli, F., Forsberg, R., … Griggs, J. A. (2013). Bedmap2: improved ice bed, surface and thickness datasets for Antarctica. The Cryosphere, 7(1), 375–393. https://doi.org/10.5194/tc-7-375-2013

Gallee, H., & Schayes, G. (1994). Development of a three-dimensional meso-γ primitive equation model: katabatic winds simulation in the area of Terra Nova Bay, Antarctica. Monthly Weather Review, 122(4), 671–685. https://doi.org/10.1175/1520-0493(1994)1222.0.CO;2

Grazioli, J., Madeleine, J.-B., Gallée, H., Forbes, R. M., Genthon, C., Krinner, G., & Berne, A. (2017). Katabatic winds diminish precipitation contribution to the Antarctic ice mass balance. Proceedings of the National Academy of Sciences - PNAS, 114(41), 10858–10863. https://doi.org/10.1073/pnas.1707633114

References

Hersbach, H., Bell, B., Berrisford, P., Hirahara, S., Horányi, A., Muñoz-Sabater, J., Nicolas, J., Peubey, C., Radu, R., Schepers, D., Simmons, A., Soci, C., Abdalla, S., Abellan, X., Balsamo, G., Bechtold, P., Biavati, G., Bidlot, J., Bonavita, M., … Thépaut, J. (2020). The ERA5 global reanalysis. Quarterly Journal of the Royal Meteorological Society, 146(730), 1999–2049. https://doi.org/10.1002/qj.3803

Hines, K. M., Bromwich, D. H., & Marshall, G. J. (2000). Artificial Surface Pressure Trends in the NCEP–NCAR Reanalysis over the Southern Ocean and Antarctica. Journal of Climate, 13(22), 3940–3952. https://doi.org/10.1175/1520-0442(2000)0132.0.CO;2

Holland, P. R., & Kwok, R. (2012). Wind-driven trends in Antarctic sea-ice drift. Nature Geoscience, 5(12), 872–875. https://doi.org/10.1038/ngeo1627

Hosking, J. S., Orr, A., Marshall, G. J., Turner, J., & Phillips, T. (2013). The Influence of the Amundsen–Bellingshausen Seas Low on the Climate of West Antarctica and Its Representation in Coupled Climate Model Simulations. Journal of Climate, 26(17), 6633–6648. https://doi.org/10.1175/JCLI-D-12-00813.1

Hudson, S. R., & Brandt, R. E. (2005). A Look at the Surface-Based Temperature Inversion on the Antarctic Plateau. Journal of Climate, 18(11), 1673–1696. https://doi.org/10.1175/JCLI3360.1

Huybrechts, P., Gregory, J., Janssens, I., & Wild, M. (2004). Modelling Antarctic and Greenland volume changes during the 20th and 21st centuries forced by GCM time slice integrations. Global and Planetary Change, 42(1), 83–105. https://doi.org/10.1016/j.gloplacha.2003.11.011

King, J. C., & Turner, J. (1997). Antarctic Meteorology and Climatology. Cambridge University Press. https://doi.org/10.1017/CBO9780511524967

King, J.C., & Anderson, P. S. (1994). Heat and water vapour fluxes and scalar roughness lengths over an Antarctic ice shelf. Boundary-Layer Meteorology, 69(1–2), 101–121. https://doi.org/10.1007/BF00713297

References

King, J. C., Anderson, P. S., & Mann, G. (2001). The seasonal cycle of sublimation at Halley, Antarctica. Journal of Glaciology, 47(156), 1–8. https://doi.org/10.3189/172756501781832548

Kittel, C. (2021). Present and future sensitivity of the Antarctic surface mass balance to oceanic and atmospheric forcings: insights with the regional climate model MAR. Unpublished doctoral thesis, ULiège - Université de Liège

Kittel, C., Amory, C., Agosta, C., Delhasse, A., Doutreloup, S., Huot, P.-V., Wyard, C., Fichefet, T., & Fettweis, X. (2018). Sensitivity of the current Antarctic surface mass balance to sea surface conditions using MAR. The Cryosphere, 12(12), 3827–3839. https://doi.org/10.5194/tc-12-3827-2018

Kittel, Amory, C., Agosta, C., Jourdain, N. C., Hofer, S., Delhasse, A., Doutreloup, S., Huot, P.-V., Lang, C., Fichefet, T., & Fettweis, X. (2021). Diverging future surface mass balance between the Antarctic ice shelves and grounded ice sheet. The Cryosphere, 15(3), 1215–1236. https://doi.org/10.5194/tc-15-1215-2021

Kittel, C., Amory, C., Hofer, S., Agosta, C., Jourdain, N. C., Gilbert, E., Le Toumelin, L., Vignon, É., Gallée, H., & Fettweis, X. (2022). Clouds drive differences in future surface melt over the Antarctic ice shelves.

Lai, C.-Y., Kingslake, J., Wearing, M. G., Chen, P.-H. C., Gentine, P., Li, H., & Spergel, J. J. (2020). Vulnerability of Antarctica's ice shelves to meltwater-driven fracture. Nature (London), 584(7822), 574–578. https://doi.org/10.1038/s41586-020-2627-8

Lenaerts, J. T. M., & van den Broeke, M. R. (2012). Modeling drifting snow in Antarctica with a regional climate model: 2. Results. Journal of Geophysical Research: Atmospheres, 117(D5), D05109/1–n/a. https://doi.org/10.1029/2010JD015419

Lenaerts, J. T. M., Fyke, J., & Medley, B. (2018). The Signature of Ozone Depletion in Recent Antarctic Precipitation Change: A Study with the Community Earth System Model. Geophysical Research Letters, 45(23), 12,931–12,939. https://doi.org/10.1029/2018GL078608

References

Lenaerts, J. T. M., Medley, B., van den Broeke, M. R., & Wouters, B. (2019). Observing and Modeling Ice-Sheet Surface Mass Balance. Reviews of Geophysics (1985), 57(2), 376–420. https://doi.org/10.1029/2018RG000622

Li, L., & Pomeroy, J. W. (1997). Estimates of Threshold Wind Speeds for Snow Transport Using Meteorological Data. Journal of Applied Meteorology (1988), 36(3), 205–213. https://doi.org/10.1175/1520-0450(1997)0362.0.CO;2

Loewe, F. (1962). On the mass economy of the interior of the Antarctic Ice Cap. Journal of Geophysical Research, 67(13), 5171–5177. https://doi.org/10.1029/JZ067i013p05171

Marshall, G. J. (2003). Trends in the Southern Annular Mode from Observations and Reanalyses. Journal of Climate, 16(24), 4134–4143. https://doi.org/10.1175/1520-0442(2003)0162.0.CO;2

Marshall, G. J. (2007). Half-century seasonal relationships between the Southern Annular mode and Antarctic temperatures. International Journal of Climatology, 27(3), 373–383. https://doi.org/10.1002/joc.1407

Marshall, G. J. & Thompson, D. W. J. (2016). The signatures of large-scale patterns of atmospheric variability in Antarctic surface temperatures. Journal of Geophysical Research. Atmospheres, 121(7), 3276–3289. https://doi.org/10.1002/2015JD024665

Marshall, G. J., Orr, A., & Turner, J. (2013). A Predominant Reversal in the Relationship between the SAM and East Antarctic Temperatures during the Twenty-First Century. Journal of Climate, 26(14), 5196–5204. https://doi.org/10.1175/JCLI-D-12-00671.1

Marshall, G. J., Thompson, D. W. J., & Broeke, M. R. (2017). The Signature of Southern Hemisphere Atmospheric Circulation Patterns in Antarctic Precipitation. Geophysical Research Letters, 44(22), 11,580–11,589. https://doi.org/10.1002/2017GL075998

Marshall, G. J., Orr, A., van Lipzig, N. P. M., & KING, J. C. (2006). The Impact of a Changing Southern Hemisphere Annular Mode on Antarctic Peninsula Summer Temperatures. Journal of Climate, 19(20), 5388–5404. https://doi.org/10.1175/JCLI3844.1

Marshall, G. J., Di Battista, S., Naik, S. S., & Thamban, M. (2009). Analysis of a regional change in the sign of the SAM–temperature relationship in Antarctica. Climate Dynamics, 36(1–2), 277–287. https://doi.org/10.1007/s00382-009-0682-9

Marshall, G. J., Fogt, R. L., Turner, J., & Clem, K. R. (2022). Can current reanalyses accurately portray changes in Southern Annular Mode structure prior to 1979? Climate Dynamics. https://doi.org/10.1007/s00382-022-06292-3

McKnight, D. M., Tate, C., Andrews, E., Niyogi, D., Cozzetto, K., Welch, K., Lyons, W., & Capone, D. (2007). Reactivation of a cryptobiotic stream ecosystem in the McMurdo Dry Valleys, Antarctica: A long-term geomorphological experiment. Geomorphology (Amsterdam), 89(1), 186–204. https://doi.org/10.1016/j.geomorph.2006.07.025

Medley, B. & Thomas, E. R. (2019). Increased Snowfall over the Antarctic Ice Sheet Mitigated Twentieth-Century Sea-Level Rise. Nature Climate Change, 9(1), 34–39. https://doi.org/10.1038/s41558-018-0356-x

Meehl, G. A., Arblaster, J. M., Chung, C. T. Y., Holland, M. M., DuVivier, A., Thompson, L., Yang, D., & Bitz, C. M. (2019). Sustained ocean changes contributed to sudden Antarctic sea ice retreat in late 2016. Nature Communications, 10(1), 14–19. https://doi.org/10.1038/s41467-018-07865-9

Monaghan, A. J., Bromwich, D. H., & Schneider, D. P. (2008). Twentieth century Antarctic air temperature and snowfall simulations by IPCC climate models. Geophysical Research Letters, 35(7), L07502–n/a. https://doi.org/10.1029/2007GL032630

Monaghan, A. J., Bromwich, D. H., Fogt, R. L., Wang, S.-H., Mayewski, P. A., Dixon, D. A., Ekaykin, A., Frezzotti, M., Goodwin, I., Isaksson, E., Kaspari, S. D., Morgan, V. I., Oerter, H., Van Ommen, T. D., Van der Veen, C. J., & Wen, J. (2006). Insignificant Change in Antarctic Snowfall since the International Geophysical Year. Science (American Association for the Advancement of Science), 313(5788), 827–831. https://doi.org/10.1126/science.1128243

References

Mottram, R. H., Hansen, N., Kittel, C., van Wessem, M., Agosta, C., Amory, C., Boberg, F., van de Berg, W. J., Fettweis, X., Gossart, A., van Lipzig, N., van Meijgaard, E., Orr, A., Phillips, T., Webster, S., Simonsen, S., Souverijns, N., Sub Dynamics Meteorology, & Marine and Atmospheric Research. (2021). What is the surface mass balance of Antarctica? An intercomparison of regional climate model estimates. The Cryosphere, 15(8), 3751–3784. https://doi.org/10.5194/tc-15-3751-2021

Munneke, P. K., Picard, G., van den Broeke, M. R., Lenaerts, J. T. M., & van Meijgaard, E. (2012). Insignificant change in Antarctic snowmelt volume since 1979. Geophysical Research Letters, 39(1), L01501/1–n/a. https://doi.org/10.1029/2011GL050207

Munneke, P. K., Luckman, A. J., Bevan, S. L., Smeets, C. J. P. P., Gilbert, E., van den Broeke, M. R., Wang, W., Zender, C., Hubbard, B., Ashmore, D., Orr, A., King, J. C., Kulessa, B., Sub Dynamics Meteorology, Sub SIM overig, & Marine and Atmospheric Research. (2018). Intense Winter Surface Melt on an Antarctic Ice Shelf. Geophysical Research Letters, 45(15), 7615–7623. https://doi.org/10.1029/2018GL077899

Murray, J. (1898). The scientific advantages of an Antarctic expedition. Proceedings of the Royal Society of London, 62(379–387), 424–451. https://doi.org/10.1098/rspl.1897.0131

Nicolas, J. P., & Bromwich, D. H. (2014). New Reconstruction of Antarctic Near-Surface Temperatures: Multidecadal Trends and Reliability of Global Reanalyses. Journal of Climate, 27(21), 8070–8093. https://doi.org/10.1175/JCLI-D-13-00733.1

Orr, A., Marshall, G. J., Hunt, J. C. R., Sommeria, J., Wang, C.-G., van Lipzig, N. P. M., Cresswell, D., & King, J. C. (2008). Characteristics of Summer Airflow over the Antarctic Peninsula in Response to Recent Strengthening of Westerly Circumpolar Winds. Journal of the Atmospheric Sciences, 65(4), 1396–1413. https://doi.org/10.1175/2007JAS2498.1

Orr, A., Deb, P., Clem, K., Gilbert, E., Boberg, F., Bromwich, D. H., Colwell, S., Hansen, N., Lazzara, M., Mottram, R., Niwano, M., Phillips, T., Pishniak, D., Reijmer, C., van de Berg, W. J., Webster, S., & Zou, X. (2022). Summer air temperature extremes over Antarctic ice shelves and potential "hotspots" of surface melting. Journal of Climate. (Manuscript Draft)

Paolo, F. S., Padman, L., Fricker, H. A., Adusumilli, S., Howard, S., & Siegfried, M. R. (2018). Response of Pacific-sector Antarctic ice shelves to the El Niño/Southern Oscillation. Nature Geoscience, 11(2), 121–126. https://doi.org/10.1038/s41561-017-0033-0

Parkinson, C. L., & Cavalieri, D. J. (2012). Antarctic sea ice variability and trends, 1979–2010. The Cryosphere, 6(4), 871–880. https://doi.org/10.5194/tc-6-871-2012

Pertierra, L. R., & Hughes, K. A. (2019). Evaluating ecosystem services in Antarctica - why are we falling behind? Antarctic Science, 31(5), 229–230. https://doi.org/10.1017/S0954102019000312

Raphael, M. N., Marshall, G. J., Turner, J., Fogt, R. L., Schneider, D., Dixon, D. A., Hosking, J. S., Jones, J. M., & Hobbs, W. R. (2016). THE AMUNDSEN SEA LOW: Variability, Change, and Impact on Antarctic Climate. Bulletin of the American Meteorological Society, 97(1), 111–122. https://doi.org/10.1175/BAMS-D-14-00018.1

Rintoul, S. R., Silvano, A., Pena-Molino, B., van Wijk, E., Rosenberg, M., Greenbaum, J. S., & Blankenship, D. D. (2016). Ocean heat drives rapid basal melt of the Totten Ice Shelf. Science Advances, 2(12), e1601610–e1601610. https://doi.org/10.1126/sciadv.1601610

Scambos, T. A., Frezzotti, M., Haran, T., Bohlander, J., Lenaerts, J. T., Van Den Broeke, M., Jezek, K., Long, D., Urbini, S., Farness, K., Neumann, T., Albert, M., & Winther, J.-G. (2012). Extent of low-accumulation "wind glaze" areas on the East Antarctic plateau: implications for continental ice mass balance. Journal of Glaciology, 58(210), 633–647. https://doi.org/10.3189/2012JoG11J232

Scott, R. C., Nicolas, J. P., Bromwich, D. H., Norris, J. R., & Lubin, D. (2019). Meteorological Drivers and Large-Scale Climate Forcing of West Antarctic Surface Melt. Journal of Climate, 32(3), 665–684. https://doi.org/10.1175/JCLI-D-18-0233.1

Shepherd, A., Ivins, E., Rignot, E., Smith, B., van den Broeke, M., Velicogna, I., Whitehouse, P., Briggs, K., Joughin, I., Krinner, G., Nowicki, S., Payne, T., Scambos, T., Schlegel, N., Geruo, A., Agosta, C., Ahlstrom, A., Babonis, G., Barletta, V., Blazquez, A., Bonin, J., Csatho, B., Cullather, R., Felikson, D., Fettweis, X., Forsberg, R., Gallee, H., Gardner, A., Gilbert, L.,

Groh, A., Gunter, B., Hanna, E., Harig, C., Helm, V., Horvath, A., Horwath, M., Khan, S., Kjeldsen, K. K., Konrad, H., Langen, P., Lecavalier, B., Loomis, B., Luthcke, S., McMillan, M., Melini, D., Mernild, S., Mohajerani, Y., Moore, P., Mouginot, J., Moyano, G., Muir, A., Nagler, T., Nield, G., Nilsson, J., Noel, B., Otosaka, I., Pattle, M. E., Peltier, W. R., Pie, N., Rietbroek, R., Rott, H., Sandberg-Sørensen, L., Sasgen, I., Save, H., Scheuchl, B., Schrama, E., Schröder, L., Seo, K.-W., Simonsen, S., Slater, T., Spada, G., Sutterley, T., Talpe, M., Tarasov, L., van de Berg, W. J., van der Wal, W., van Wessem, M., Vishwakarma, B. D., Wiese, D., Wouters, B., and team, T. I. (2018). Mass balance of the Antarctic Ice Sheet from 1992 to 2017. Nature (London), 558(7709), 219–222. https://doi.org/10.1038/s41586-018-0179-y

Thompson, D. W. J., & Solomon, S. (2002). Interpretation of Recent Southern Hemisphere Climate Change. Science (American Association for the Advancement of Science), 296(5569), 895–899. https://doi.org/10.1126/science.1069270

Trusel, L. D., Frey, K. E., Das, S. B., Karnauskas, K. B., Kuipers Munneke, P., van Meijgaard, E., & van den Broeke, M. R. (2015). Divergent trajectories of Antarctic surface melt under two twenty-first-century climate scenarios. Nature Geoscience, 8(12), 927–932. https://doi.org/10.1038/ngeo2563

Turner, J. (2004). The El Niño–southern oscillation and Antarctica. International Journal of Climatology, 24(1), 1–31. https://doi.org/10.1002/joc.965

Turner, J., Colwell, S. R., Marshall, G. J., Lachlan-Cope, T. A., Carleton, A. M., Jones, P. D., Lagun, V., Reid, P. A., & Iagovkina, S. (2004). The SCAR READER Project: Toward a High-Quality Database of Mean Antarctic Meteorological Observations. Journal of Climate, 17(14), 2890–2898. https://doi.org/10.1175/1520-0442(2004)0172.0.CO;2

Turner, J., Lu, H., White, I., King, J. C., Phillips, T., Hosking, J. S., Bracegirdle, T. J., Marshall, G. J., Mulvaney, R., & Deb, P. (2016). Absence of 21st century warming on Antarctic Peninsula consistent with natural variability. Nature (London), 535(7612), 411–415. https://doi.org/10.1038/nature18645

References

Turner, J., Marshall, G. J., Clem, K., Colwell, S., Phillips, T., & Lu, H. (2020). Antarctic temperature variability and change from station data. International Journal of Climatology, 40(6), 2986–3007. https://doi.org/10.1002/joc.6378

Turton, J. V., Kirchgaessner, A., Ross, A. N., & King, J. C. (2018). The spatial distribution and temporal variability of föhn winds over the Larsen C ice shelf, Antarctica. Quarterly Journal of the Royal Meteorological Society, 144(713), 1169–1178. https://doi.org/10.1002/qj.3284

van de Berg, W. J., Medley, B., Sub Dynamics Meteorology, & Marine and Atmospheric Research. (2016). Brief Communication: Upper-air relaxation in RACMO2 significantly improves modelled interannual surface mass balance variability in Antarctica. The Cryosphere, 10(1), 459–463. https://doi.org/10.5194/tc-10-459-2016

van den Broeke, M. R. (1997). Spatial and temporal variation of sublimation on Antarctica: Results of a high-resolution general circulation model. Journal of Geophysical Research: Atmospheres, 102(D25), 29765–29777. https://doi.org/10.1029/97JD01862

Wace, N. M. (1960). The Botany of the Southern Oceanic Islands. Proceedings of the Royal Society of London. Series B, Biological Sciences, 152(949), 475–490. https://doi.org/10.1098/rspb.1960.0055

Wachter, P., Beck, C., Philipp, A., Höppner, K., & Jacobeit, J. (2020). Spatiotemporal Variability of the Southern Annular Mode and its Influence on Antarctic Surface Temperatures. Journal of Geophysical Research. Atmospheres, 125(23). https://doi.org/10.1029/2020JD033818
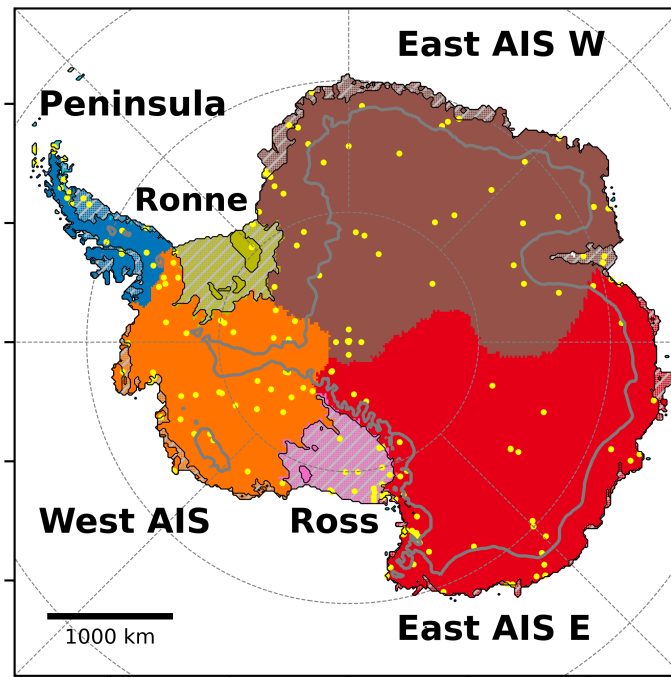
7. Appendix

Figure A.1: Map illustrating the separation into regions used in this study (from Kittel *et al.*, 2021)
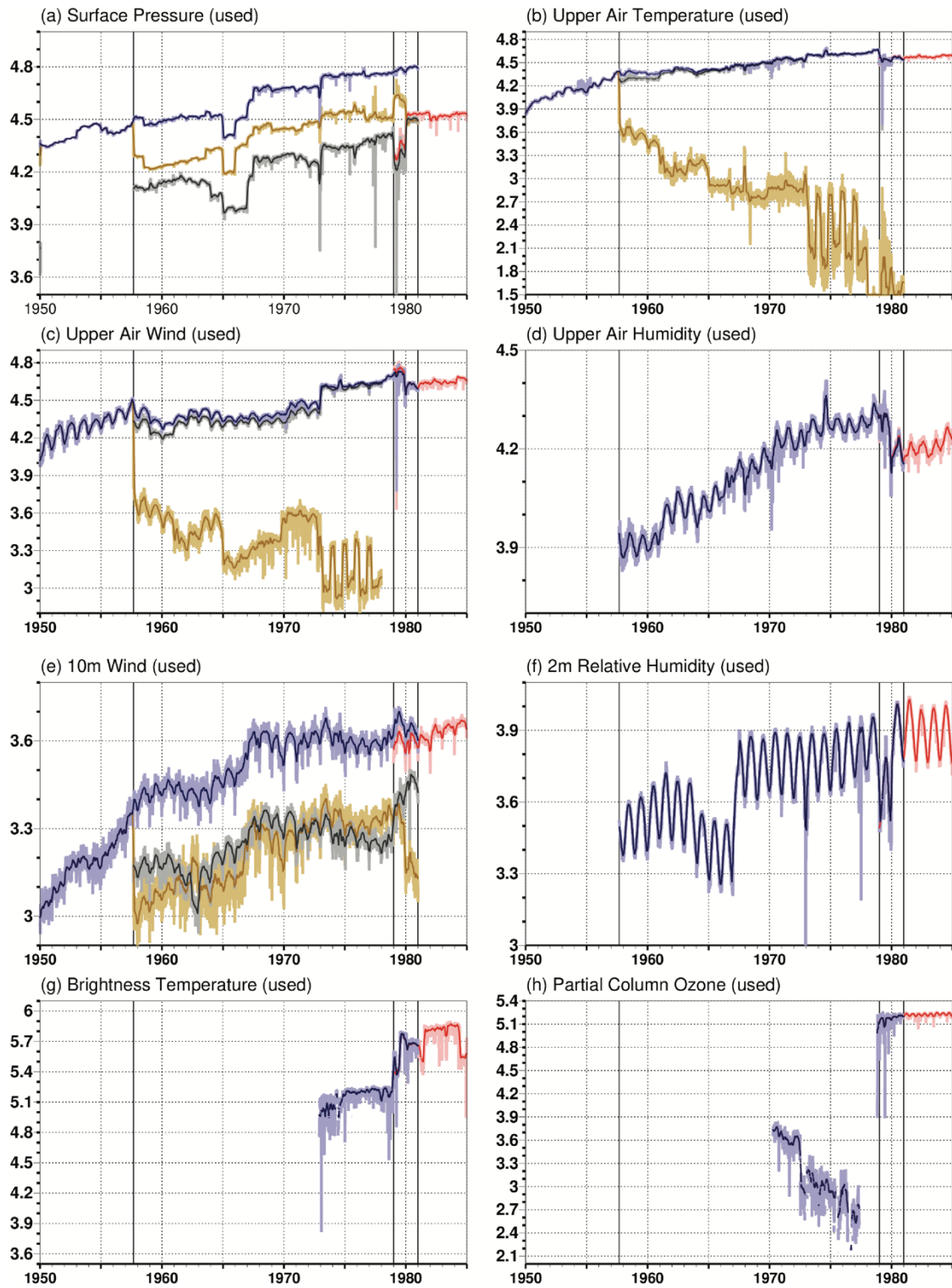
Figure A.2: Evolution of the data assimilated into the ERA5 reanalyis. For a complete description, we refer to Bell *et al.* (2021) (from Bell *et al.*, 2021)
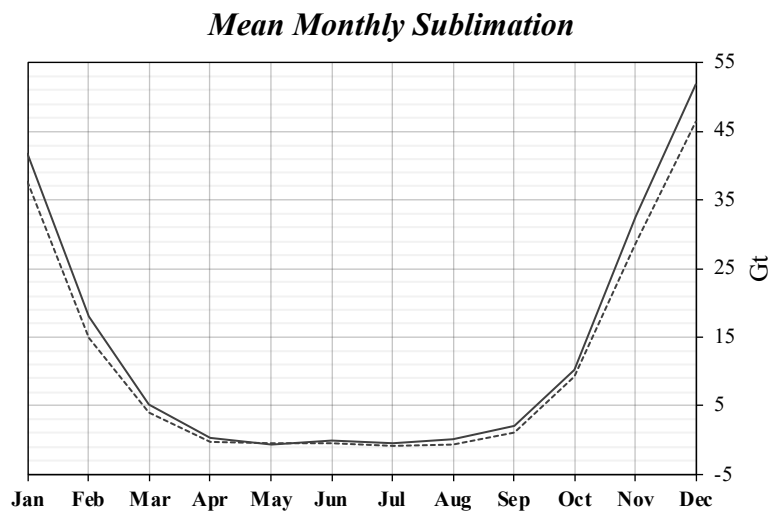
Mean Monthly Sublimation

Figure A.3: Seasonal cycle of sublimation (Gt) across the AIS from MAR $_{v3.12}$ forced by ERA5 over 1951-2010 (dashed line) and 1981-2010 (straight line)
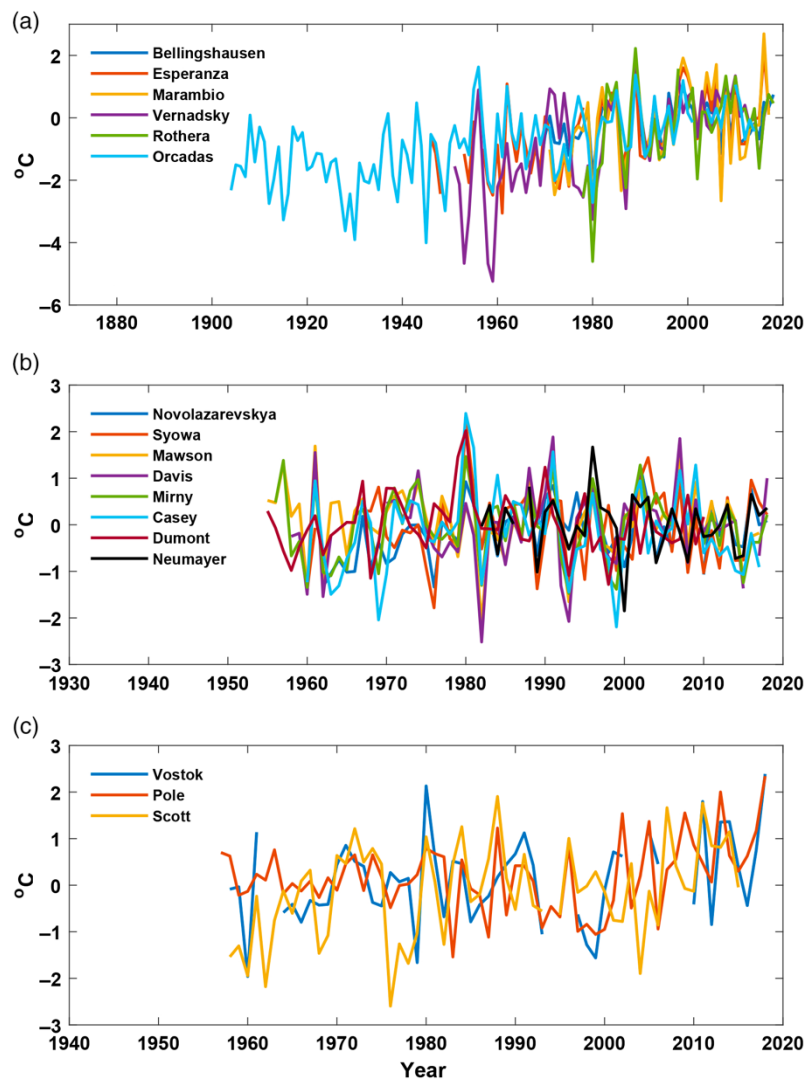

Figure A.4: Station-based temperature anomalies (from Turner *et al.,* 2020)